

**Sampling of tissues using picosecond infrared laser (PIRL) for Redox  
Proteomics**

**Dissertation**

zur Erlangung des akademischen Grades eines Doktors der Naturwissenschaften  
(Dr. rer. nat.)

Fakultät für Mathematik, Informatik und Naturwissenschaften  
am Fachbereich Chemie der Universität Hamburg

**Atef Manna**  
**Aus Dakahlia, Ägypten**

**Hamburg, September 2017**

**Supervisor: Professor Dr. Hartmut Schlüter**

**Co-advisor: Professor Dr. Dr. Christian Betzel**

**Date of disputation: 17.11.2017**

This work has been done from July 2015 to September 2017, at the Department of Clinical Chemistry, at the University Medical Centre Eppendorf, Hamburg, in the working group of proteomics and mass spectrometry, under the supervision of Professor Dr. Hartmut Schlüter.

**Dedicated to my mother and my father,  
my brothers, my sister,  
my wife and my son**

## **Publications**

- Homogenization of tissues via picosecond-infrared laser (PIRL) ablation: Giving a closer view on the in-vivo composition of protein species as compared to mechanical homogenization. M. Kwiatkowski, M. Wurlitzer, A. Krutilin, P. Kiani, R. Nimer, M. Omidi, **A. Manna**, T. Bussmann, K. Bartkowiak, S. Kruber, S. Uschold, P. Steffen, J. Lübberstedt, N. Küpker, H. Petersen, R. Knecht, N.O. Hansen, A. Zarrine-Afsar, W.D. Robertson, R.J.D. Miller, H. Schlüter. *Journal of proteomics* 134 (2016): 193-202.

## **Poster presentations**

- Sampling of tissues with the picosecond-infrared-laser ablation for Redox Proteomics. **Atef Manna** , Marcel Kwiatkowski, Nils-Owe Hansen, R. J. Dwayne Miller, Hartmut Schlüter.  
50th Annual Meeting of the German Society for Mass Spectrometry (DGMS),05.03-08.03.2017, Kiel.

## Table of contents

<b>Dedication</b>	iii
<b>Publications</b>	iv
<b>Table of content</b>	v
<b>List of abbreviations</b>	viii
<b>Abstract</b>	1
<b>Zusammenfassung</b>	2
<b>1. Introduction</b>	4
1.1. Proteins are targets for ROS/Protein oxidation	4
1.1.2. Sources of ROS	6
1.1.2.A Exogenous sources	6
1.1.2.B Endogenous sources	7
1.1.3. Oxidative PTMs and biological effects	9
1.1.4. Oxidative PTMs in disease	9
1.1.5 Proteomic approaches in redox field	10
1.1.6. Methionine oxidation	11
1.1.7. Characterization of Methionine oxidation	14
1.1.8. Cysteine oxidation	15
1.1.9. Mass spectrometry (MS) in Redox Proteomics	16
1.1.10. Picosecond Infrared Laser (PIRL)	18
1.1.10A Laser Physics	18
1.1.10B Protein homogenization via PIRL-DIVE	19
<b>Aim of work</b>	21
<b>2. Materials and Methods</b>	22
2.1. Chemicals	22
2.1.1 Chemicals and reagents	22
2.1.2. Devices	24
2.1.3. Softwares	25
2.2. Jurkat cells	25
2.2.1. Cell Culture and H <sub>2</sub> O <sub>2</sub> Treatment	25
2.3. Human tonsils	26
2.4. Rat Pancreas	26

2.5.	Histology	27
2.6.	PIRL Homogenization	27
2.6.1.	DIVE Homogenization of Jurkat cells and protein homogenization	28
2.6.2.	DIVE Homogenization of Human tonsil and protein extraction	29
2.6.3.	DIVE Homogenization of Rat Pancreas and protein extraction	29
2.7.	Classical Homogenization	30
2.7.1.	Classical Homogenization of Jurkat cells and protein extraction	30
2.7.2.	Classical Homogenization of Human tonsil and protein extraction	30
2.7.3.	Classical Homogenization of Rat Pancreas and protein extraction	31
2.8.	Tryptic in-solution digestion of Jurkat cells	31
2.9.	1D-gel electrophoresis of of Human tonsil and Rat pancreas	32
2.10.	Tryptic in-gel digestion of tissues	32
2.11.	LC-MS/MS analysis	32
2.12.	Data analysis	34
2.12.1.	Proteome Discoverer 2.0	34
2.12.2.	MaxQuant (version 1.5.2.8)	34
2.13.	Data analysis of rat pancreas and human tonsil tissues	35
2.13.1.	Rat Pancreas tissue	36
2.13.2.	Human tonsil tissue	36
<b>3.</b>	<b>Results</b>	<b>37</b>
3.1.	Detection of oxidized methionine containing peptides after cell treatment with H <sub>2</sub> O <sub>2</sub>	37
3.2.	Comparison between classical and PIRL homogenization	40
3.3.	Classical homogenization	41
3.3.1.	Peptide 1 (GGIMLPEK)	41
3.3.2.	Peptide 2 (VMLGETNPADSKPGTIR)	47
3.4.	PIRL homogenization	53
3.4.1.	Peptide 3 (MVVESAYEVIK)	53
3.4.2.	Peptide 4 (AILVDLEPGTMDSVR)	59
3.5.	Classical versus PIRL-DIVE homogenization	65
3.5.1.	Peptide 5 (EITALAPSTMK)	65
3.6.	Validation of results Proteomics result of rat pancreas tissue	68
3.6.1.	Peptide 6 (AANEAGYFNEEMAPIEVK)	68

3.7.	Proteomics result of rat pancreas tissue	69
3.7.1.	Classical versus PIRL-DIVE homogenization of rat pancreas	70
3.8.	Proteomics result of human tonsil tissue	76
3.8.1.	Classical versus PIRL-DIVE homogenization of human tonsil	76
<b>4.</b>	<b>Discussion</b>	<b>83</b>
<b>5.</b>	<b>Future outlook</b>	<b>90</b>
<b>6.</b>	<b>References</b>	<b>91</b>
<b>7.</b>	<b>Appendix</b>	<b>100</b>
<b>8.</b>	<b>Acknowledgement</b>	<b>102</b>
<b>9.</b>	<b>Declaration on oath</b>	<b>104</b>



## List of abbreviations

ACN	Acetonitril
DTT	Dithiothreitol
IAA	Iodoacetamide
SDS	Sodium Dodecyl Sulfate
SDS-PAGE	Sodium Dodecyl Sulfate-Poly acrylamide gel electrophoresis
1DE	One dimensional electrophoresis
2DE	Two dimensional electrophoresis
MeOH	Methanol
EtOH	Ethanol
FA	Formic acid
TFA	Trifluoro acetic acid
MS	Mass spectrometry
HPLC	High pressure liquid chromatography
MS/MS	Tandem mass spectrometry
ESI	Electrospray ionization
MALDI	Matrix assisted laser desorption/ionization
TOF	Time of flight
XIC	Extracted ion chromatogram
AUC	Area under curve
ROS	Reactive oxygen species
Met	Methionine
MetO	Methionine sulfoxide
MetO <sub>2</sub>	Methionine slfone
TR	Thioredoxin
TRX	Thioredoxin reductase
Prx	Peroxiredoxin
Cys	Cysteine
OS	Oxidative stress

SOD	Superoxide dismutase
H <sub>2</sub> O <sub>2</sub>	Hydrogen peroxide
RNS	Reactive nitrogen species
PTMs	post-translational modifications
NOXs	NADPH oxidases
XO	Xanthine oxidase
MPO	Myeloperoxidase
Msr	Methionine sulfoxide reductase
SOH	Sufenic acid
SO <sub>2</sub> H	Sufinic acid
SO <sub>3</sub> H	Sulfonic acid
DNA	Deoxy ribonucleic acid
COFRADIC	Combined fractional diagonal chromatography
PIRL	Picosecond infrared laser
Ps	Picoseconds
OPA	Optical parametric amplifier
LASER	Light amplification by stimulated emission of radiation
Nd: YAG	Neodymium-doped Yttrium Aluminium Garnet
Nd: YLF	Neodymium-doped Yttrium Lithium Fluoride
RPC	Reversed phase chromatography
LC	Liquid chromatography
Q	quadrupole
HCD	High energy collision induced dissociation
DDA	Data dependant acquisition
AGC	Automatic gain control
Tris	Tris-hydroxymethyl-aminomethane
PBS	Phosphate buffer saline
SILAC	Stable isotope labeling amino acids by cell culture
MH	Mechanical homogenization
DIVE	Desorption by impulsive vibrational excitation

DH	Dive homogenization
BCA	Bicinconinic acid
min	Minutes
W	Watt
V	Volt
mA	Milliampère
J	Joule
μ	micro
MW	Molecular weight
m/z	Mass to charge
RT	Room temperature
T	Temperature
IP	Isoelectric points
UV	Ultra violet
λ	Wavelength

**Abstract**

Oxidative post-translational modifications (Ox-PTMs) including protein oxidation are associated with regulation of different cellular functions as well as disease mechanisms such as cancer, diabetes and neurodegenerative diseases. Recent studies showed that methionine oxidation plays a crucial role in various physiological and pathophysiological contexts. Therefore, new advances in redox proteomics tools will provide a better understanding of different disease mechanisms such as cancer. Here, we present a novel, ultrafast and soft technology for cold vaporization of cell and tissue through desorption by impulsive vibrational excitation (DIVE) of intramolecular vibrational states of intracellular water molecules within picoseconds range using a picosecond-infrared-laser (PIRL), for the investigation of redox proteome involved in either physiological or pathophysiological processes.

For the comparison of the PIRL-DIVE and the classical homogenization method, three different rat pancreases as well as three different human tonsils were cut in two comparable pieces each and then underwent mechanical and PIRL-DIVE homogenization. After tryptic digestion, the samples were analyzed by LC-MS/MS.

In order to compare the influence of the homogenization method (classical and PIRL homogenization) on the extent of protein oxidation, rat pancreas and human tonsil tissues were homogenized by both methods and the degree of methionine oxidation determined for pairs of methionine-containing peptides identified in both data sets.

After the comparison of pairs of peptides in each tissue and classifying them in two groups (1 - methionine oxidation higher in the classically homogenized sample and 2 - methionine oxidation higher in the PIRL homogenized sample), it was shown that in rat pancreas 1, 2 and 3, the percentage of methionine-containing peptides in group 1 was 92.83%, 57.85% and 52.41% respectively. In human tonsil 1, 2 and 3, the percentage of methionine containing peptides in group 1 was 80.80%, 42.41% and 50.63% respectively.

By comparing pairs in different tissues and different biological replicates, it was shown that by using PIRL-DIVE there was a case in each tissue model gives less oxidation compared to conventional approaches in the field of redox proteomics. This can suggest that PIRL mechanism itself does not generate oxidation. This technology can also be adapted to detect other oxidative PTMs such as cysteine oxidation, protein carbonylation.

### Zusammenfassung

Oxidative post-translationale Modifikationen (Ox-PTMs) von Proteinen spielen eine Rolle bei der Regulation unterschiedlicher zellulärer Funktionen ebenso wie bei der Entstehung von Krankheiten wie Krebs, Diabetes und neurodegenerativen Erkrankungen. Neuere Untersuchungen haben gezeigt, dass dabei die Oxidation des Methionins in verschiedenen physiologischen und pathophysiologischen Zusammenhängen eine Schlüsselrolle spielt. Daher sollte die Entwicklung neuer Techniken für die Untersuchung des Redox-Proteoms zu einem besseren Verständnis von Krankheitsursachen, etwa bei Krebserkrankungen, führen. In der vorliegenden Arbeit wird die Anwendung einer neuen, ultraschnellen und schonenden Technik für die Untersuchung von Redox-Proteomen vorgestellt, die an physiologischen und pathophysiologischen Prozessen beteiligt sind. Dabei wird durch „desorption by impulsive vibrational excitation“ (DIVE), bei der Schwingungen des intrazellulären Wassers innerhalb von Picosekunden durch einen Picosekunden-Infrarot-Laser angeregt werden, eine kalte Verdampfung von Zellen und Gewebe erreicht. Für den Vergleich der PIRL-DIVE- mit der klassischen Homogenisierungsmethode wurden drei Ratten-Bauchspeicheldrüsen und drei menschliche Tonsillen jeweils in gleiche Teile geschnitten und einer mechanischen bzw. einer PIRL-DIVE-Homogenisierung unterzogen. Nach Trypsin-Verdau wurden die Proben durch LC-MS/MS analysiert. Um den Einfluss der Homogenisierungs-Methode (klassische bzw. PIRL-Homogenisierung) auf die Protein-Oxidation zu vergleichen, wurden das Ratten-Bauchspeicheldrüsen- und das menschliche Tonsillen-Gewebe mit beiden Methoden homogenisiert und das Ausmaß der Methionin-Oxidation für Paare von methionin-enthaltenden Peptiden bestimmt, die jeweils in beiden Datensätzen identifiziert worden waren. Nach dem Vergleich von Paaren von Peptiden in den jeweiligen Geweben und ihrer Klassifizierung in zwei Gruppen (1 - Methionin-Oxidation höher in der klassisch homogenisierten Probe und 2 - Methionin-Oxidation höher in der durch PIRL homogenisierten Probe) zeigten die Ergebnisse, dass in den Ratten-Bauchspeicheldrüsen 1, 2 und 3 der Prozentsatz der methionin-enthaltenden Peptide in Gruppe 1 92.83%, 57.85% und 52.41% betrug. In den menschlichen Tonsillen 1, 2 und 3 betrug der Prozentsatz der methionin-enthaltenden Peptide in Gruppe 1 80.80%, 42.41% und 50.63%. Durch den Vergleich von Peptid-Paaren in verschiedenen Geweben und biologischen Replikaten konnte gezeigt werden, dass mit PIRL-DIVE in jeweils einem der Replikate der betrachteten Gewebe weniger Oxidationen beobachtet wurden als mit konventionelle Methoden, die in der Redox-Proteomanalyse verwendet werden. Daraus lässt sich schließen, dass die PIRL-DIVE Methode selbst keine Oxidationen erzeugt. Somit kann

diese Methode auch für die Identifikation anderer oxidativer PTMs wie der Cystein-Oxidation und der Protein-Carbonylierung genutzt werden.

**1. Introduction****1.1. Proteins are targets for ROS/Protein oxidation**

Aerobic organisms cannot exist without oxygen however oxygen can be dangerous to their existence due to the possibility of the conversion of oxygen to reactive oxygen species (ROS) via biological mechanisms under oxidative stress (OS) [1]. As a result of their highly reactive nature, free radicals including superoxide anion ( $O_2^{\cdot -}$ ), hydrogen peroxide ( $H_2O_2$ ), and the toxic hydroxyl radical are called ROS [2, 3]. Consequently, excessive production of ROS in living organisms can lead to severe injury or even death by damaging different biomolecules such as proteins, lipids, and nucleic acids [4-6].

Free radicals and other highly reactive oxidants including, superoxide, hydrogen peroxide, and others, are constantly formed within cells as a result of aerobic metabolism [7, 8]. Under basal physiological conditions, reactive oxygen species (ROS) and reactive nitrogen species (RNS) are normally generated at physiological levels and in a regulated manner by various mechanisms [9, 10]. Elevated levels of ROS or impairment of cellular antioxidant defenses including thioredoxin (Trx) [11], superoxide dismutase (SOD) [12], catalase [13], glutathione (GSH) [10] among others lead to oxidative stress (OS) that can increase oxidative modifications within biomolecules such as proteins, nucleic acids, and lipids, altering/losing their function, hence activity, leading to cell death [14-16].

Proteins are main targets of oxidants such as  $H_2O_2$ , due to their high abundance in biological systems. They can undergo reversible modifications and irreversible oxidative damage (see figure 1) [14]. The reaction of ROS and RNS with proteins results in three different kinds of oxidative protein modifications. The first type is the oxidation of the side chains of amino acids, where, for example, the thiol group of cysteine (Cys) is the primary target for oxidation reactions. Methionine and the aromatic amino acids such as tyrosine and tryptophan are also sensitive targets of ROS however to a lesser extent than Cys [17]. The second oxidative modification is the oxidation of the carbon–nitrogen skeleton of the protein resulting in the fragmentation of polypeptide chains or the formation of intra- or inter-molecular crosslinks [18, 19].

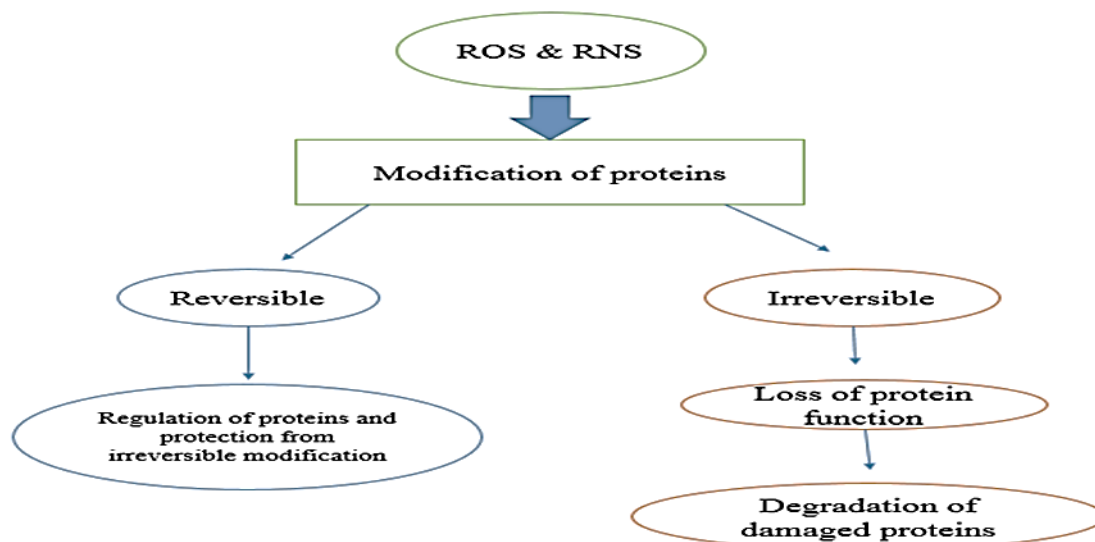


Figure. 1. Effect of ROS (reversible modifications and irreversible modifications) attack on protein function and activity [9, 14].

The third mechanism is the formation of protein carbonylation. Protein carbonylation is an irreversible modification resulting from ROS attack, leading to the introduction of carbonyl group to the polypeptide chain of protein [20]. The formation of proteins that suffer carbonyl formation can occur either by direct oxidation of sensitive amino acid side chains (lysine, arginine, and threonine) resulting in different carbonyl derivatives [20-22] or due to the fragmentation of the carbon chain [23, 24]. In this context, it is worthy to mention that protein carbonylation can also take place by reacting with reactive carbonyl species that result from the peroxidation of lipids or from the oxidation of reducing sugars [23].

Indeed, research on the reversible nature of thiol oxidation has shown that these modifications are non-toxic and have been usually attributed with a dual role: a) protection from irreversible damage, b) modulation of protein function [25]. Therefore, redox reversible protein modifications of methionine (Met) and cysteine (Cys) are normally an early cellular response to moderate oxidative stress, hence thiol modifications play a key role in different process, e.g., redox signaling processes [18, 25].



Protein oxidation includes the modifications of 3D- structures which leads to the aggregation, fragmentation, hence increasing the susceptibility to proteolysis [21, 26, 27]. It has been also reported that high levels of oxidized protein is connected to the loss of proteasomal activity that degrades oxidized proteins [17, 28].

### 1.1.2. Sources of ROS

#### 1.1.2. A. Exogenous sources

ROS are generated by various mechanisms and produced from different sources (exogenous and endogenous sources). Exogenous sources include molecular oxygen (O<sub>2</sub>), ozone (O<sub>3</sub>), ionizing radiations, industrial contaminants, air pollutants and pathogens among others. Food can be also one of exogenous sources that can include a great variety of oxidants such as peroxides, oxidized fatty acids, transition metals (e.g., Fe<sup>2+</sup>) and others [14, 29]. ROS production can take place in the process of the complete reduction of O<sub>2</sub> into two molecules of H<sub>2</sub>O [14]. This reduction process requires four electrons, however O<sub>2</sub> accepts one electron at a time (see figure 2A) [14].

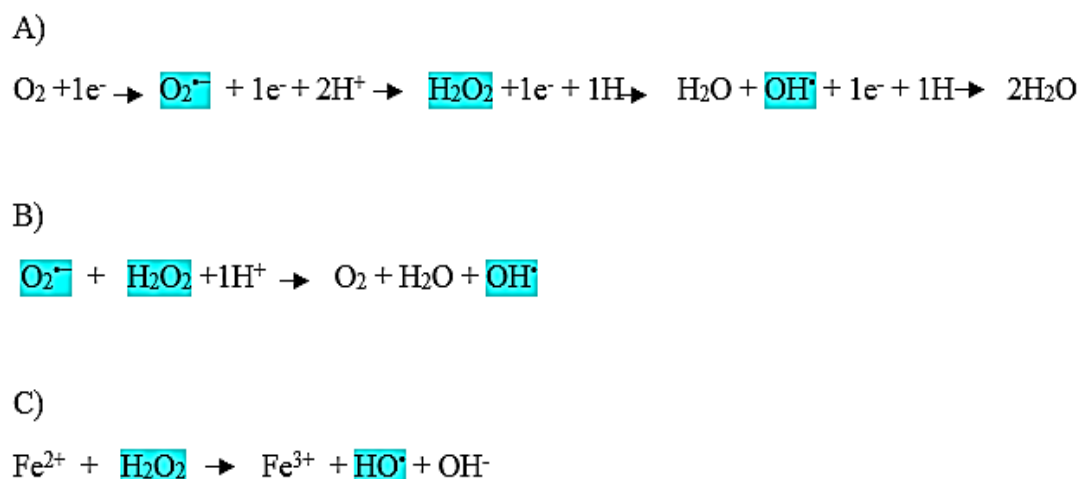


Figure 2. ROS generation within three different exogenous sources [14]. Blue colored species representing ROS.

Addition of the first electron to O<sub>2</sub> generates O<sub>2</sub><sup>·-</sup>. When the second electron is added O<sub>2</sub><sup>·-</sup>, H<sub>2</sub>O<sub>2</sub> is formed. Then, third electron is added forming toxic hydroxyl (OH<sup>·</sup>). Finally, the fourth electron is added producing two molecules H<sub>2</sub>O. OH<sup>·</sup> can be produced through the electron

exchange between  $O_2^{\cdot-}$  and  $H_2O_2$  in a reaction called (Haber–Weiss reaction, figure 2B).  $OH^{\cdot}$  can be also generated by the reduction of  $H_2O_2$  in the presence of endogenous transition metals (e.g,  $Fe^{2+}$ ), in Fenton reaction (figure 2C).

### 1.1.2.B. Endogenous sources

ROS can be generated not only by exogenous sources but also through endogenous cellular systems (see figure 3). ROS can be produced through three major endogenous cellular sources: (i) the leakage of activated oxygen from the respiratory chain within the inner mitochondrial membrane during oxidative phosphorylation [30]; (ii) monoamine oxidase (MAO)-catalyzed generation of  $H_2O_2$  during oxidative deamination of biogenic amines within the outer mitochondrial membrane [30-32]; (iii) oxygen-metabolizing enzymatic reactions catalyzed by xanthine oxidase (XO), cytochromes P450 and NADPH oxidases (NOXs) among others [32]. Existence of multiple isoforms of these enzymes in a variety of tissues and cells introduces evidence that the deliberate generation of low levels of oxidants plays a pivotal role in different cellular processes of many cells [32]. However, metals such as  $Fe^{2+}$  and  $Cu^{2+}$  can easily lose electrons, leading to generation of ROS. Therefore high levels of heavy transition metals can cause an accumulation of ROS, resulting in oxidative damage of a tissue [33].

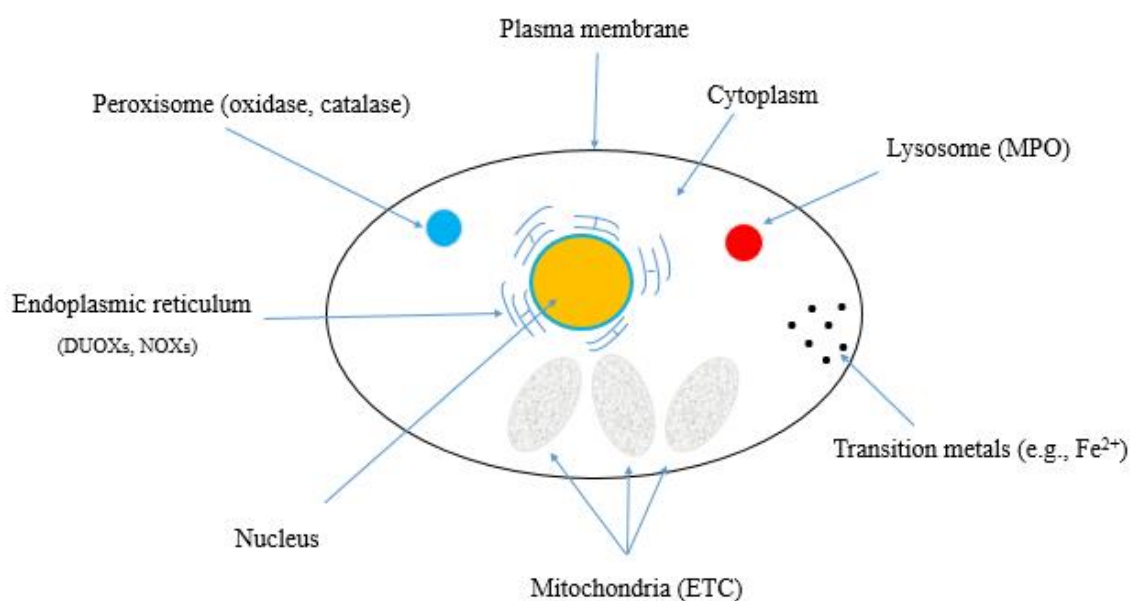


Figure 3. Main endogenous cellular systems generating ROS [14, 30]. An electron-transferring protein or enzymatic system generate ROS as “byproducts” of electron transfer reactions. A significant source of ROS in mitochondria is the electron transport chain (ETC) within the inner mitochondrial membrane of mitochondria [30]. ETC and monoamine oxidase (MAO) together catalyze the generation of H<sub>2</sub>O<sub>2</sub> during oxidative deamination of biogenic amines within the outer membrane of mitochondria. Plasma membrane is a main source of ROS via NADPH oxidases (NOXs) [30, 34]. Endoplasmic reticulum (ER) involves enzymes, such as dual oxidases (DUOXs) and NOXs [35]. It also contains cytochrome P-450 and b5 families that catalyze a variety of reactions to remove (detoxify) harmful metabolic products [14, 35, 36]. Enzymes of the same class displaying low activity are also present as free species within the cytoplasm [14, 36, 37].

Peroxisomes are an important source of total cellular H<sub>2</sub>O<sub>2</sub> production. Peroxisomes include a series of H<sub>2</sub>O<sub>2</sub> generating enzymes such as the oxidase family [31, 35]. Therefore, they are a significant source of total H<sub>2</sub>O<sub>2</sub> production in the cell. In neutrophils, once lysosomes fuse with the phagosome, enzymes, for example, myeloperoxidase (MPO) are released to it producing reactive halide-derived oxidants such as hypochlorous acid (HOCl) in the presence of H<sub>2</sub>O<sub>2</sub> [31]. Cytoplasmic soluble enzymes including xanthine oxidase (XO), dehydrogenase among others, are able to produce ROS during catalytic cycling [29]. Transition metals (e.g., Fe<sup>2+</sup>), because of their ability to lose electrons, have the capacity to produce ROS, thus oxidative damage [26, 38].

In this context, it should be mentioned that the NADPH oxidase (NOX) family of enzymes is one of the major ROS-generating enzymatic systems. It generates O<sub>2</sub><sup>•-</sup> in a highly regulated manner by catalyzing electron transfer from NADPH onto molecular oxygen (O<sub>2</sub>) [39]. The NOX family presenting seven members (NOX1–5 and DUOX1&2) representing different tissue distribution and cell-type-specific subcellular localization [40, 41]. The primary function of NOXs enzymes is ROS production, particularly for phagocytic killing of pathogens in the innate immune response. They are essential for redox signaling as well [40].

### 1.1.3. Oxidative PTMs and biological effects

ROS activity is associated with variance of biological effects, therefore under physiological conditions, specific ROS are important intracellular signal transducers of a great variety of molecular effectors including growth factors, extracellular matrix receptors, and cytokines [34, 42]. Thus, they act as second messengers to activate various downstream signaling processes [42-44]. Numerous cellular processes, such as gene expression, proliferation and apoptosis can be regulated by subtle changes in cellular redox balance [43, 45]. For example, activation of certain redox-dependent nuclear transcription factors that control antioxidant response genes including OxyR and nuclear factor  $\kappa$ B (NF- $\kappa$ B), translate cellular redox signaling to inducible expression of genes implicated in different cellular events (e.g., differentiation and detoxification) [45-47].

### 1.1.4. Oxidative PTMs in disease

Redox proteomics research area is an ideal approach for the characterization of ROS-induced protein modifications in oxidative stress conditions [48-50]. A numerous of redox proteomic publications have characterized specific oxidized proteins in different human diseases including cancer, associated with oxidative damage, providing mechanistic information on their onset, development and insights into the pathways involved in their pathogenesis as well as into downstream functional consequences [14, 51]. Recent advances in redox proteomic approaches are utilized to specify the functional impact of ROS of the cellular signaling events and to recognize the functional relationships between disease hallmarks and protein functional changes, enabling a significant contribution in the discovery of novel diagnostic biomarkers that are used for detection of many diseases at early stage as well as in the identification of new therapeutic drugs [50, 52, 53]. As a result, understanding in more details how the mechanistic pathways during oxidative damage conditions act is an extremely crucial issue. Consequently, further work in the field of redox proteomics has been devoted [53, 54], especially, investigation of novel bio-analytical methods to selectively identify and quantify oxidative modifications of proteins with high sensitivity, either for individual proteins or redox-sensitive residues of proteins [53-55]. Therefore, further advancements can be expected in the understanding of regulatory mechanisms associated with oxidative modifications of proteins, which are involved in these mechanisms and result in the illustration of function of protein oxidation within both physiological and pathological states [54, 56].

### 1.1.5. Proteomic approaches in redox field

Proteomics techniques are continuously being developed to further understanding of biology and diseases including, particularly cancer, and others (23). Many of the pathways which are associated with disease pathways rely, among others, on the characterization of PTMs such as protein oxidation. Extensive effort has been devoted on oxidative PTMs such as methionine oxidation, cysteine oxidation, protein carbonylation and others [57-60]. For example, various redox proteomics methodologies have been used to identify protein thiol oxidations that result as a part of normal cell signaling processes and oxidative stress as well [19, 60].

Indeed, one of problems in redox proteome study is that an altered oxidation status of proteins is one of the PTMs which may lead to a severe failure of biological functions, hence to cell death. Indeed, OS is associated with the start and progression of cancer [51, 61] and accumulating evidence has suggested that abnormal protein oxidation may play an important role in the development of neurodegenerative diseases such as Alzheimer (AD), and Parkinson (PD) [62, 63]. Thus, if the oxidized proteins are not adequately repaired (by antioxidant defenses), toxic cell damage may take place.

Nowadays, two main techniques are utilized in the field of redox proteomics, namely are gel-based and non-gel approaches. In gel-based approaches, the extracted oxidized proteins out of a biological tissue are separated using one or two-dimensional gel electrophoresis (1DE or 2DE respectively) separation whereby proteins migrate on a polyacrylamide gel according to their molecular weights in 1DE, and to isoelectric points (IP) and relative mobilities in 2DE [64-66]. Gels can be further transferred to a Western blot and specific antibodies utilized to visualize targeted oxidized protein spots [66, 67]. The targeted spots can be excised out of the gel, digested and identified using a peptide mass fingerprinting (PMF) MS approach [26, 65, 68] via electrospray ionization (ESI)-MS or matrix-assisted laser desorption ionization (MALDI)-MS. The benefit of using gel-based techniques is that gel-based methods are able to target a particular subset of the proteome and several gels can be applied and aligned using sophisticated software tools [62, 69]. The second approach are non-gel (gel free) methods, that include liquid chromatography (LC), followed by MS and tandem MS (MS/MS) [62, 70]. Non-gel approaches involve the digestion of proteins into peptides (in-solution digestion), then LC separation of peptides, MS and MS/MS data acquisition (see figure 4). Because of the availability of human and other databases and raw MS data, the search can be applied against protein databases by utilizing different search engine tools including SEQUEST (Yates laboratory) [71] and

MASCOT [69]. Compared to the gel-based approach, the in-solution digestion (bottom-up) method is more suited for the identification of low abundant, highly acidic/basic and hydrophobic proteins [70].

In non gel-based techniques, the fast MS scan times and automation of MS can improve the throughput compared to gel-based approaches [70], which is also a significant goal in redox proteomics research to quantify different redox levels in two or more physiological states.

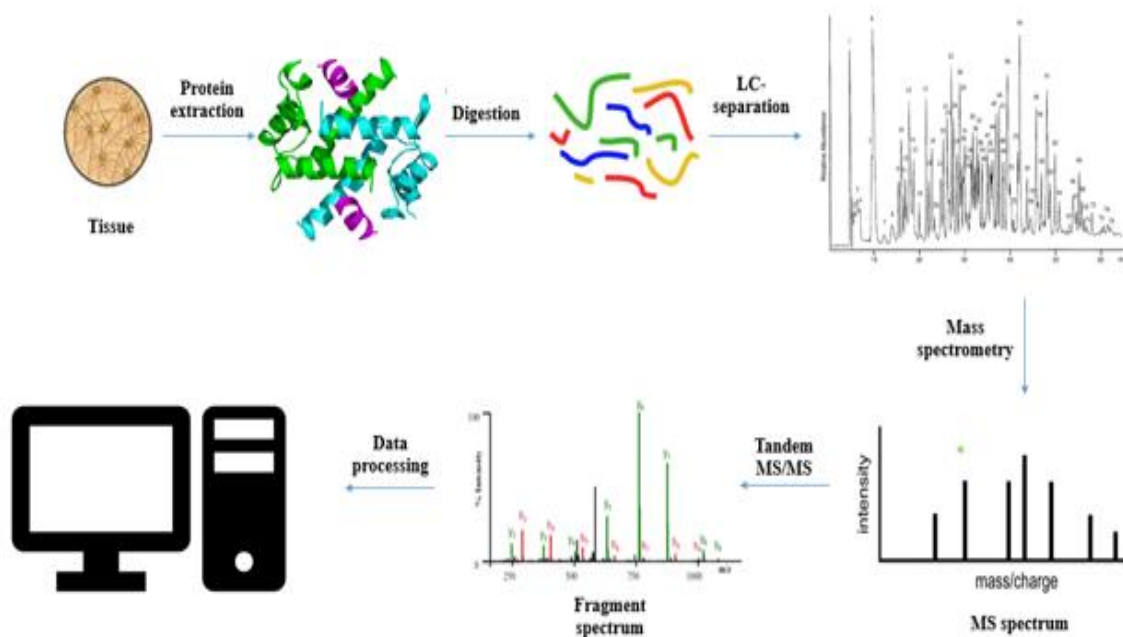


Figure 4. In-solution digestion workflow, adapted from [72].

Protein structure was taken from, <https://www.slideshare.net/damarisb/protein-structure-details>.

### 1.1.6. Methionine oxidation

Different amino acids (e.g., methionine) are exposed to be oxidized in living cells. Under normal oxidation conditions, the attack of ROS on protein induces the oxidation of methionine (Met) to methionine sulfoxide (MetSO) [73], which can be further oxidized to methionine sulfone (MetO<sub>2</sub>) under strong oxidation condition [74]. Met is the most sensitive amino acid to oxidation, and the oxidation of Met to MetSO can cause changes in hydrophobicity (MetSO, is more hydrophilic due to the oxidation of side chain of Met amino acid), alterations in protein conformation, loss of function, hence loss of biological activity of the proteins [75-77]. The

non-enzymatic oxidation of surface-exposed Met residues of proteins by ROS produces mixtures of two diastereoisomers of MetSO, referred to as Met-S-SO and Met-R-SO, due to the asymmetric position of the sulfur atom in the lateral chain [17]. Because of the toxicity arising from the oxidation of Met, living organisms have developed Met sulfoxide reductases (Msr) to repair the oxidized Met [76, 78]. Msr converts hydrophilic MetSO to hydrophobic Met [75, 76] and could participate in the scavenging of ROS intermediates in cells by reversible oxidation/reduction of Met in proteins [79]. There are two distinct isozymes of Msr, Met sulfoxide reductase A (MsrA) and Met sulfoxide reductase B (MsrB) as shown in figure 5 [80], specific for the conversion of the S and R diastereomer forms of MetSO, respectively [77, 81]. MsrA and MsrB do not share homology neither at the level of the primary sequence nor the tertiary structure [77]. In this context, it is worth mentioning that orthologs of MsrA and MsrB genes are present in most living organisms, and there is great diversity in the organization and copy number of the Msr genes in different organisms [75, 82].

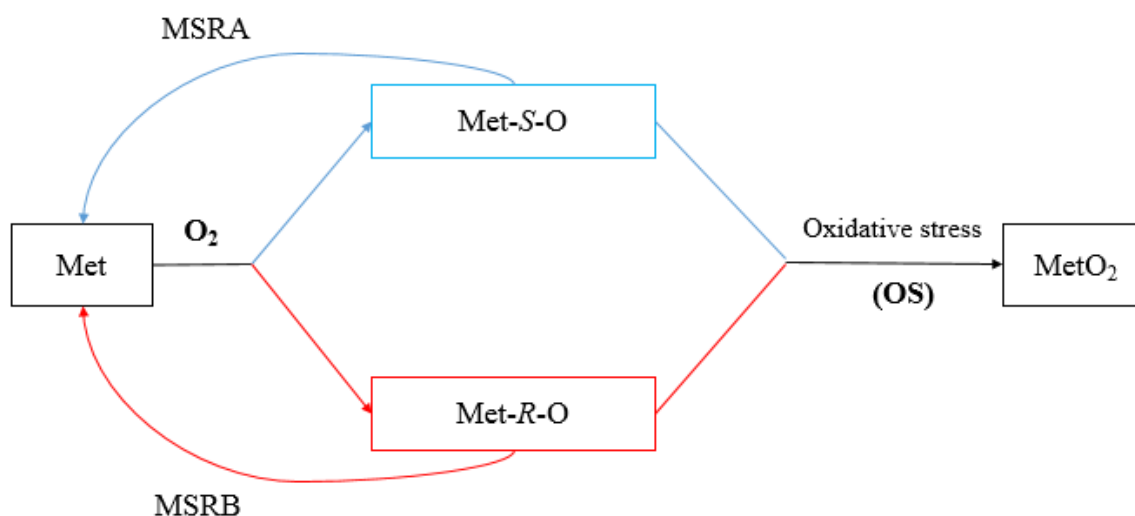


Figure 5. Chemistry of methionine oxidation/reduction in the cell [80].

The Msr enzyme reduces MetSO to Met, leading to the generation of disulfide bond (S-S) within an active site of the Msr making it inactive [79]. Reformation of an active thiol form of Msr demands the action of the thioredoxin (TRX)/thioredoxin reductase (TR) system (see figure 6), to reduce the disulfide bond within Msr via thiol exchange reactions [15, 77, 79, 80]. This

system of reversible methionine oxidation/reduction by (ROS and MSR respectively) is arising as a common biological mechanism for cellular regulation [77].

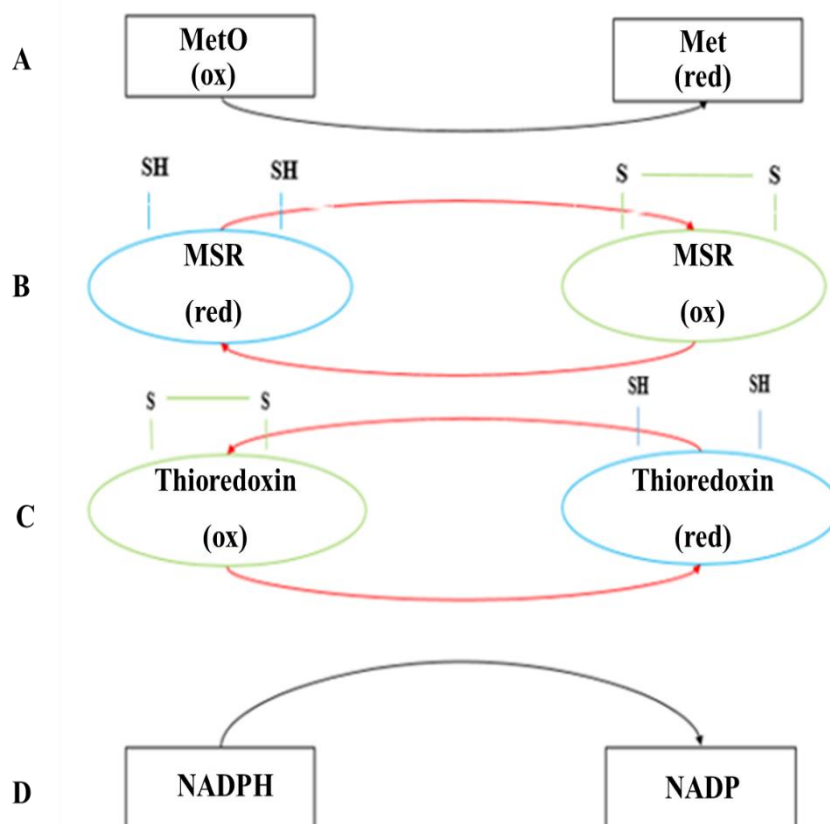


Figure 6. Main pathway of methionine sulfoxide reductase (Msr). Adapted from [80, 83], and illustrates also the reproduction of MSR occurs via thioredoxin system as the following: Reduction of methionine sulfoxide (MetO) to methionine (Met) by MSR (as shown in A), leading to the transient formation of intramolecular disulfide bond that inactivates the enzyme (as shown in B). Disulfide exchange reaction with thioredoxin (TRX) reproduces an active form of MSR (as shown in C), resulting in inactive form of TRX. Finally, reproduction of an active/reduced form of TRX takes place via the transfer of electrons from NADPH in a reaction catalyzed by thioredoxin reductase (TR) leading to NADP (as shown in D). Note that, blue-colored represents an active (reduced) forms and green ones indicates inactive forms of enzymes [84].

Protein methionine oxidation plays a crucial role within various physiological processes in many living organisms. For example, research on bacteria reported the function of methionine oxidation and its regulation by Msr for the viability of bacteria [84]. It has been shown that the lack of Msr in bacteria leads to elevated levels of ROS-induced killing, which can be rescued by restoration of Msr expression [85]. It has also been also reported that the depletion of MsrA



in knockout mice (-/-) promotes oxidative stress (OS) [85]. Thus, Msr can also have a protective role in redox regulated processes connected to diseases such as cancer and others [86-89].

### 1.1.7. Characterization of Methionine oxidation

The identification of in vivo methionine oxidation of proteins using proteomic techniques available, especially, by using mass spectrometry (MS) has been described by Ghesquière in 2011 [89]. Methionine sulfoxide (MetO) and sulfone (MetO<sub>2</sub>) containing peptides are easily detected by a mass increase of +16 and +32 Da in Met oxidized peptides compared to their unmodified counterparts (Table. 1) within electrospray ionization (ESI) and by MALDI as well [90-92]. Most of the utilized methods to study methionine oxidation depend on MS of non-enriched peptides. However, Ghesquière introduced the largest proteomic identification and quantification of Met oxidation in mammalian cells (e.g., Jurkat cells) obtained which has been described with a combined fractional diagonal chromatography (COFRADIC) technique. COFRADIC technique isolates a specific set of peptides and is based on two identical peptide separations within reversed phase liquid chromatography (RP-LC) coupled to MS/MS analysis [91]. In COFRADIC, within the first and the second chromatographic separation steps, peptides are exhibited to a sorting reaction that consists of an enzymatic or a chemical modification performed to selectively affect a specific amino acid, therefore change the chromatographic properties of the oxidized peptides containing the targeted residue [89]. It has been shown that the proteins extracted within SILAC-labeled Jurkat cells exposed to H<sub>2</sub>O<sub>2</sub> were trypsinized and peptides were separated via RP-LC and reduced with MetO reductase A and B3 (MsrA & MsrB3) [93]. Thus MetO-containing peptides were converted to more hydrophobic Met-containing counterparts in a higher retention time in the second RP-LC compared with oxidized Met-containing peptides [89, 92]. Those peptides with altered column retention time in the second chromatography, representing those peptides which have been initially oxidized, and consequently are collected for subsequent MS/MS identification [89].

Table 1. Selected Main Chemical Modifications on cysteine and methionine side chains induced by OS.

Amino Acid	Product	Composition	$\Delta m$ (mass shift)
Met	Methionine sulfoxide	+1O	+15.99492
Met	Methionine sulfone	+2O	+31.98983
Met	Homocysteic acid	-2H-1C+3O	+33.96910

### 1.1.8. Cysteine oxidation

The deprotonated thiolate anion of cysteine is a reactive group at physiological pH [94]. In reacting with cysteine, two-electron oxidants including reactive oxygen species (ROS) and second messenger hydrogen peroxide ( $H_2O_2$ ) produce a sulfenic acid (SOH) derivative as their initial oxidation product [94-96]. In the presence of available proximal thiol groups, SOH can form intra- (PSSP) or inter- (PSSP') molecular disulfide bonds, or mixed disulfides with low molecular weight thiols such as glutathione (GSH) [96, 97]. Exposure to elevated levels of oxidants (strong oxidative stress) SOH can be further irreversibly oxidized to sulfinic ( $SO_2H$ ) or sulfonic ( $SO_3H$ ) acid [98, 99]. Understanding the effects of environmental variances of ROS-mediated molecular pathways, and genetic variations for reversible cysteine oxidation, is important to investigate redox signaling events that modulate different essential intracellular processes [97-99].

One of the obstacles/drawbacks of the study of sulfenic acid modifications is that cys sulfenic acids are difficult to detect due to high chemical instability of this species. Therefore, sulfenic acids are not only products of thiol oxidation either for reversible or irreversible modifications as mentioned above. Nevertheless, they also have a specific chemical property; acting as electrophiles or nucleophiles depending on the surrounding environment. Thus, this property has been utilized for the development of probes for their detection within proteins [23].

### 1.1.9. Mass spectrometry (MS) in Redox Proteomics

Proteomics approaches are constantly being developed for understanding of biology and disease. A variety of pathways which are associated with disease mechanisms depend on the characterization (identification) of post-translational modifications (PTMs) including oxidative PTMs (e.g., methionine oxidation, protein carbonylation, cysteine oxidation and others) [14, 23, 62]. One of the main and powerful proteomic tools is mass spectrometry (MS) technology [100, 101]. Mass spectrometry (MS) is generally a key feature in proteomics, particularly in the area of redox proteomics [62]. Proteomics allows the detection of thousands of proteins in a single experiment and can provide significant insights on the identification and quantification of proteins, as well as cellular localization and protein interactions [102-104]. It can specifically provide important information in the context of understanding disease states and, by the discovery of biomarkers, facilitate early diagnosis. Proteomics also gives insight into post-translational modifications (PTMs) in the cell including, among others, protein oxidation (e.g, methionine oxidation, cysteine oxidation) among others [51, 88].

Investigations of oxidative PTMs which occur *in vitro* or *in vivo* are presently being applied using focused redox proteomics methodologies. Redox proteomics depends on gel electrophoresis (e.g., SDS-PAGE) and/or liquid chromatography separations (e.g., reversed phase chromatography) of peptides or intact proteins, followed by the detection of resulting oxidative PTMs by mass spectrometry [23, 49, 105, 106].

Briefly, the main components of a mass spectrometry instrument are an ion source, a mass analyzer and a detector (see figure 7). An ion source (e.g, electrospray ionization“ESI”) is set to ionize the molecules, the mass analyzer separates analytes/ions in gas phase depending on their mass/charge ( $m/z$ ) ratio, and ions are then detected via the detector, followed by visualization of data as an intensity on y-axis vs  $m/z$  on x-axis in a mass spectrum. Finally, the measured mass spectrum is compared to the theoretical spectra of known sequences provided by different data bases [101, 107].

Mass spectrometry technology revolution has begun by introducing the soft ionization approaches [108, 109]. In this context, it should be mentioned that ionization techniques are classified on the basis of the sample source, for instance, if the ionization occurs in a liquid phase, then electrospray ionization (ESI) is suited for LC-MS/MS coupling, and if the ionization takes place in a solid phase, MALDI (Matrix Assisted Laser Desorption/Ionization) is used then as an ionization technique [108]. The name of soft ionization techniques has been driven as they provide the transfer of biomolecules including proteins and peptides from liquid either or solid

to gas phase without any fragmentation of ions [110]. Consequently, those target molecules are analyzed using mass spectrometry instrument.

Afterwards, using a combination of two mass analyzers, it was manageable to isolate molecules/ions with certain mass/charge ratio from the complex mixture. These ions are then fragmented using a variety of techniques such as high energy collision induced dissociation (HCD), then the fragment spectrum (MS/MS) is acquired [110]. MS/MS enables us the intact mass of the molecule and its fragmentation allowing information about the identification of that molecule through available database. Currently, mass spectrometry is the most essential technique utilized in all omics applications (which include proteomics, metabolomics and lipidomics) allowing their identification, quantification, determination of post-translational modifications and structural elucidation [111, 112].

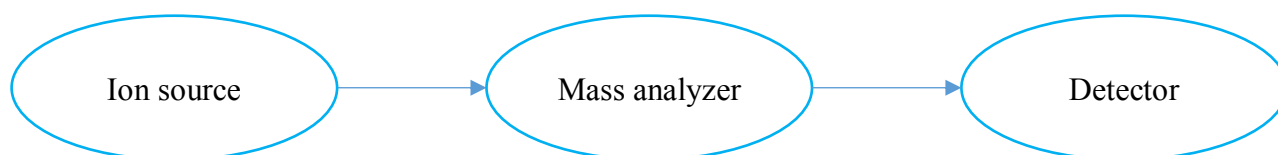


Figure 7. Main components of a mass spectrometer [101].

### 1.1.10. Picosecond Infrared Laser (PIRL)

Several classical/conventional homogenization methods with different protocols are utilized in the field of redox proteomics. As the classical homogenization procedure is not performed under an inert condition such as nitrogen gas, the redox status of classical homogenate can be changed, resulting in a high possibility to obtain artificial oxidative modifications of proteins. Therefore, the development of new techniques is needed to improve the quality of homogenization process for sampling of tissues for redox proteomics, and to have a close view to the original redox state in the cell.

Thus, the picosecond infrared laser (PIRL) homogenization technology was proposed to be used, as there was a hypothesis that PIRL technique might have an advantage in the field of redox proteomics, hence, it might work better compared to classical methods. Therefore, the PIRL method was used in comparison to the conventional method to investigate our hypothesis.

#### 1.1.10A. Laser Physics

The LASER term stands for light amplification by stimulated emission of radiation [111]. It generally refers to a device that is able to emit light within a process of optical amplification based on the stimulated emission of electromagnetic radiation. Some decades ago, physicists like Max Planck paved the way for modern day physics when he concluded the relationship between energy and the frequency of radiation in 1900, implying that energy could be emitted or absorbed only in discrete segments which he referred to as quanta. This was a crucial point that was the basis of other physicists work [113]. Later on, Planck received a Nobel Prize in physics in 1918 for the discovery of elementary energy quanta. The roots of the laser date back to 1917 with Albert Einstein's discovery of stimulated emission [113]. Then, Theodore Harold Maiman in 1960 constructed the first functioning laser device which was a Pulsed Solid-State ruby laser [111, 114]. Since that time, the laser technology has rapidly advanced and is used nowadays across a wide range of applications including biomedical research (e.g., laser surgery) [115], and others.

The term amplification in laser physics refers to a process in which the medium converts part of its energy to the emitted electromagnetic radiation, leading to an increase in optical power.

Laser systems are categorized into five sub-types based on the lasing medium : i) gas lasers such as nitrogen laser, ii) chemical lasers such as deuterium fluoride laser, iii) metal-vapor lasers such as helium–selenium and iv) solid-state lasers such as Nd: YAG (Neodymium-doped Yttrium Aluminium Garnet) laser or ruby, and v) dye lasers.

### 1.1.10B. Tissue homogenization via PIRL-DIVE

Miller and his group have introduced, in 2010, a novel laser system that has been termed picosecond infrared laser (PIRL) [116, 117]. PIRL is an example of a solid state laser which uses Nd: YLF (Neodymium-doped Yttrium Aluminium Garnet) medium with pulses in the picoseconds (ps) range. In medical application, lasers have been used in departments of dermatology and otolaryngology and ophthalmology. The main problem however has been the degree of surrounding tissue damage by the lasers used. Recently, the PIRL has been demonstrated to exhibit significantly less tissue coagulation and tissue damage when used as an incisor in surgical applications compared to other surgical tools including conventional lasers and cold instruments [118, 119]. Thus, PIRL provides a precise ablation in cellular dimension leading to much less cellular damage of the surrounding tissue [120].

The ablation mechanism by using PIRL is called desorption by impulsive vibrational excitation (DIVE), which is described below.

The PIRL delivers a wavelength ( $\lambda$ ) of 2.9  $\mu\text{m}$  with a pulse duration of of 300 picoseconds (ps). This wavelength is tuned to excite the OH bond stretch/vibration stretch in the water molecule changing its vibrational degree [119]. The water molecules in the target biological material (tissue/cells) absorb this laser pulse creating mechanical stress that leads to material fracture and ejection [119]. This wavelength and pulse duration is short enough to prevent acoustic (thermal) damage or nucleation growth and as such creating the possibility of ablating intact biological molecules such as proteins. Besides the water molecules, different biomolecules are transferred into the gaseous phase included in the plume [117]. This is known as the photo-mechanical ablation and is described as desorption by impulsive vibrational excitation (DIVE) [117, 121].

In this context, it is worth mentioning that the tissue homogenization using PIRL technology is a superior efficient method for tissues [122-124], including even hard tissues like bone or tooth [117].

**Aim of the current work**

Previous studies as described in the introduction showed that the homogenization is possible by irradiating tissues with PIRL and that during this process the chemical composition of labile biomolecules like proteins is not changed. Furthermore in homogenates obtained with PIRL significantly less enzymatical conversions of proteins were observed compared with classical homogenization techniques (Kwiatkowski et al, 2015). Consequently the total number of intact protein species detected in tissue homogenates, obtained with PIRL, was higher compared with classical homogenization methods (Kwiatkowski et al, 2016). It was assumed that this advantage of PIRL induced homogenization of tissue is based on the extremely fast process of tissue disruption and transfer of the proteins from the intact tissue into the frozen condensate of the PIRL-induced tissue aerosol. Because of the speed of this process enzymes, which are released from the compartments within the cells during homogenization, can not degrade many of the other tissue molecules. It is hypothesized, that the special mechanism and the speed by which the tissue is homogenized with PIRL may also result in less oxidation of proteins occurring during homogenization, which will be advantageous for redox proteomics.

Thus the goal of this thesis is to investigate to which extend proteins are oxidized during homogenization of tissues with PIRL in comparison to conventional homogenization.



**2. Materials and Methods****2.1. Chemicals**

Water, methanol (MeOH) and acetonitrile (ACN; all HPLC-grade) were obtained from Merck (Darmstadt, Germany). Hydrogen peroxide (H<sub>2</sub>O<sub>2</sub>) was purchased from Calbiochem (California, United states). Sequence-grade trypsin and resuspension buffer was purchased from Promega (Mannheim, Germany), protease inhibitors cocktail (complete tablets) from Roche Diagnostics, Mannheim, Germany). Other chemicals were obtained from Sigma-Aldrich (Steinheim, Germany), Amersham (Freiburg, Germany), and others as shown in the following table.

**2.1.1. Chemicals and reagents**

---

<b>Chemical name</b>	<b>Provider</b>
Iodoacetamide (IAA)	Sigma-Aldrich (Taufheim, Germany)
Dithiotrietol (DTT)	Sigma-Aldrich (Steinheim, Germany)
Urea	Amersham (Freiburg, Germany)
Formic acid (FA)	Merck (Darmstadt, Germany)
Methanol (MEOH)	Merck (Darmstadt, Germany)
Acetonitril (ACN)	Merck (Darmstadt, Germany)
Ammonium bicarbonate	Merck (Darmstadt, Deutschland)
Trypsin buffer (Promega)	(Mannheim, Germany)
Protease inhibitor cocktail	(Roche Diagnostics Ltd, Mannheim, Germany)
Water (H <sub>2</sub> O <sub>2</sub> )	Merck (Darmstadt, Germany)
Thiourea	Sigma-Aldrich (Steinheim, Germany)
2-beta mercaptoethanol Bio-Rad Laboratories (Germany)	Bio-Rad Laboratories (Germany)

---

---

## 2. Materials and Methods

---

Sodium dodecyl sulfate	Fluka
2x Laemmli Buffer	Bio-Rad Laboratories (Germany)
Hydrogen peroxide (H <sub>2</sub> O <sub>2</sub> )	Calbiochem (California, United states)
Tris	Bio-Rad Laboratories (Munich, Germany)
Reducing agent 20x	Bio-Rad Laboratories (Munich, Germany)
2D Quant Kit	GE Healthcare (Freiburg, Germany)
BCA test kit	(Thermo scientific, Germany)
Glycerol	Sigma-Aldrich (Steinheim, Germany)
2β-Mercaptoethanol	Sigma-Aldrich (Steinheim, Ger,many)
Thiourea	Sigma-Aldrich (Steinheim, Ger,many)
Trifluoroacetic acid	Sigma-Aldrich (Steinheim, Ger,many)
Oligo R3 bulk medium	Applied Biosystems (Darmstadt, Germany)

---

## 2.1.2. Devices

Device name	Provider
ACQUITY UPLC PST C18 nanoACQUITY Column 10K psi, 130Å, 1.7 µm, 75 µm X 200 mm	Waters (Manchester, UK)
ACQUITY UPLC PST C18 nanoACQUITY Trap 10K psi MV, 100Å, 5 µm, 180 µm X 20 mm	Waters (Manchester, UK)
Falcon tubes 15 mL, 50 mL	Greiner (Melsungen, Germany)
Pico second-Infrared-Laser PIRL-HP2-1064 OPA-3000	Attodyne, Toronto, Canada
Ablation box; dimensions: 9 * 7.5 * 10.5 cm	Constructed by Wesley Robertson (Max Planck Institute for Structure and Dynamics of Matter, Hamburg, Germany)
pH-Meter	Beckman Coulter (Krefeld, Germany)
Eppendorf Safe-Lock Tubes (1,5 mL, 2 mL)	Eppendorf (Hamburg, Germany)
Speed Vac concentrator 5301	Eppendorf (Hamburg, Germany)
Orbitrap fusion mass spectrometer	Thermo Scientific (Bremen, Germany)
Orbitrap Q-Exactive mass spectrometer	Thermo Scientific (Bremen, Germany)
Thermo mixer 5320	Eppendorf (Hamburg, Germany)
Balance	Kern/Sohn GmbH (Balingen-Frommern, Germany)
Vacuum pump CVC 2000	(Vacuubrand, Germany)
Vacuum centrifuge Jouan RC1010	Thermo Scientific (Waltham, USA)
Cooling trap RCT90	Thermo Scientific (Waltham, USA)
GELoader	Eppendorf (Hamburg, Germany)
Centrifuge 4-16K	Sigma-Aldrich (Osterode, Germany)
Dionex UltiMate 3000 RSLCnano	Thermo Scientific (Bremen, Germany)

**2.1.3. Softwares**

---

<b>Device name</b>	<b>Provider</b>
Proteome discoverer 2.0	Thermo Scientific (Bremen, Germany)
MaxQuant (1.5.2.8)	www.maxquant.org
Andromeda	Thermo Scientific (Bremen, Germany)
Sequest HT	Yates laboratory, USA
Xcalibur™ 2.1	Thermo Scientific (Bremen, Germany)
Image Lab™ 5.0	Bio-Rad Laboratories
Microsoft word, powerpoint and Excel 2013 as well as powerpoint 2016	Microsoft Co.

---

**2.2. Jurkat cells**

All experiments were performed three times (n=3).

**2.2.1. Cell Culture and H<sub>2</sub>O<sub>2</sub> Treatment.**

Jurkat cells were cultivated in suspension using RPMI-1640 Medium (SIGMA) supplemented with 10% FBS (Biochrom) at 37°C, 5% CO<sub>2</sub> and 100% humidification. The cells were singularized using a pipette and the cell number was determined using a Coulter-Counter (Beckman). Cells were centrifugated and washed two times with PBS. For H<sub>2</sub>O<sub>2</sub> treatment (Calbiochem, stock concentration 10 mM) 5x10<sup>6</sup> cells per sample were resuspended in 3 ul media and were treated with different concentrations as indicated (0, 50, 100, 200 μM) . The cells were incubated for 25 min at 37°C before harvest.

### 2.3. Human tonsils

We investigated this experiment before for Human tonsil tissue and the same was for rat pancreas, the data has been acquired before with respect to protein degradation (Kwiatkowski et al, 2016), however, the data is reanalyzed now with respect to methionine oxidation. Human tonsils were obtained from three different patients during tonsillectomy. Immediately following the tonsillectomy, one piece of tissue from the center of the tonsil of each patient was prepared. Each sample was cut into two comparable pieces (approx. dimension: 5 mm × 5 mm and 2 mm in depth) for conventional homogenization and PIRL-DIVE homogenization to provide direct comparison of identically prepared tissue. In addition, from each sample sections were used for histological staining. The pieces dedicated for further experiments were frozen in liquid nitrogen right after preparation and stored at – 80 °C.

### 2.4. Rat Pancreas

We investigated this experiment before for rat pancreas tissue and the data has been acquired before with respect to protein degradation [123], however, the data in this study is reanalyzed with respect to methionine oxidation. Pancreas was obtained from six different Wistar rats. The rats were killed in line of another experiment which was approved by the local licensing authority (Behörde für Soziales, Familie, Gesundheit, Verbraucherschutz; Amt für Gesundheit und Verbraucherschutz; Billstr. 80, D-20539 Hamburg, Germany) and supervised by the institutional animal welfare officer at the UKE. The pancreas was extracted and prepared immediately after euthanasia of the animals by carbon dioxide inhalation. Each of the six pancreas samples was prepared into 2 equal pieces of tissue. A separate tissue slice was prepared from each piece of tissue for histology. The pieces dedicated for further experiments were frozen in liquid nitrogen right after preparation and stored at – 80 °C. One piece was homogenized either mechanically (MTH) and with PIRL-DIVE (DTH) to enable a direct comparison of effectively identically prepared tissue.

### 2.5. Histology

For histological staining tissue samples were fixed in phosphate buffered 3.5% formaldehyde. Specimens were then embedded in paraffin, cut into 4- $\mu\text{m}$  thick sections, and stained with hematoxylin and eosin (H.E., Merck, Darmstadt, Germany). Stained samples were then scanned using MIRAX SCAN (Carl Zeiss Microimaging GmbH, Jena, Germany) [123].

### 2.6. PIRL Homogenization

The PIRL (PIRL-HP2-1064 OPA-3000, Attodyne Inc. Toronto, Canada) operated at a wavelength of 3  $\mu\text{m}$ , a repetition rate of 1 kHz and a pulse width of 300 picoseconds (ps). The PIRL beam was delivered and focused onto the sample surface with a home-built optical system. The optical power at the sample surface was approximately 450 mW for a tissue, and 380 mW for cells. The optical energy density at the sample surface was 3.39 J/cm<sup>2</sup> and the average optical power density was  $3.39 \times 10^3$  W/cm<sup>2</sup>. The PIRL beam was scanned at the speed of 130 mm/s during the ablation process. Frozen human tonsil tissue was placed in a home-built ablation chamber equipped with a funnel, which was connected with a wash-bottle within a cryo-trap. For homogenization tissues with a dimension of approximately 5 mm  $\times$  5 mm and 2 mm in depth were irradiated with PIRL. The DIVE ablation plume was captured inside the wash-bottle (condensate of the DIVE aerosol, DIVE homogenate, DH). Figure 8, shows the schematic diagram of PIRL including the ablation process. Table (2) summarizes PIRL parameters.

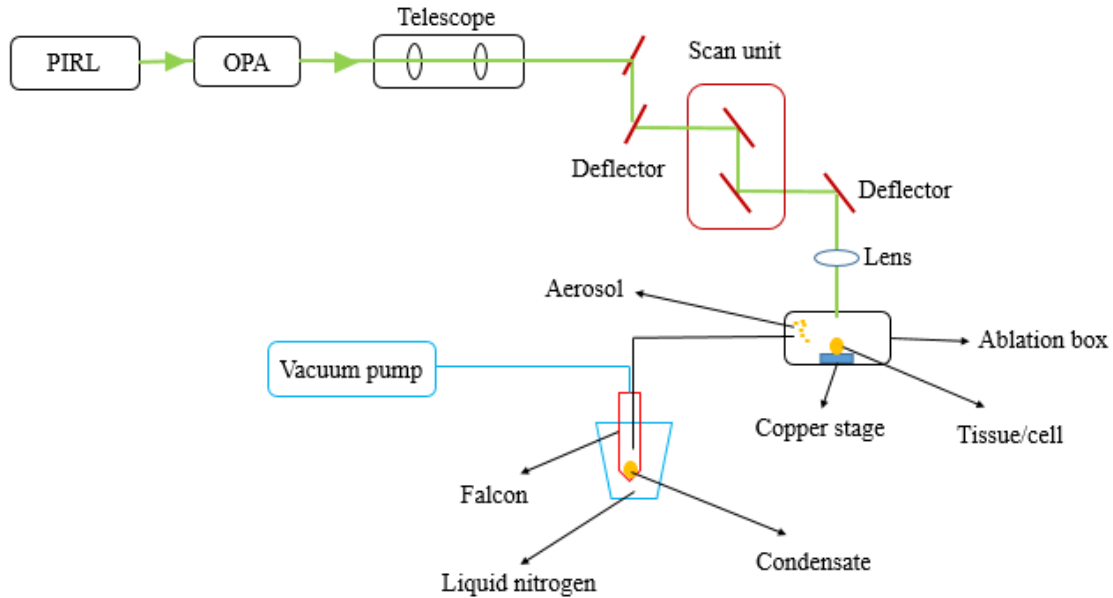


Figure 8. Schematic diagram of PIRL.

Table 2. Displays PIRL parameters for a tissue and cells ablation.

Parameters	Values
Wavelength ( $\lambda$ )	3 $\mu\text{m}$
Pulse duration	300 picoseconds
Optical power at the sample surface	450 mW (tissue), 380 mW (cells)
Repetition rate	1 kHz
Optical energy density at the sample surface	3.39 J/cm <sup>2</sup>

### 2.6.1. DIVE Homogenization of Jurkat cells and protein extraction

For homogenization of Jurkat cell samples the DIVE ablation plume was captured in a wash-bottle filled with a powder of urea which was a final concentration of 8 M urea. The frozen condensates were thawed on ice for 20 min, and centrifuged at 5200 g for 10 min at +4 °C. The supernatants were transferred into a 2 mL reaction vial. Protein quantification of PIRL homogenization for Jurkat cells was measured using the pierce BCA protein assay kit (Thermo Scientific, Germany). The samples, working reagent and dilution of bovine serum albumin

(BSA) standards have been prepared and determined following the BCA assay kit instruction. Figure 2, in the appendix displaying the calibration curve of BCA test by plotting different BSA standards concentrations versus their corresponding absorbances, hence calculated protein concentration of Jurkat cells. The samples were ready for in-solution digestion and desalting.

The BCA test kit is a colorimetric assay, in which cupric ion ( $\text{Cu}^{2+}$ ) is reduced to cuprous ion ( $\text{Cu}^{1+}$ ). The reduction process is occurred through peptide bonds of proteins. One ( $\text{Cu}^{1+}$ ). Is chelated with two molecules of bicinchoninic acid (BCA) in approximately 37 °C for 30 min producing a purple colored complex which displays a strong absorbance of light at  $\lambda = 562 \text{ nm}$  [125, 126].

### 2.6.2. DIVE Homogenization of Human tonsil and protein extraction

In case of human tonsil experiments the wash bottle was filled with a powder of urea ( $m = 210.21 \text{ mg}$ ), thiourea ( $m = 76.12 \text{ mg}$ ) and Tris-HCl ( $m = 1.82 \text{ mg}$ ). The DIVE condensates were thawed and adjusted to a total volume of 500  $\mu\text{L}$  with HPLC- $\text{H}_2\text{O}$  and 1.23  $\mu\text{L}$  2-hydroxyethyl disulfide (HED) resulting in a concentration of 7 M urea, 2 M thiourea, 30 mM Tris-HCl and 20 mM HED (DIVE homogenate, DH). DIVE homogenates were incubated for 1 h at room temperature. After incubation, samples were centrifuged at  $15,000 \times g$  for 5 min. The supernatants were transferred into a 2 mL reaction vial. Proteins were precipitated and protein concentrations were determined using the 2-D Quant Kit (GE Healthcare Life Sciences, Freiburg, Germany) following the manufacturer's instruction. For each sample 200  $\mu\text{g}$  was used for two dimensional gel electrophoresis and 40  $\mu\text{g}$  was used for SDS-PAGE.

### 2.6.3. DIVE Homogenization of Rat Pancreas and protein extraction

For homogenization of rat pancreas tissue samples the DIVE ablation plume was captured in a wash-bottle. The frozen condensates were thawed with 100  $\mu\text{L}$  five times concentrated Laemmli buffer (0.225 M Tris-HCl, pH 6.8; 50% glycerol; 5% SDS; 0.05% bromophenol blue; 0.25 M DTT,  $T = 95 \text{ }^\circ\text{C}$ ) and immediately transferred in a boiling water bath. The volume was adjusted with MS- $\text{H}_2\text{O}$  to 500  $\mu\text{L}$  and the DIVE homogenates were incubated in the boiling



water bath for 5 min. DIVE homogenates were centrifuged at  $15,000 \times g$  for 3 min. The supernatants were transferred into a 2 mL reaction vial. Protein concentration of the condensates was determined using 2-D Quant Kit (GE Healthcare Life Sciences, Freiburg, Germany) following the manufacturer's instruction. For each sample 30  $\mu\text{g}$  was loaded on SDS-PAGE.

### 2.7. Classical Homogenization method

#### 2.7.1. Classical Homogenization of Jurkat cells and protein extraction

Cells were centrifuged and washed two times with PBS. The cell pellets were stored at  $-80^\circ\text{C}$ . Cells were washed and then scraped in a lysis buffer containing 8 M urea, protease inhibitors cocktail (Complete tablets; Roche Diagnostics, Mannheim, Germany), and 1  $\mu\text{L}$  benzonase. The lysates were sonicated for 1 cycles of 15 seconds each, incubated for 1h at  $+4^\circ\text{C}$  and centrifuged for 10 minutes at 5200 g to remove cellular debris. Protein concentration of classical homogenization for Jurkat cells was measured using the pierce BCA protein assay kit (Thermo Scientific, Germany). The samples, working reagent and dilution of bovine serum albumin (BSA) standards have been prepared and determined following the BCA assay kit instruction. Figure 3, in the appendix displaying the calibration curve of BCA test by plotting different BSA standards concentrations versus their corresponding absorbances, hence calculated protein concentration of Jurkat cells.

#### 2.7.2. Classical Homogenization of Human tonsil and protein extraction

For classical (mechanical) tissue homogenization, human tonsil tissues were lyophilized for 24 h. The lyophilized and frozen tissues were grinded with a cryo-grinder in the presence of liquid nitrogen. The homogenates were dissolved in 500  $\mu\text{L}$  lysis buffer (7 M urea, 2 M thiourea, 30 mM Tris-HCl, 20 mM HED, dissolved in HPLC- $\text{H}_2\text{O}$ ) and incubated for 1 h at room temperature. After incubation, samples were centrifuged at  $15,000 \times g$  for 5 min. The supernatants were transferred into a 2 mL reaction vial. Proteins were precipitated and protein concentrations were determined using the 2-D Quant Kit (GE Healthcare Life Sciences,

Freiburg, Germany) following the manufacturer's instruction. For each sample 200 µg was used for two dimensional gel electrophoresis and 40 µg was used for SDS-PAGE.

### 2.7.3. Classical Homogenization of Rat Pancreas and protein extraction

Frozen rat pancreas tissue samples were homogenized in the presence of 500 µL lysis buffer (45 mM M Tris–HCl, pH 6.8; 10% glycerol; 1% SDS; 0.01% bromophenol blue; 0.05 M DTT) using a bead mill (TissueLyser II, Quiagen, Hamburg, Germany) with a 3 mm stainless steel bead (time: 3.3 min, frequency: 25/s). Mechanical homogenates of pancreas tissues were centrifuged at 15,000 × *g* for 3 min. The supernatants were transferred into a 2 mL reaction vial. Protein concentration of the condensates was determined using 2-D Quant Kit (GE Healthcare Life Sciences, Freiburg, Germany) following the manufacturer's instruction. For each sample 30 µg was loaded on SDS-PAGE.

### 2.8. Tryptic in-solution digestion of Jurkat cells

The protein extract solution to be digested was filled into a 10 kDa centrifuge filter. The protein solution was concentrated to max. 50 µl via centrifuging with 14000 rpm at + 4 °C, for 20 minutes. A 450 µl of 6M Urea was added to the retentate. The protein solution was again concentrated to max. 50 µl by centrifuging with 14000 rpm at +4 °C, for 20 minutes. The mentioned step was performed twice to obtain a complete buffer exchange. For in-solution reduction 1.3 µl of 100 mM of dithiothreitol (DTT, dissolved in 100 mM NH<sub>4</sub>HCO<sub>3</sub>) was used, then the samples were incubated for 10 min at 56 °C, and alkylation was achieved with 1.3 µl of 300 mM of iodoacetamide (IAA, dissolved in 100 mM NH<sub>4</sub>HCO<sub>3</sub>). The samples were incubated in dark for 40 min at room temperature. Then, 425 µl of NH<sub>4</sub>HCO<sub>3</sub> (AmbiCa) was added. Modified trypsin (Promega) was added to the Jurkat cell samples with the ratio of 1:100 (Trypsin:Protein) and incubated for 16h at 37 °C. Then, a new tube was added to the 10 kDa centrifuge filter and the digested peptides were collected within the filtrate after centrifugation with 14000 rpm at + 4 °C, for 20 minutes. Then, the desalting of peptides was performed on ice using an Oasis HLB short cartridge. The cartridge was washed with 3 mL 100% methanol twice. Then, the column was washed with 3ml wash buffer (5% Methanol, 0.2% FA in HPLC-H<sub>2</sub>O), for the sample loading. The sample was dissolved in 1 mL wash buffer and loaded onto the column. After that, the column was washed with 3 mL wash buffer. The samples were eluted with 1.5 mL 50% Methanol to a new tube. Then, the samples were evaporated. For further LC–

MS/MS analysis, samples were dissolved in 20  $\mu$ L 0.1% formic acid (FA), vortexed for 3 minutes, then sonicated for 5 minutes, and centrifuged for a short run (30 seconds) at 14000 rpm.

### 2.9. 1D-gel electrophoresis of Human tonsil and Rat pancreas

The samples were dissolved in 5  $\mu$ L 4  $\times$  sample buffer (XT sample buffer, Bio-Rad, Munich, Germany), 1  $\mu$ L 20  $\times$  reducing agent (XT reducing agent, Bio-Rad, Munich, Germany) and filled up to 20  $\mu$ L with HPLC-grade water. The samples were incubated at 95  $^{\circ}$ C for 5 min and loaded onto a 10% Criterion<sup>TM</sup> XT Bis-Tris gel (Bio-Rad, Munich, Germany). Proteins were separated at a constant voltage of 120 V for 45 min. The gel was stained for 2 h with a Coomassie solution (40% MeOH, 10% acetic acid, 0.025% Coomassie blue-250, dissolved in H<sub>2</sub>O) and destained with 40% MeOH. For tryptic in-gel digest the SDS-PAGE lanes of the DIVE homogenate (DH) and the classical, mechanical homogenate (MH) were cut in comparable bands.

### 2.10. Tryptic in-gel digestion of tissues

In-gel digestion was performed in accordance with Shevchenko et al [127]. Briefly, shrinking and swelling was achieved with pure ACN and 100 mM NH<sub>4</sub>HCO<sub>3</sub>. For in-gel reduction 10 mM dithiothreitol (dissolved in 100 mM NH<sub>4</sub>HCO<sub>3</sub>) was used and alkylation was achieved with 55 mM iodoacetamide (dissolved in 100 mM NH<sub>4</sub>HCO<sub>3</sub>). For trypsin digestion the gel pieces were covered with a trypsin solution (13 ng/ $\mu$ L sequencing-grade trypsin, dissolved in 10 mM NH<sub>4</sub>HCO<sub>3</sub> containing 10% ACN) and incubated at 37  $^{\circ}$ C for 12 h. Tryptic peptides were extracted from the gel pieces with 5% FA, 50% ACN and the extract evaporated. For further LC-MS/MS analysis, samples were dissolved in 20  $\mu$ L 0.1% FA.

### 2.11. LC-MS/MS analysis

For Jurkat cells, LC-MS/MS measurements were performed by injecting the samples on a nano liquid chromatography system (nanoACQUITY (reversed phase, type 1), Waters, Manchester, UK) coupled via electrospray-ionization (ESI) to a quadrupole orbitrap mass spectrometer (Orbitrap QExactive, Thermo Scientific, Bremen, Germany). The samples were loaded on a

trapping column (Acclaim PepMap  $\mu$ -precolumn, C18, 300  $\mu\text{m} \times 5 \text{ mm}$ , 5  $\mu\text{m}$ , 100  $\text{\AA}$ , Thermo Scientific, Bremen, Germany; nanoACQUITY UPLC Symmetry C18 trap column, 180  $\mu\text{m} \times 20 \text{ mm}$ , 5  $\mu\text{m}$ , 100  $\text{\AA}$ ; **buffer A**: 0.1% FA in HPLC- $\text{H}_2\text{O}$ ; **buffer B**: 0.1% FA in ACN) with 2% buffer B. After sample loading, the trapping column was washed for 5 min with 2% buffer B with a flow rate of (5  $\mu\text{L}/\text{min}$ ) and after that, the peptides were eluted (200  $\text{nL}/\text{min}$ ) onto the separation column (Acclaim PepMap 100, C18, 75  $\mu\text{m} \times 250 \text{ mm}$ , 2  $\mu\text{m}$ , 100  $\text{\AA}$ , Thermo Scientific, Bremen, Germany; nanoAcquity UPLC column, BEH 130 C18, Waters; 75  $\mu\text{m} \times 250 \text{ mm}$ , 1.7  $\mu\text{m}$ , 100  $\text{\AA}$ ; 200  $\text{nL}/\text{min}$ , gradient: 2–30% B in 30 min). The spray was generated from a fused-silica emitter (I.D. 10  $\mu\text{m}$ , New Objective, Woburn, USA) at a capillary voltage of 1650 V. Mass spectrometric analysis was performed in positive ion mode. LC–MS/MS analysis with the orbitrap QExactive was performed on MS level (The  $m/z$  window for precursor ion) over a  $m/z$  range from 400 to 1300, with a resolution of 70,000 FWHM at  $m/z$  200 (transient length = 256 ms, injection time = 100 ms, AGC target =  $3e6$ ). MS/MS measurements were carried out in DDA (data-dependent acquisition) mode, with a HCD collision energy of 30%, a resolution of 17,000 FWHM at  $m/z$  200 (transient length = 64 ms, injection time = 100 ms, AGC target =  $3e6$ ), and an isolation width of 2  $m/z$ .

For pancreas tissue, LC–MS/MS measurements were performed by injecting the samples on a nano liquid chromatography system (nanoACQUITY, Waters, Manchester, UK) coupled via electrospray-ionization (ESI) to a quadrupole orbitrap mass spectrometer (Orbitrap QExactive, Thermo Scientific, Bremen, Germany) and the same settings as mentioned above. Fragment MS/MS spectra were recorded in the orbitrap (scan-rate = 66 kDa/s, maximum injection time = 200 ms, AGC target =  $1e4$ ), and an isolation width of 2  $m/z$ .

For tonsil tissue, LC–MS/MS measurements were performed by injecting the samples on a nano liquid chromatography system (Dionex UltiMate 3000 RSLCnano (reversed phase, type 2), Thermo Scientific, Bremen, Germany) coupled via electrospray-ionization (ESI) to a linear trap quadrupole (LTQ) orbitrap mass spectrometer (Orbitrap Fusion, Thermo Scientific, Bremen, Germany), and the same settings as mentioned above. However, LC–MS/MS analysis with orbitrap Fusion was carried out in data dependent acquisition mode (DDA) using top speed mode, a HCD collision energy of 28%, an intensity threshold of  $2e5$  and an isolation width of 1.6  $m/z$ . Every second a MS scan was performed over a  $m/z$  range from 400 to 1500, with a resolution of 120,000 FWHM at  $m/z$  200 (transient length = 256 ms, maximum injection time = 50 ms, AGC target =  $2e5$ ). Fragment spectra (MS/MS spectra) were detected in the ion trap (scan-rate = 66 kDa/s, maximum injection time = 200 ms, AGC target =  $1e4$ ).

### 2.12. Data analysis

#### 2.12.1. Proteome Discoverer 2.0

For Jurkat cells, LC–MS raw data from the tryptic in solution digestion were processed via proteome Discoverer 2.0 (Thermo Scientific, Bremen, Germany). For identification MS/MS spectra were searched with Sequest HT algorithms (search engine) against the human SwissProt database ([www.uniprot.org](http://www.uniprot.org), downloaded November 10, 2014, 20161 sequence entries). The searches were performed using the following parameters: precursor mass tolerance was set to 10 ppm and fragment mass tolerance was set to 0.02 Da. For peptide identification, a maximum of two missed cleavages were allowed and a carbamidomethylation on cysteine residues as static (fixed) modification as well as an oxidation of methionine residues as dynamic modifications. Peptides were identified with a false discovery rate (FDR) of 1% by using Percolator. Proteins were considered as correctly identified if at least two unique peptides were identified.

For tonsil tissue, LC–MS raw data from the tryptic in gel digestion were processed via proteome Discoverer 2.0 (Thermo Scientific, Bremen, Germany) as mentioned above, except that fragment mass tolerance was set to 0.2 Da, and a carbamidomethylation on cysteine residues was considered as a static modification and an oxidation of methionine as dynamic modification.

For pancreas tissue, LC–MS raw data from the tryptic in gel digestion were processed via proteome Discoverer 2.0 (Thermo Scientific, Bremen, Germany) as mentioned above, except that identification MS/MS spectra were searched with Sequest HT algorithms against against a SwissProt database of *Rattus norvegicus* ([www.uniprot.org](http://www.uniprot.org), downloaded December 22, 2016), and a carbamidomethylation on cysteine residues was considered as a static modification and an oxidation of methionine as dynamic modification.

#### 2.12.2. MaxQuant (version 1.5.2.8)

For Jurkat cells, LC–MS raw data from the tryptic in solution digestion were processed with MaxQuant (version 1.5.2.8). Peptide and protein identification was done with Andromeda search engine against a human SwissProt database ([www.uniprot.org](http://www.uniprot.org), downloaded November 10, 2014). The searches were performed using the following parameters: precursor mass tolerance was set to 20 ppm and fragment mass tolerance was set to 20 ppm for orbitrap Q-Excactive measurements. For peptide identification, a maximum of two miss cleavages were

allowed, a carbamidomethylation on cysteine residues as a fixed modification and an oxidation of methionine, N-terminal Acetylation as variable modifications. Peptides and proteins were identified with a FDR of 1%. For a protein identification at least two of its unique peptides were detected.

For tonsil tissue, LC–MS raw data from the tryptic in gel digestion were processed via MaxQuant (version 1.5.2.8) as mentioned above as mentioned above, except that the fragment mass tolerance was set to 0.5 Da.

For pancreas tissue, LC–MS raw data from the tryptic in gel digestion were processed via MaxQuant (version 1.5.2.8) as mentioned above, except that identification MS/MS spectra were searched with Andromeda search engine against against a SwissProt database of *Rattus norvegicus* ([www.uniprot.org](http://www.uniprot.org), downloaded September, 02, 2016).

### 2.13. Data analysis of rat pancreas and human tonsil tissues

Raw files of LC-MS/MS analysis for rat pancreatic and human tonsils tissues were processed using MaxQuant software (version 1.2.5) searching against andromeda search engine. After the processing task was done, the oxidation (M).txt file was merged to an excel sheet for each of human tonsil and rat pancreas tissues.

From the exported data, oxidation (M) probabilities and the respective ratios of mod/base (ratio of oxidized/reduced) were selected. Peptides with non-defined and zero values have been excluded from further analysis.

For the final analysis, only pairs (common) of oxidized methionine containing peptides were chosen that were found by both homogenization methods in each tissue separately in rat pancreases and in human tonsils respectively, and of which intensities for both, oxidized and reduced form, have been measured from (→Mod Spec Sites.txt file).

For any given peptide out of all common peptides (in rat pancreases and human tonsils), the ratio of oxidized to reduced form for both methods was calculated. The ratios of oxidized/reduced form (for common peptides) in each tissue separately obtained by classical homogenization have been divided by the respective matched ratios obtained by PIRL-DIVE

homogenization (``ratios of oxidized/ reduced form of classical`` divided by ``ratios of oxidized/ reduced form PIRL-DIVE``).

After the division of the ratios obtained by classical homogenization to PIRL-DIVE, the obtained results (in each rat pancreatic tissue separately ``section 2.13.1``, and in each human tonsil tissue separately ``section 2.13.2 `` ) produced values that fall in two categories.

### 2.13.1. Rat pancreas tissue

The results obtained from the classical and the PIRL homogenization methods in rat pancreas tissues are given in figures 43, 44 and 45 and tables 11, 12 and 13. Methionine containing peptides were sorted depending on the ratio of oxidized/reduced state. These values were then compared between the two homogenization methods (classical and PIRL) and were assigned to two categories:

- 1- After the division of  $\text{ratio(classical)/ratio(PIRL)}$ , values which are higher than 1, meaning that there is more methionine oxidation in the sample prepared by the classical homogenization method.
- 2- After the division of  $\text{ratio(classical)/ratio(PIRL)}$ , values which are lower than 1, meaning that there is more methionine oxidation in the sample prepared by the PIRL-DIVE homogenization technique.

### 2.13.2. Human tonsil tissue

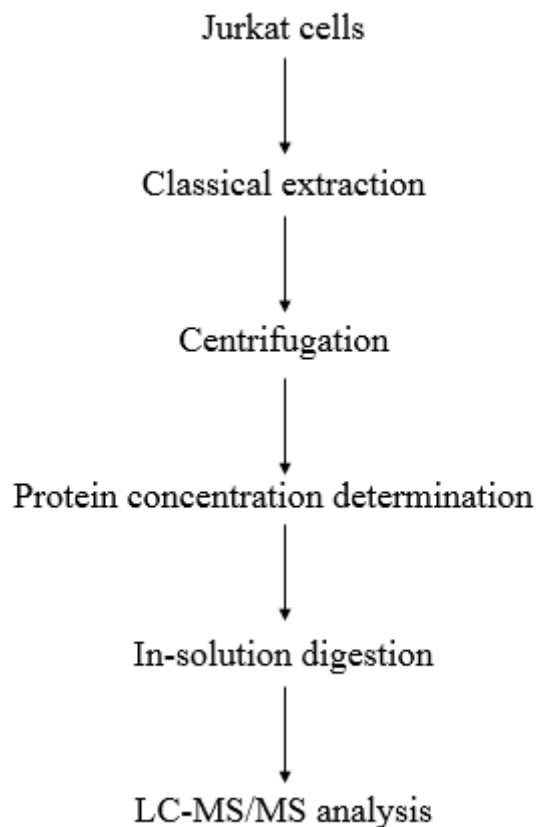
The same manner of calculation was done as in case of rat pancreatic tissues, again sorting the methionine-containing peptides into two categories:

- 1- More methionine oxidation in the sample prepared by the classical homogenization method (figures 52, 53 and 54) and tables (14, 15 and 16).
- 2- More methionine oxidation in the sample prepared by the PIRL-DIVE homogenization method.

### 3. Results

#### 3.1. Detection of oxidized methionine containing peptides after cell treatment with H<sub>2</sub>O<sub>2</sub>

In order to investigate if we can detect increase of the level of oxidation by treating Jurkat cells with oxidant in classical homogenization method, cells were treated with different concentrations of hydrogen peroxide, H<sub>2</sub>O<sub>2</sub>, (0, 50, 100, and 200 μM) as a final concentration. The experimental workflow suggested is presented in scheme 1. After classical homogenization of Jurkat cells, the lysates were sonicated (1 cycle for 15 seconds), incubated for 1h at +4 °C and centrifuged at +4 °C for 30 minutes at 5200 g to remove cellular debris.



Scheme 1. Experimental workflow of classical homogenization for Jurkat cells. Details are in materials and methods section.



Protein concentration of Jurkat cell samples was determined, the samples were in solution digested, then desalted. Finally, oxidized methionine containing peptides (in different treated samples) were identified by liquid chromatography mass spectrometry/mass spectrometry (LC-MS/MS). It is displayed in (tables 3 'A, B' & figures 9 'A, B'), the percentage of oxidized methionine containing peptides to all methionine containing peptides in classical homogenization. A and B refer that the LC-MS/MS analysis was done in the same manner except that in A, reversed phase column (type 1) was used, however in B, reversed phase column (type 2) was used; similar results were obtained. In figures 8A and 8B, it is shown that by increasing the H<sub>2</sub>O<sub>2</sub> concentration, we can detect an increase in the levels of oxidized methionine containing peptides.

Table 3A. Percentage of oxidized methionine containing peptides to all methionine containing peptides in classical homogenization.

uM of H <sub>2</sub> O <sub>2</sub>	% of OX Met containing peptides/all Met containing peptides				
	1	2	3	Mean	SD
0 μM	4.2	4.6	5.5	4.8	0.6
50 μM	4.5	5.7	6.5	5.6	1.0
100 μM	9.2	9.6	6.3	8.4	1.8
200 μM	12.0	13.2	6.2	10.5	3.7

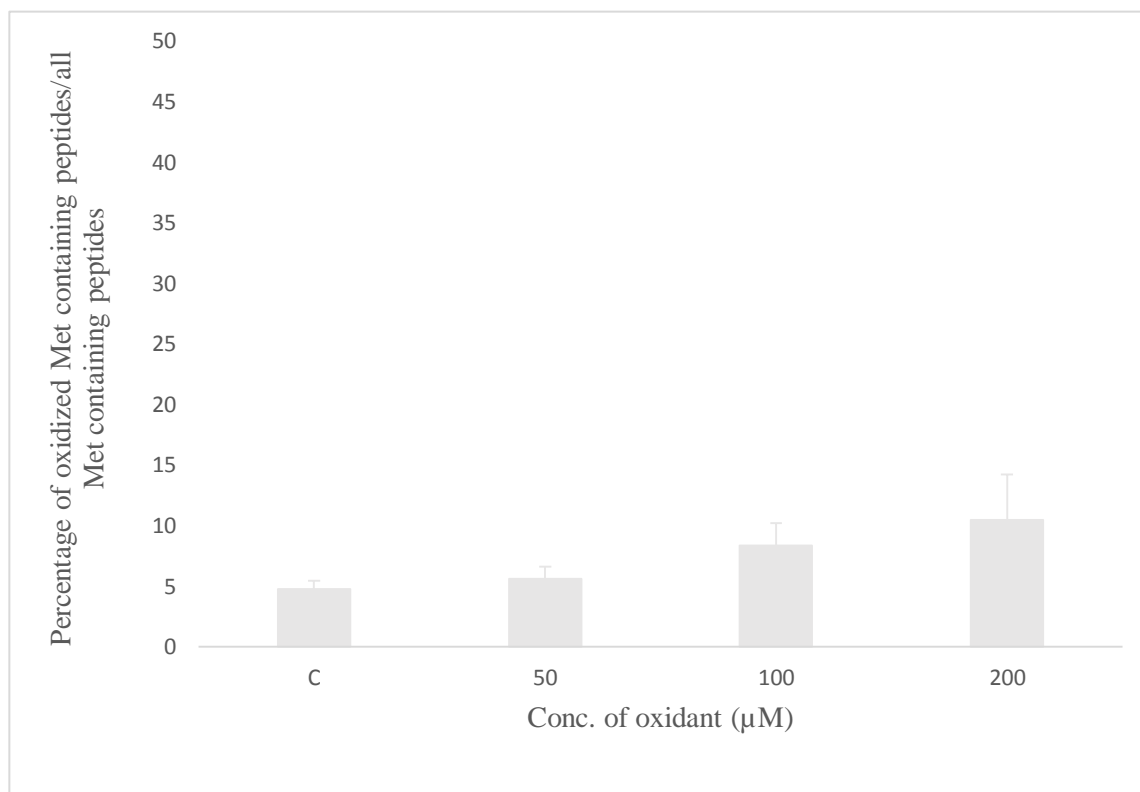


Figure 9A. Percentage of oxidized methionine containing peptides to all methionine containing peptides in classical homogenization method. reversed phase column (type 1) was used.

Table 3B. Percentage of oxidized methionine containing peptides to all methionine containing peptides in classical homogenization.

uM of H <sub>2</sub> O <sub>2</sub>	% of OX Met containing peptides/all Met containing peptides				
	1	2	3	Mean	SD
0 $\mu$ M	9.2	12.6	14	11.9	2.4
50 $\mu$ M	8.7	14.7	17.9	13.7	4.6
100 $\mu$ M	17.6	18.4	20.9	18.9	1.7
200 $\mu$ M	14.4	17.6	25.5	19.1	5.7

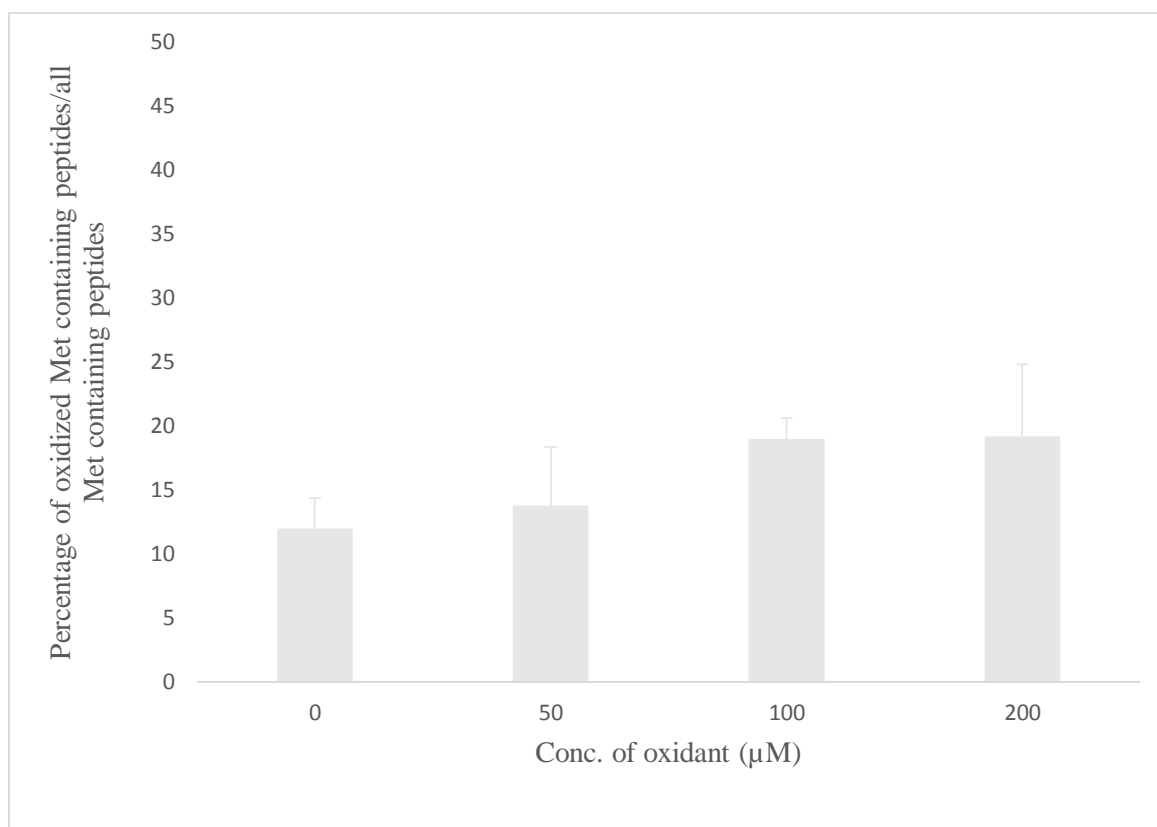


Figure 9B. Percentage of oxidized methionine containing peptides to all methionine containing peptides in classical homogenization method. reversed phase column (type 2) was used.

### 3.2. Comparison between classical and PIRL homogenization method

The cell culture experiment was performed under the same conditions as in classical approach except PIRL-DIVE technology (see scheme 1) was used instead as an homogenization method. PIRL-DIVE was used to see if there is a change compared to classical homogenization procedure. After LC/MS/MS analysis, for given peptides, the comparison of oxidized and reduced methionine form (including the following parameters; area under the curve ``AUC``, full MS scan, fragment spectra) was performed to see their behavior under using two different homogenization techniques (PIRL versus classical). The selected peptides are presented in table 4.

Table 4. Selected peptides for the comparison between PIRL and classical homogenization.

<b>Method</b>	<b>Peptide sequence</b>
Classical	GGIMLPEK (1)
Classical	VMLGETNPADSKPGTIR (2)
PIRL	MVVESAYEVIK (3)
PIRL	AILVDLEPGTMDSVR (4)
Classical and PIRL	EITALAPSTMK (5)

### **3.3. Cell homogenization via classical homogenization method**

The peptides 1 and 2 representing the sequences GGIMLPEK, and VMLGETNPADSKPGTIR, respectively, were observed in the classical homogenization method are used to study the extent of oxidation occurred. The parameters such as full MS scan, fragment spectra (MS/MS), and the area under curve (AUC) from the extracted ion chromatogram (EIC) are provided for both the oxidized and reduced forms of these peptides presented in the results. For these given peptides, it is shown that the AUC of reduced form was found to be higher than oxidized form.

#### **3.3.1. Peptide 1 (GGIMLPEK)**

The peptide **1**, which was selected from methionine containing peptides, resulting from the tryptic digestion of proteins in Jurkat cells. After LC-MS/MS analysis, the (TIC, figure 10), the (BPC, figure 11), full MS scan of reduced (figure 12 ) and of oxidized (figure 13 ) form are presented below. The fragment ion spectra of peptide **1** is shown in figure 14 as well as AUC is shown in figure 15. The peptide 1 was found in both oxidized and reduced form has the parameters of the (RT, m/z and MW) which are represented in table 5.

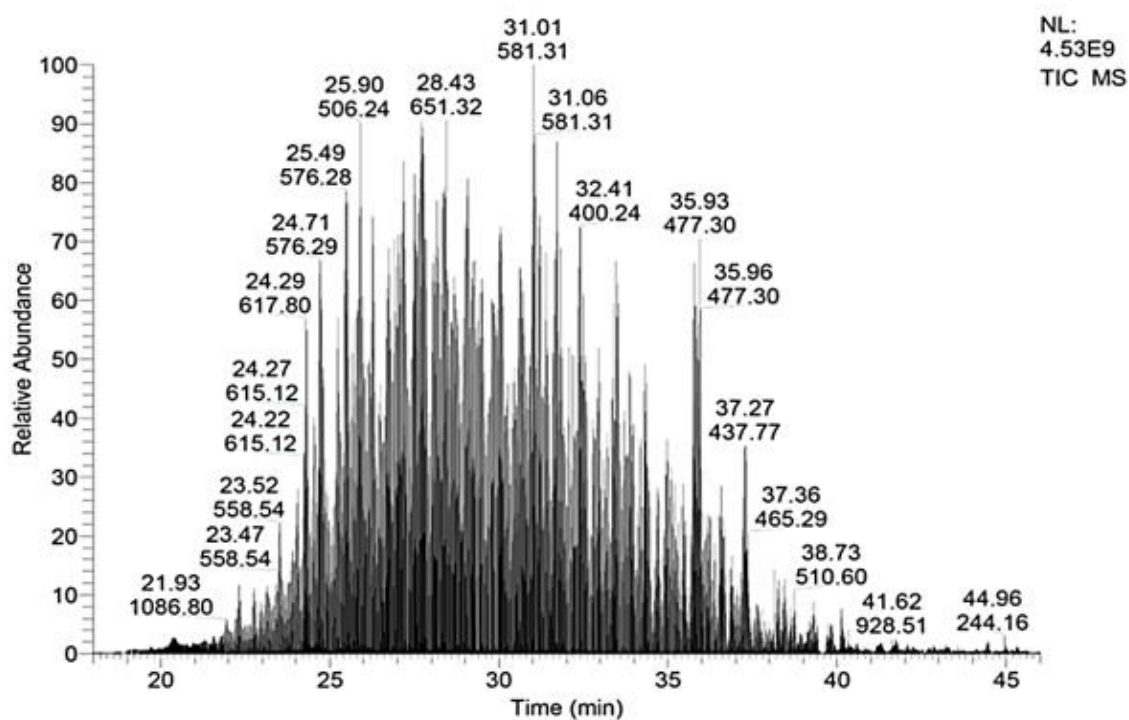


Figure 10. A part of total ion current (TIC) of Jurkat cell sample in case of classical homogenization, at RT (18.00-46.00 min).

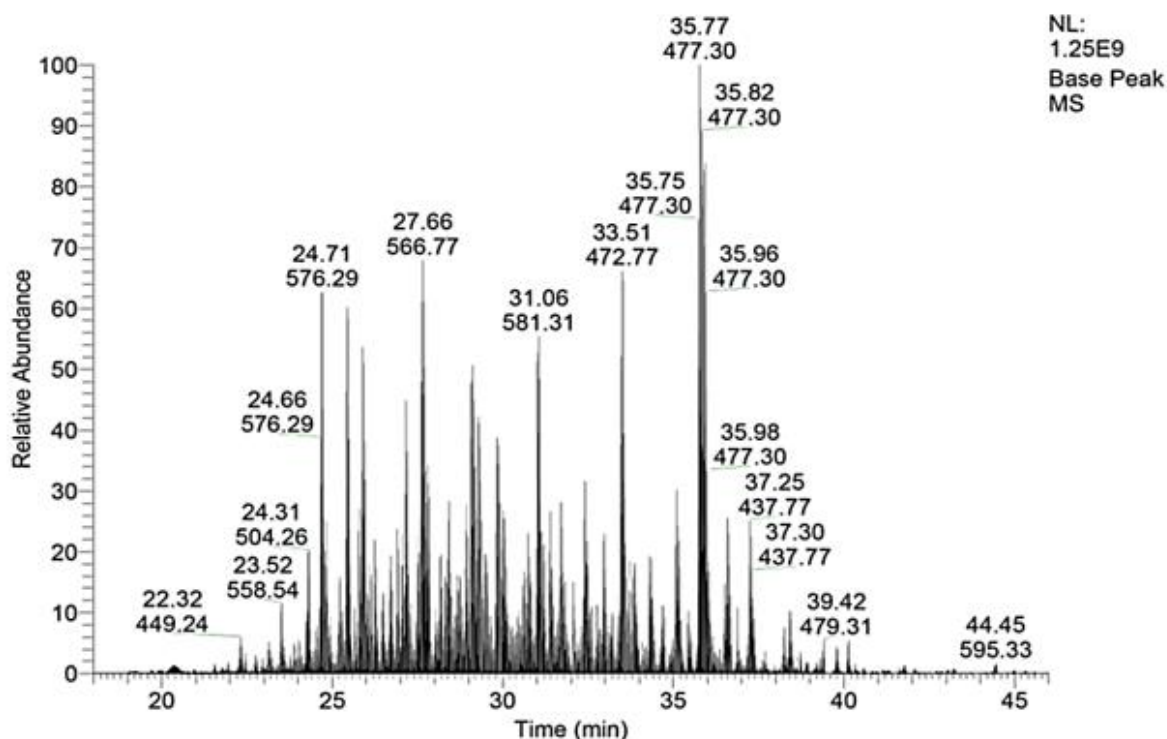


Figure 11. A part of base peak chromatogram (BPC) of Jurkat cell sample in case of classical homogenization, at RT (18.00-46.00 min).

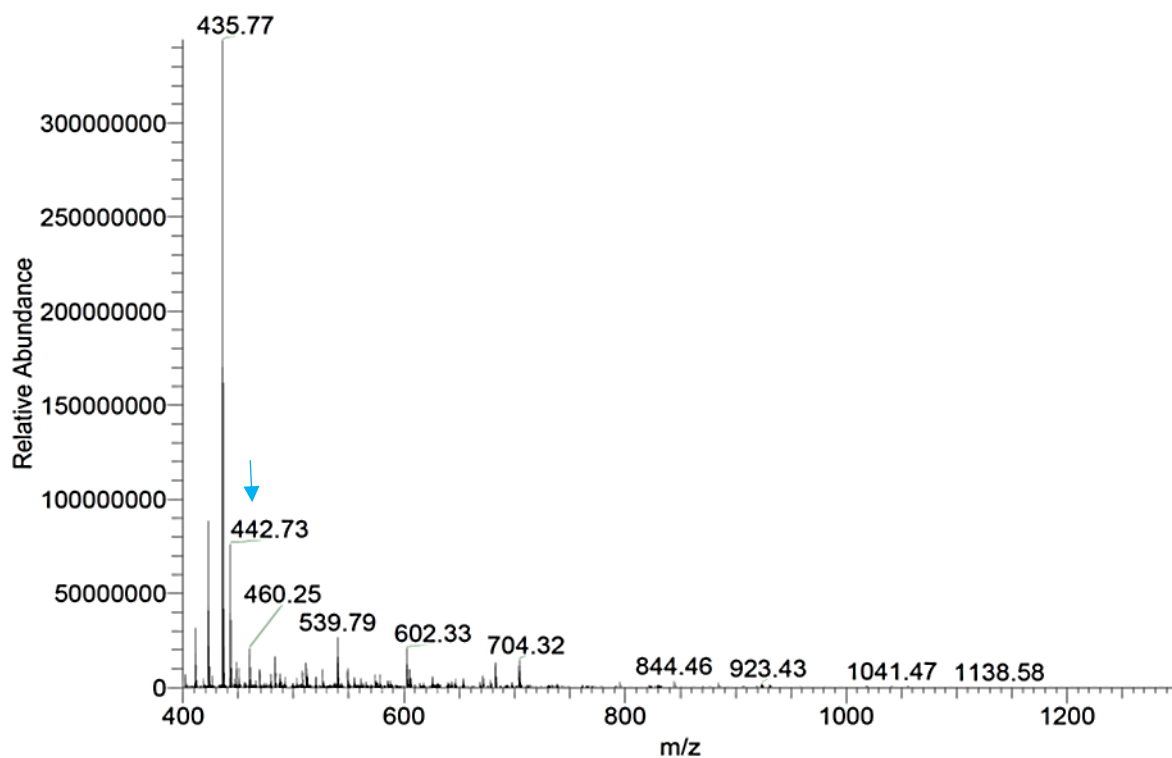


Figure 12. Full MS scan of the reduced form of GGIMLPEK, at RT 29.92 min.

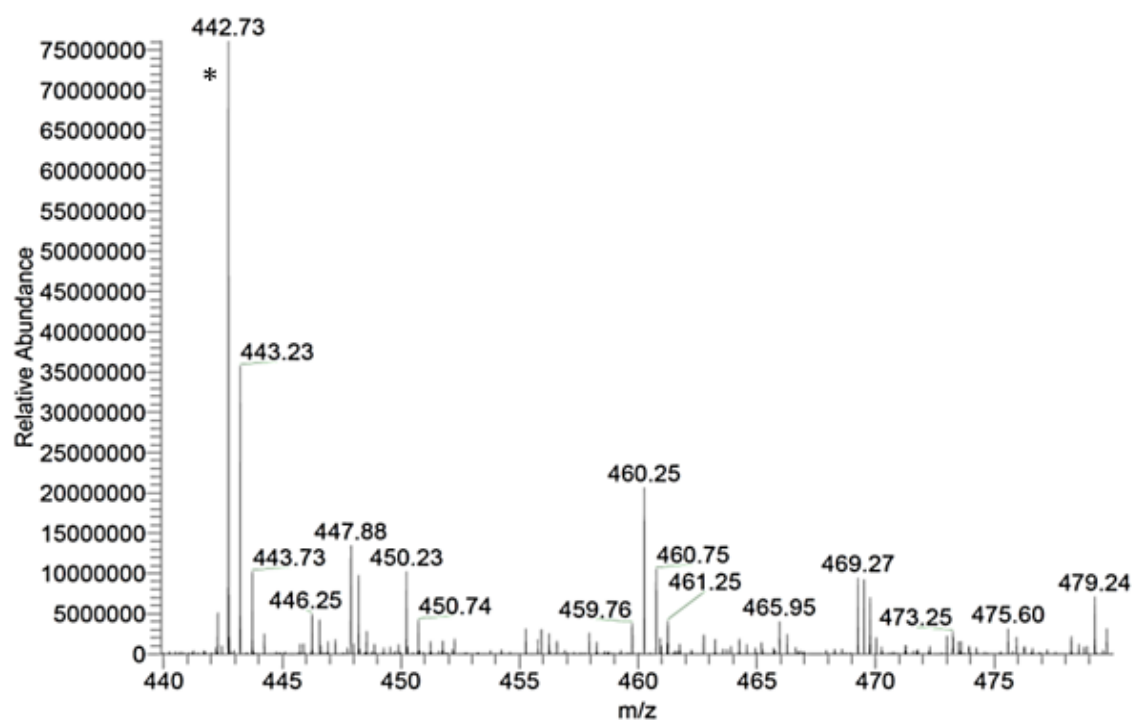


Figure 12A. Section of full MS scan of the reduced form of GGIMLPEK, at RT 29.92 min. \* representing the monoisotopic peak for the signal with (m/z, 442.73).

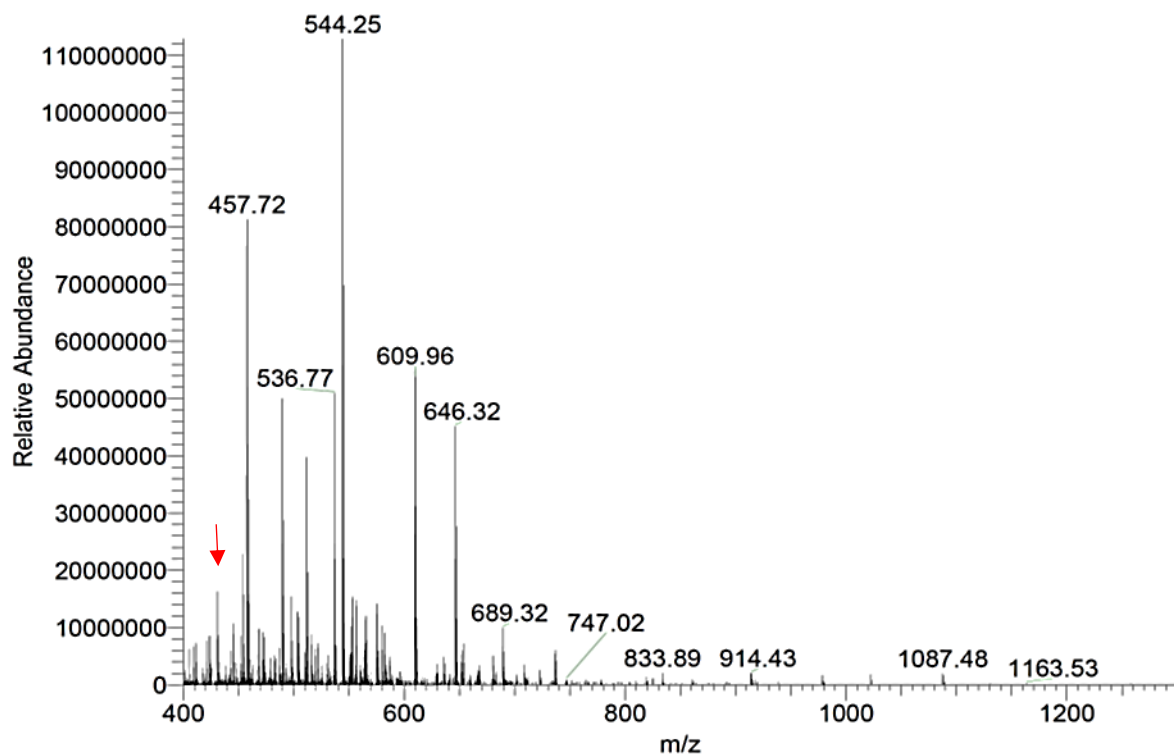


Figure 13. Full MS scan of the oxidized form of GGIM<sub>ox</sub>LPEK, at RT 28.61 min.

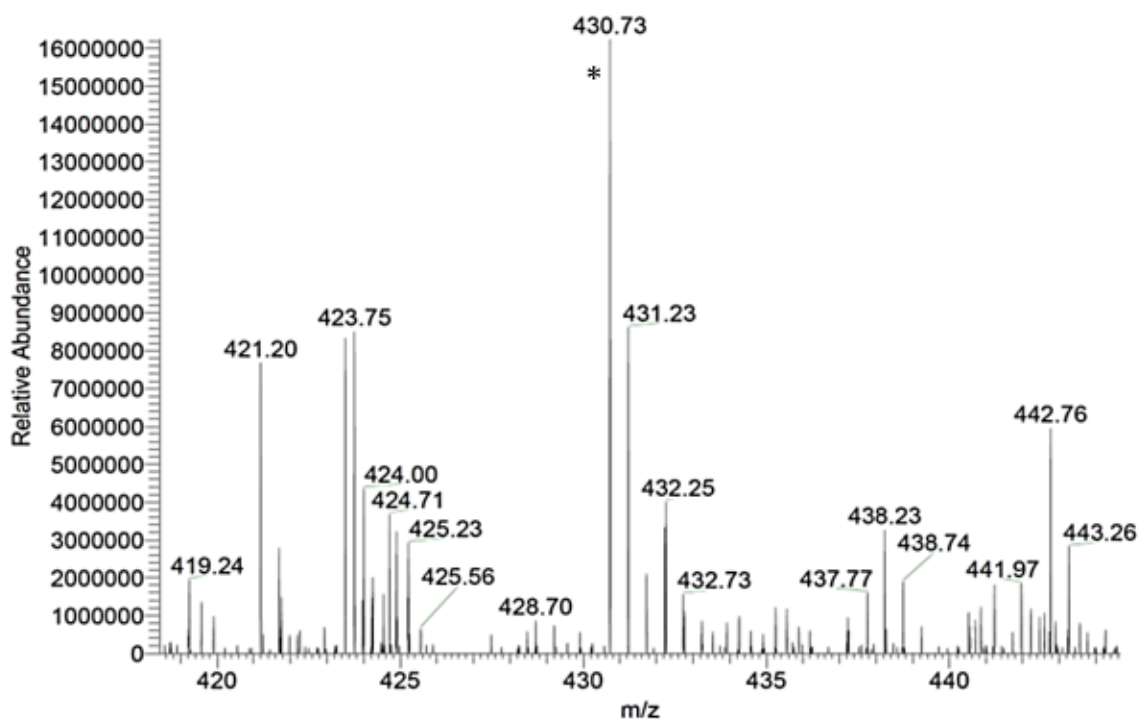


Figure 13A. Section of full MS scan of the oxidized form of GGIM<sub>ox</sub>LPEK, at RT 28.62 min. \* representing the monoisotopic peak for the signal with (m/z, 430.73).

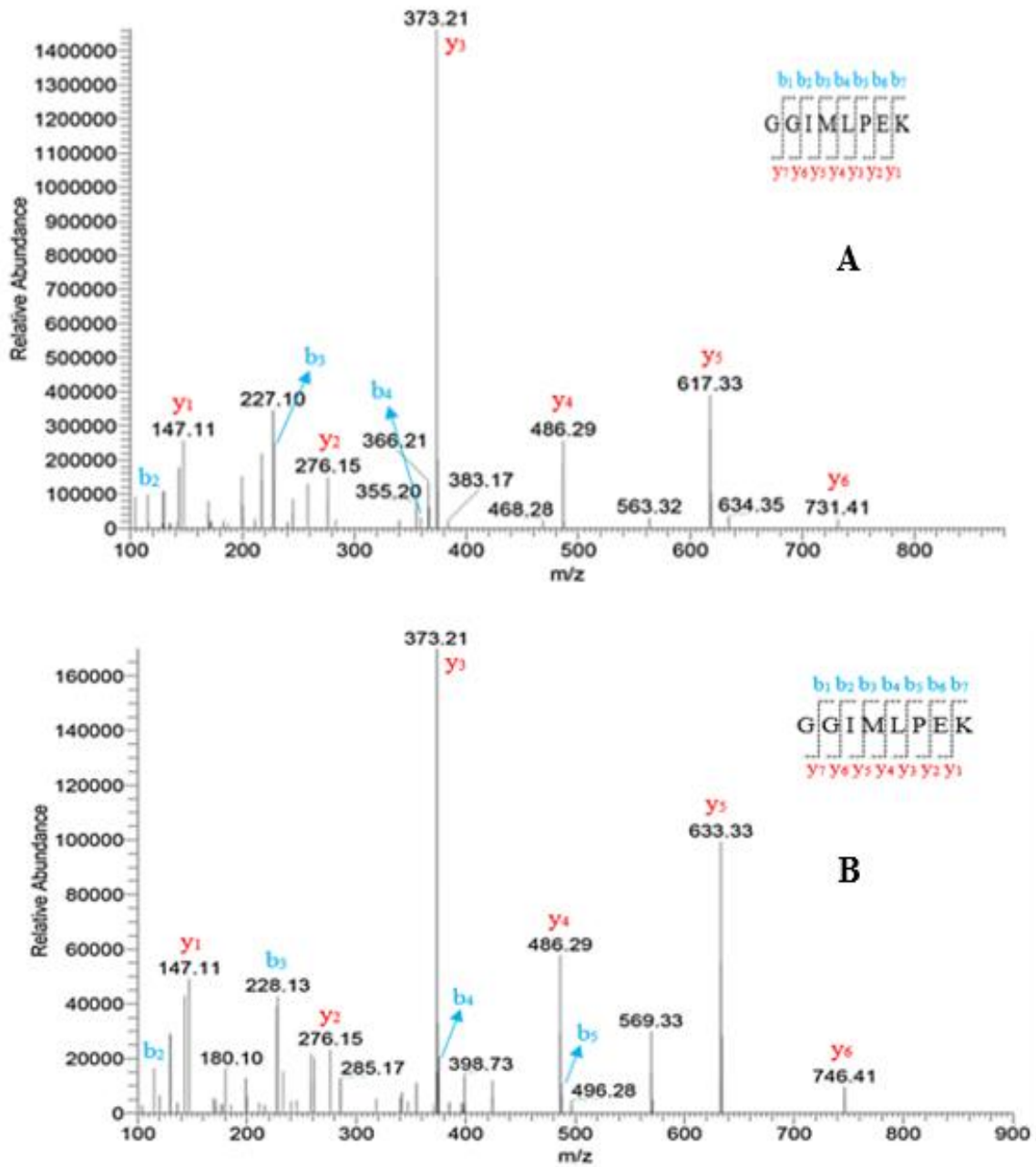


Figure 14. MS/MS spectra of the reduced GGIMLPEK (A) and the oxidized GGIM<sub>ox</sub>LPEK (B) representing the y- and b-ions of both methionine forms



Table 5. Reduced and oxidized form of peptide, GGIMLPEK, including their retention time (RT), mass/charge (m/z) and molecular weight (MW).

Peptide sequence	Retention time (RT, min)	Mass/charge (m/z)	M.W
GGIM <sub>ox</sub> LPEK	28.62	430.73 [M+2H] <sup>2+</sup>	860.45
GGIMLPEK	29.92	422.73	844.45

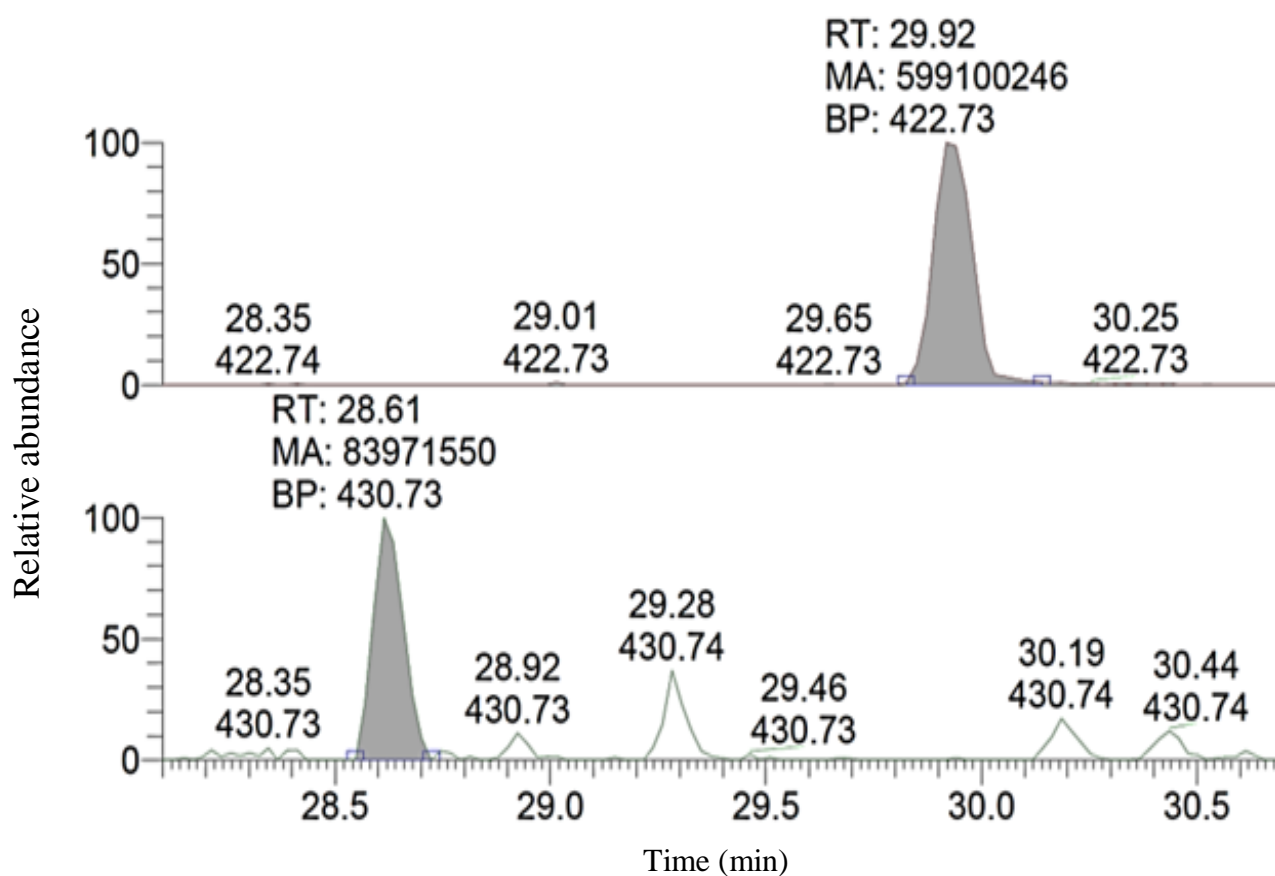


Figure 15. Extracted ion chromatogram (EIC) for the reduced GGIMLPEK and oxidized GGIM<sub>ox</sub>LPEK form.

### 3.3.2. Peptide 2 (VMLGETNPADSKPGTIR)

The peptide **2**, which was selected from methionine containing peptides, resulting from the tryptic digestion of proteins in Jurkat cells. After LC-MS/MS analysis, the (TIC, figure 16), the (BPC, figure 17), full MS scan of reduced (figure 18 ) and of oxidized (figure 19 ) form are presented below. The fragment ion spectra of peptide **2** is shown in figure 20 as well as AUC is shown in figure 21. The peptide **2** was found in both oxidized and reduced form has the parameters of the (RT, m/z and MW) which are represented in table 6.

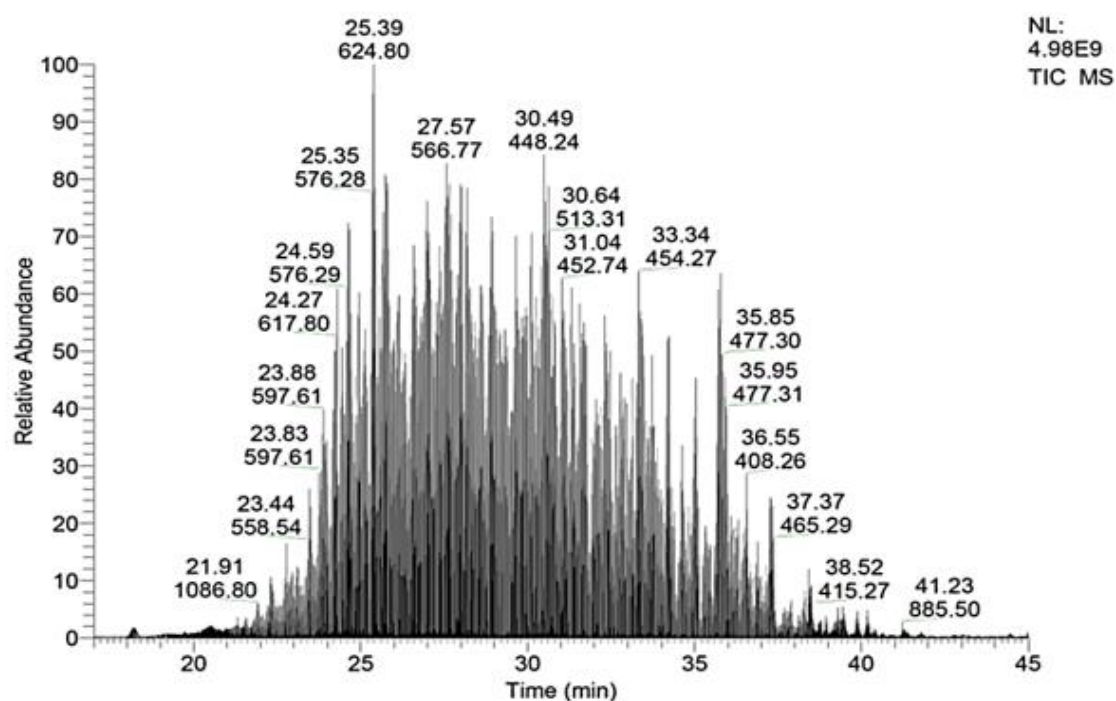


Figure 16. A part of total ion current (TIC) of Jurkat cell sample in case of classical homogenization, at RT (17.00-45.00 min).

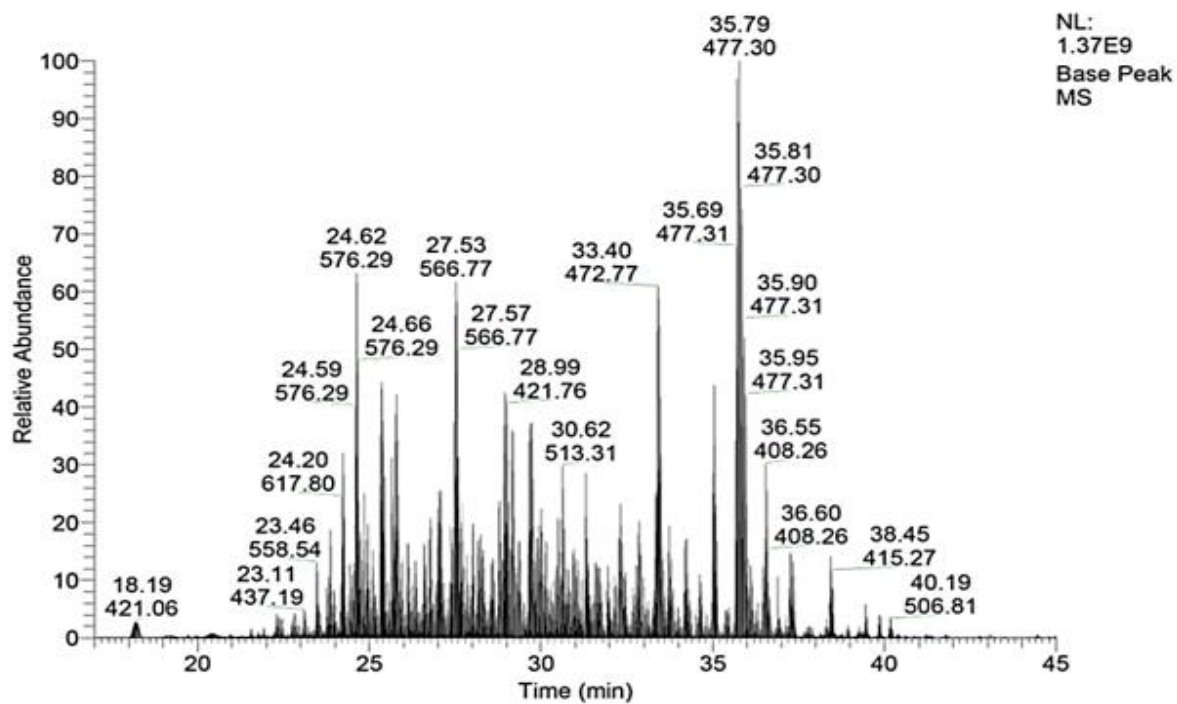


Figure 17. A part of base peak chromatogram (BPC) of Jurkat cell sample in case of classical homogenization, at RT (17.00-45.00).

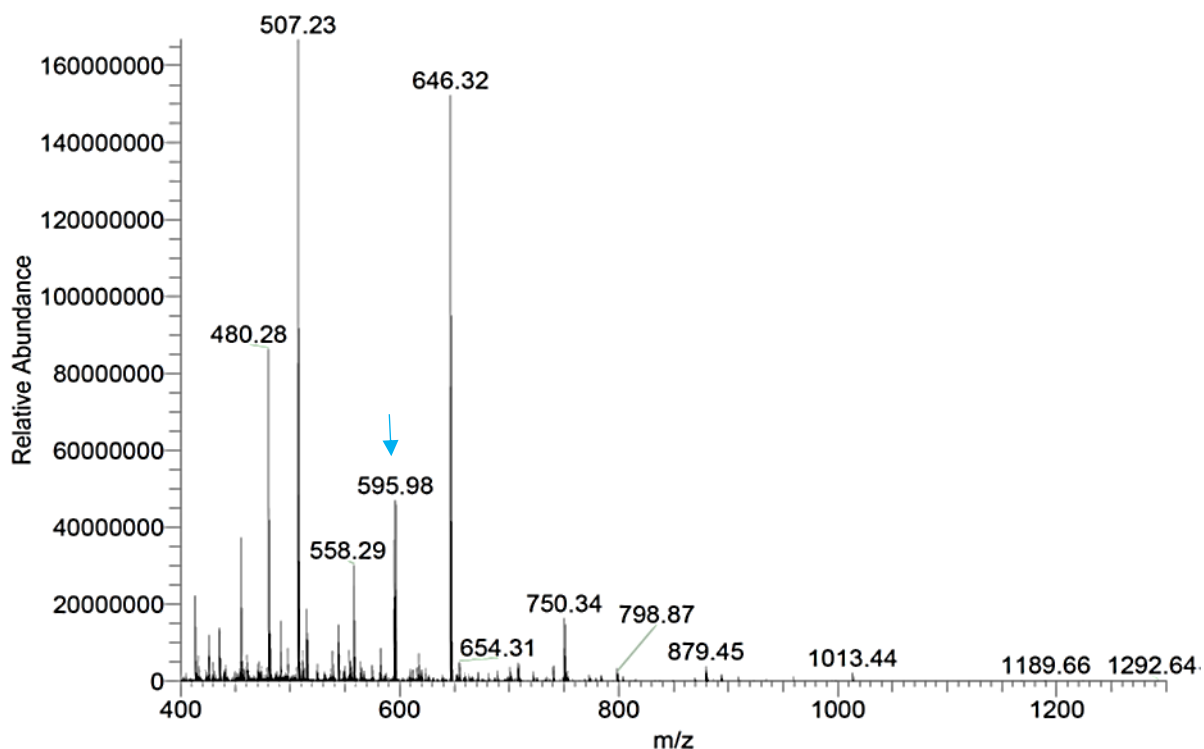


Figure 18. Full MS scan of the reduced form of VMLGETNPADSKPGTIR, at RT 28.57 min.

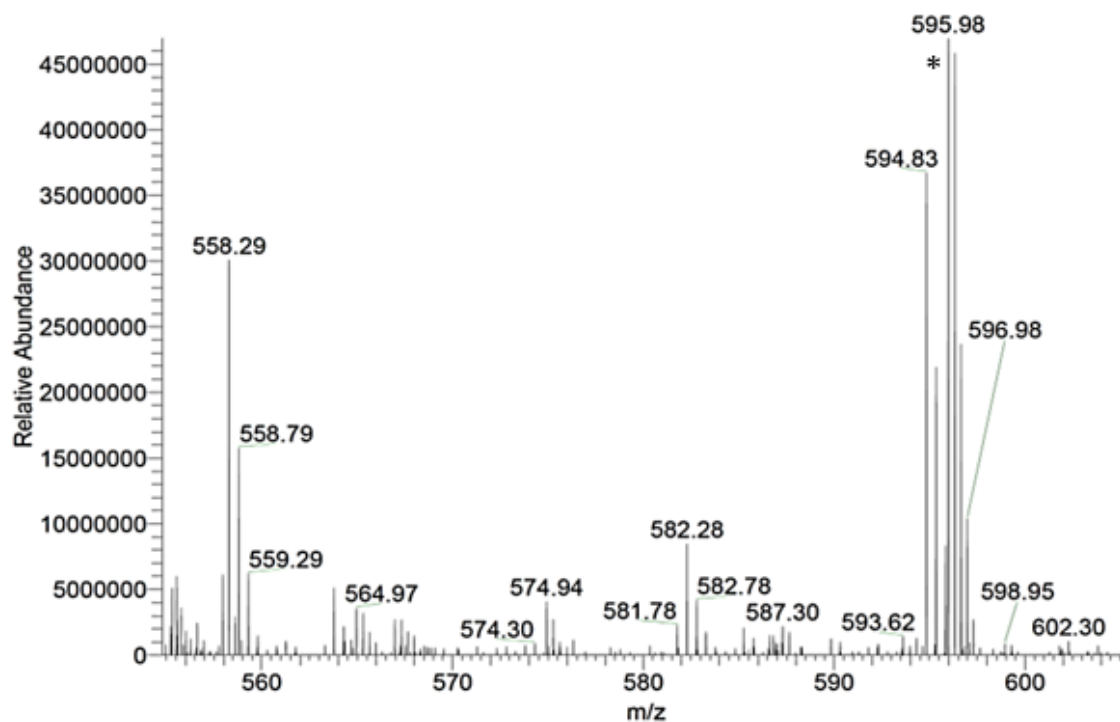


Figure 18A. Section of full MS scan of the reduced form of VMLGETNPADSKPGTIR, at RT 28.57 min. \* representing the monoisotopic peak for the signal with (m/z, 595.98).

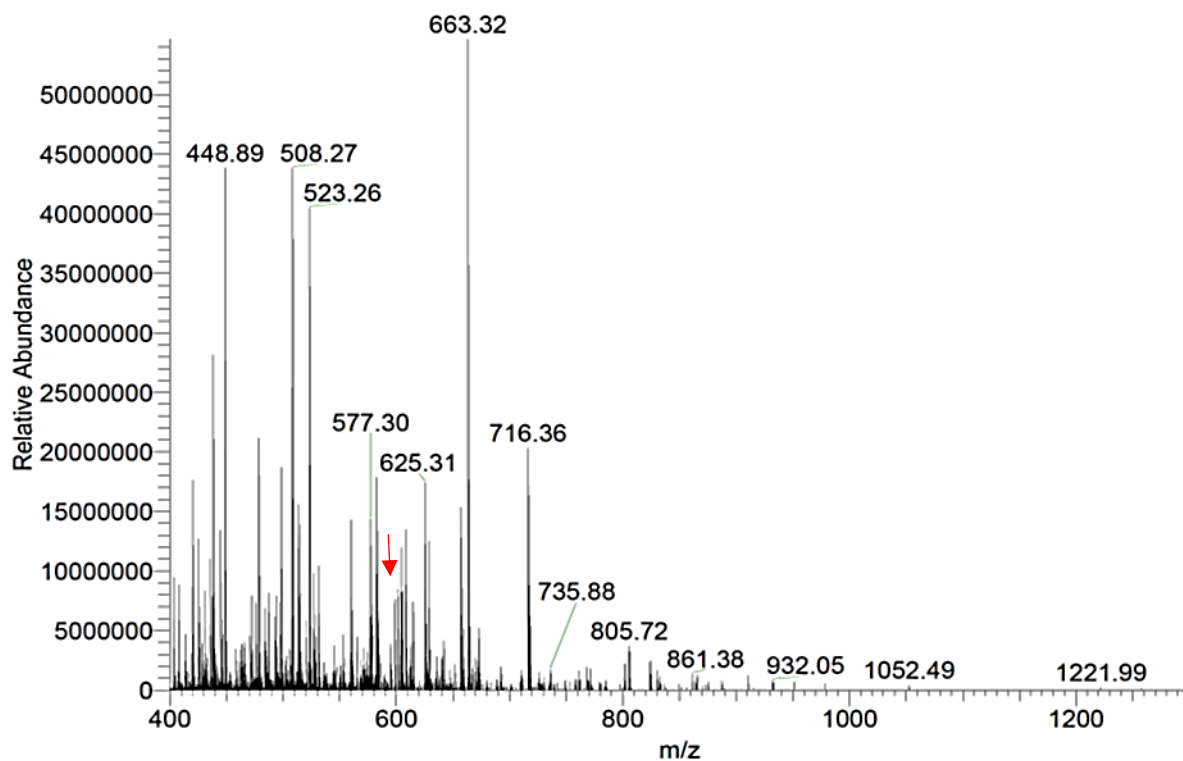


Figure 19. Full MS scan of the oxidized form of  $VM_{ox}$ LGETNPADSKPGTIR, at RT 27.24 min.

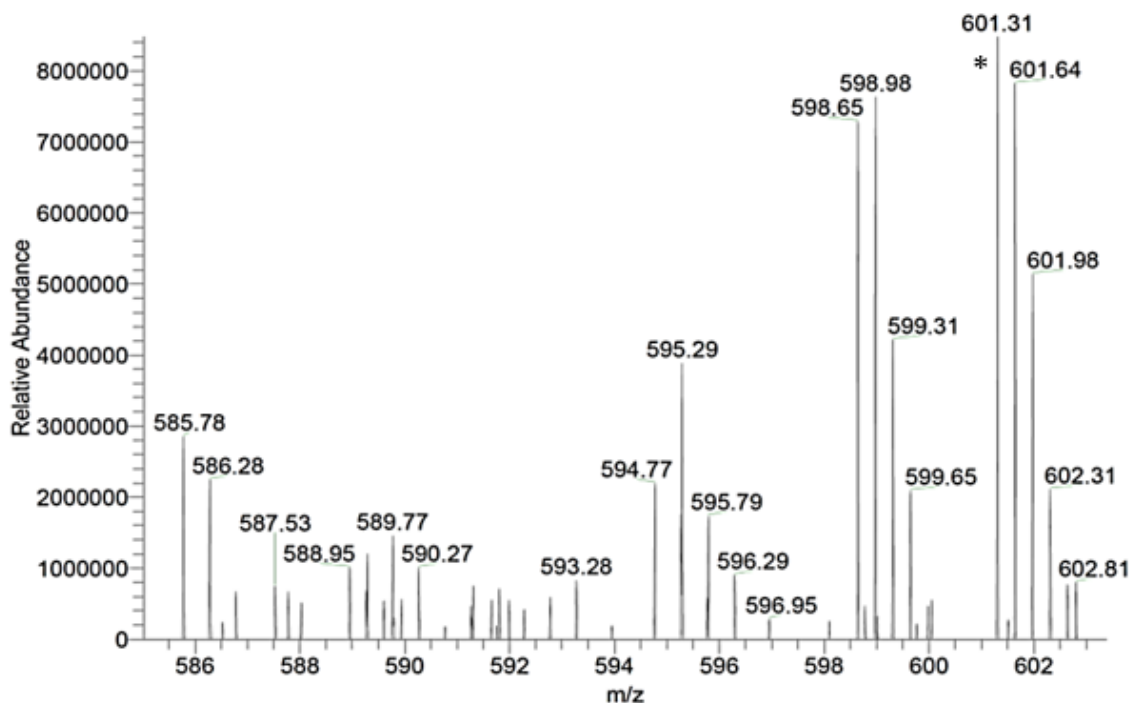


Figure 19A. Section of full MS scan of the oxidized form of  $VM_{ox}$ LGETNPADSKPGTIR, at RT 27.24 min. \* representing the monoisotopic peak for the signal with (m/z, 601.31).

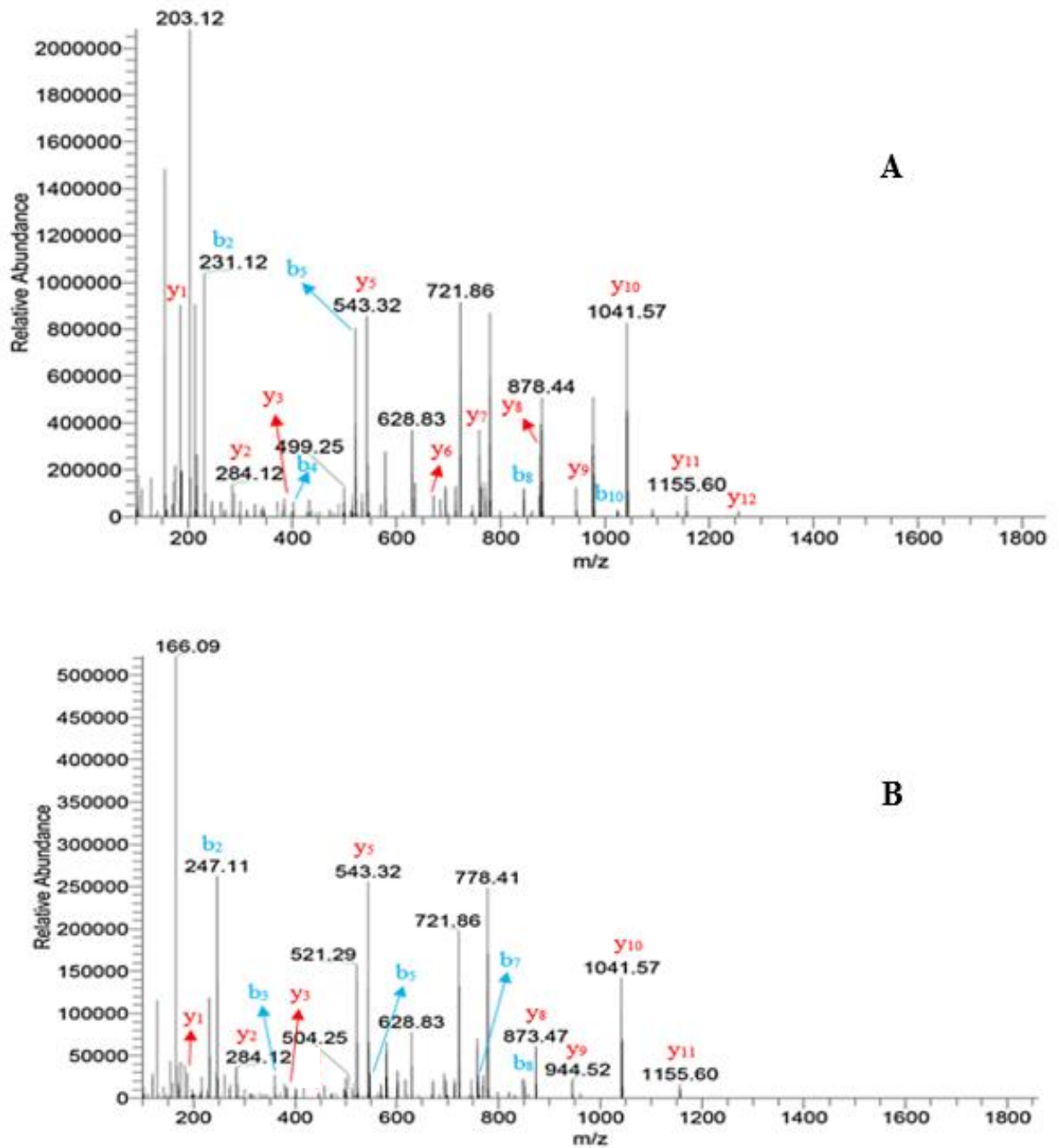


Figure 20. MS/MS spectra of the reduced VMLGETNPADSKPGTIR (A) and the oxidized VM<sub>ox</sub>LGETNPADSKPGTIR (B) representing the y- and b-ions of both methionine forms

Table 6. Reduced and oxidized form of peptide, VMLGETNPADSKPGTIR, including their retention time (RT), mass/charge (m/z) and molecular weight (MW).

Peptide sequence	Retention time (RT, min)	Mass/charge (m/z)	M.W
VM <sub>ox</sub> LGETNPADSKPGTIR	27.25	601.31 [M+3H] <sup>3+</sup>	1801.91
VMLGETNPADSKPGTIR	28.57	595.98	1785.91

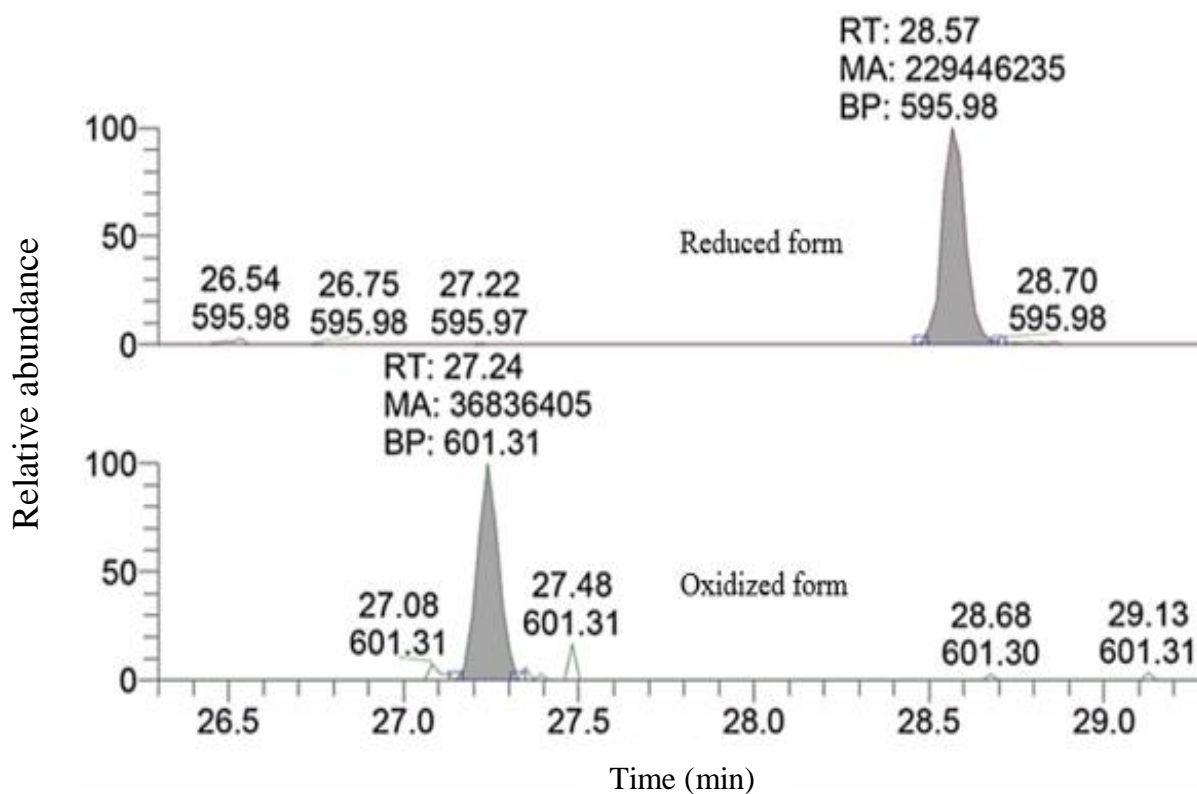


Figure 21. Extracted ion chromatogram (EIC) of the reduced VMLGETNPADSKPGTIR and the oxidized VM<sub>ox</sub>LGETNPADSKPGTIR representing the y- and b-ions of both methionine forms.

### **3.4. Jurkat cells homogenization via PIRL homogenization method**

The peptides **3** and **4** representing the sequences MVVESAYEVIK, AILVDLEPGTMDSVR, and LAVNMVPFPR, respectively, were observed in the PIRL-DIVE homogenization method are used to study the extent of oxidation occurred. As described in section 3.3, the parameters such as full MS scan, fragment spectra (MS/MS), and the area under curve (AUC) from the extracted ion chromatogram (EIC) are provided for both the oxidized and reduced forms of these peptides presented in the results. For these given peptides, it is shown that the AUC of oxidized form was found to be higher than reduced form.

#### **3.4.1. Peptide 3 (MVVESAYEVIK)**

The peptide **3**, which was selected from methionine containing peptides, resulting from the tryptic digestion of proteins in Jurkat cells. After LC-MS/MS analysis, the (TIC, figure 22), the (BPC, figure 23), full MS scan of reduced (figure 24 ) and of oxidized (figure 25 ) form are presented below. The fragment ion spectra of peptide **3** is shown in figure 26 as well as AUC is shown in figure 27. The peptide **3** was found in both oxidized and reduced form has the parameters of the (RT, m/z and MW) which are represented in table 7.



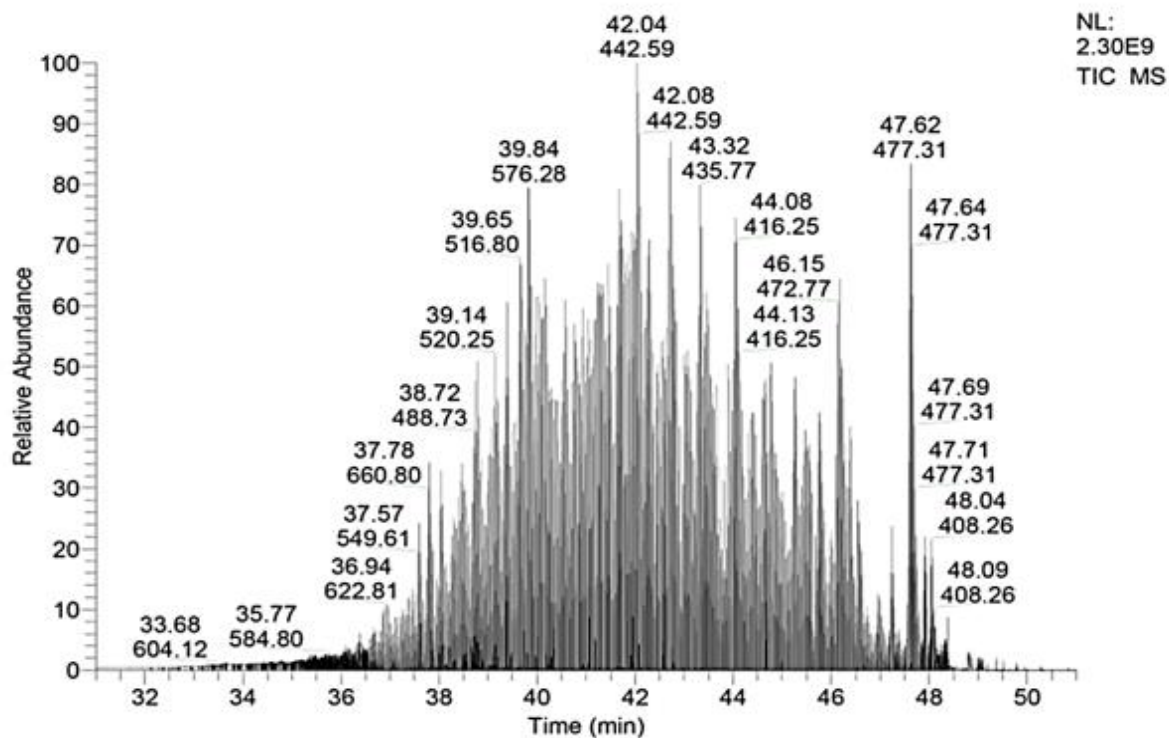


Figure 22. A part of total ion current (TIC) of Jurkat cell sample in case of PIRL homogenization, at RT (31.00-51.00 min).

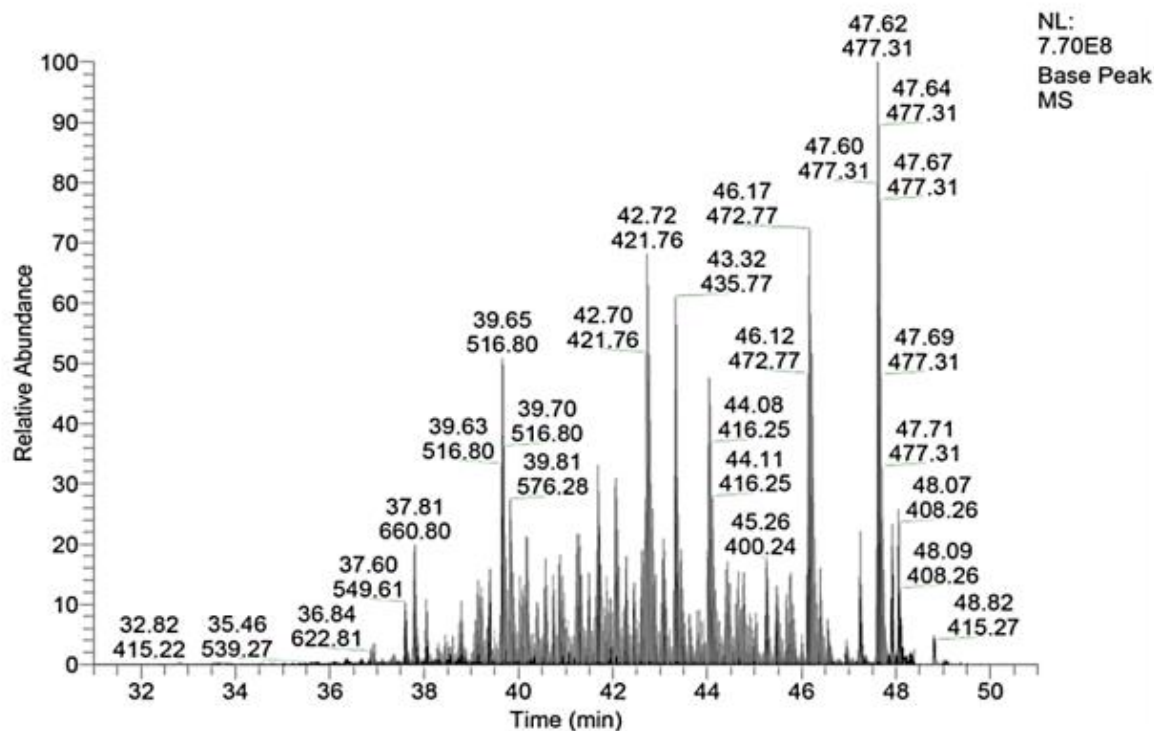


Figure 23. A part of base peak chromatogram (BPC) of Jurkat cell sample in case of PIRL homogenization, at RT (31.00-51.00 min).

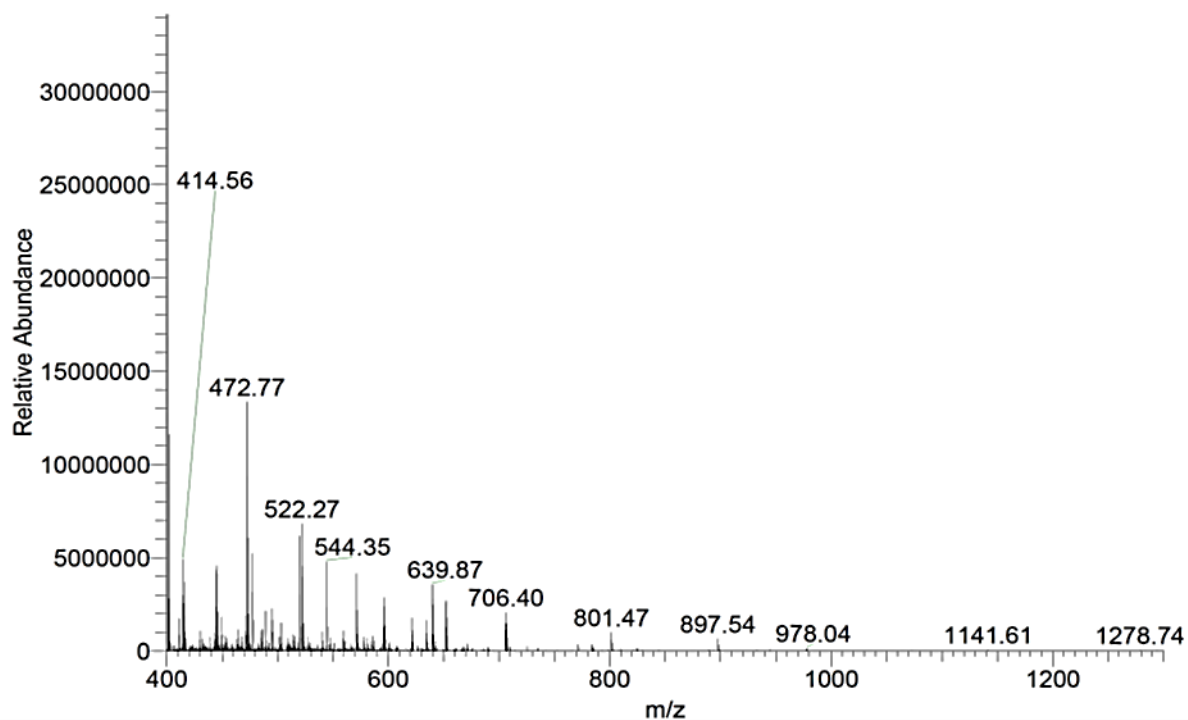


Figure 24. Full MS scan of the reduced form of MVVESAYEVIK, at RT 46.50 min.

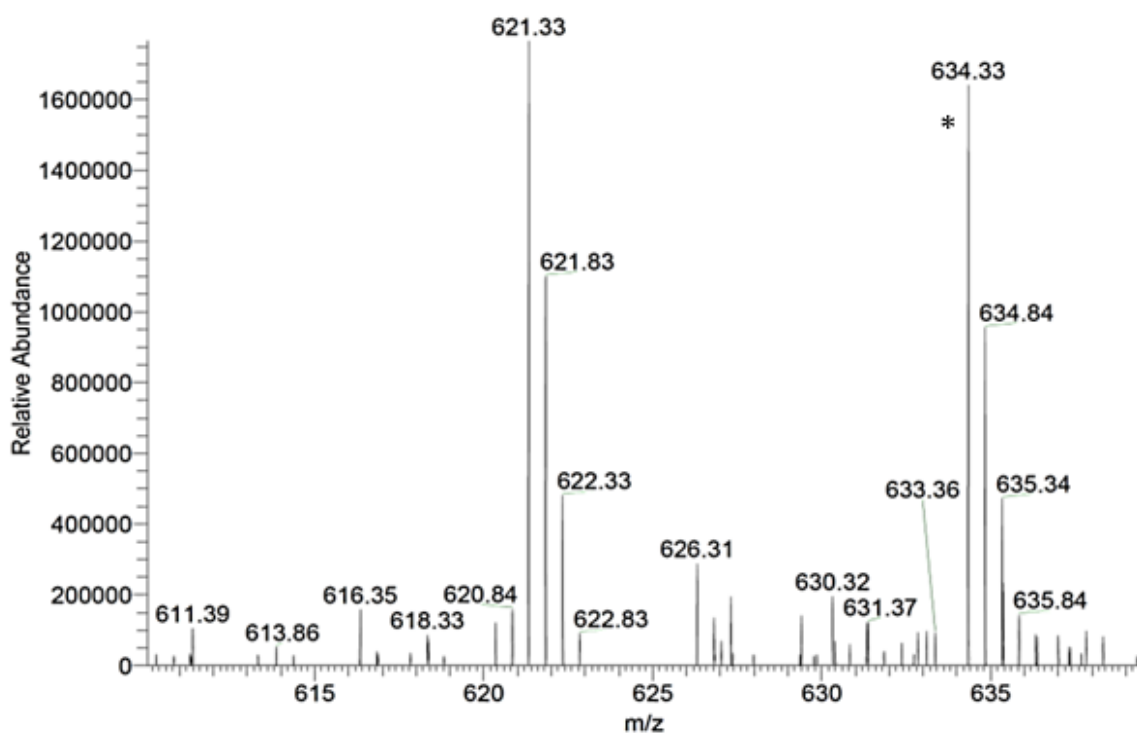


Figure 24A. Section of full MS scan of the reduced form of MVVESAYVIK, at RT 46.50 min. \* representing the monoisotopic peak for the signal with (m/z, 634.33).

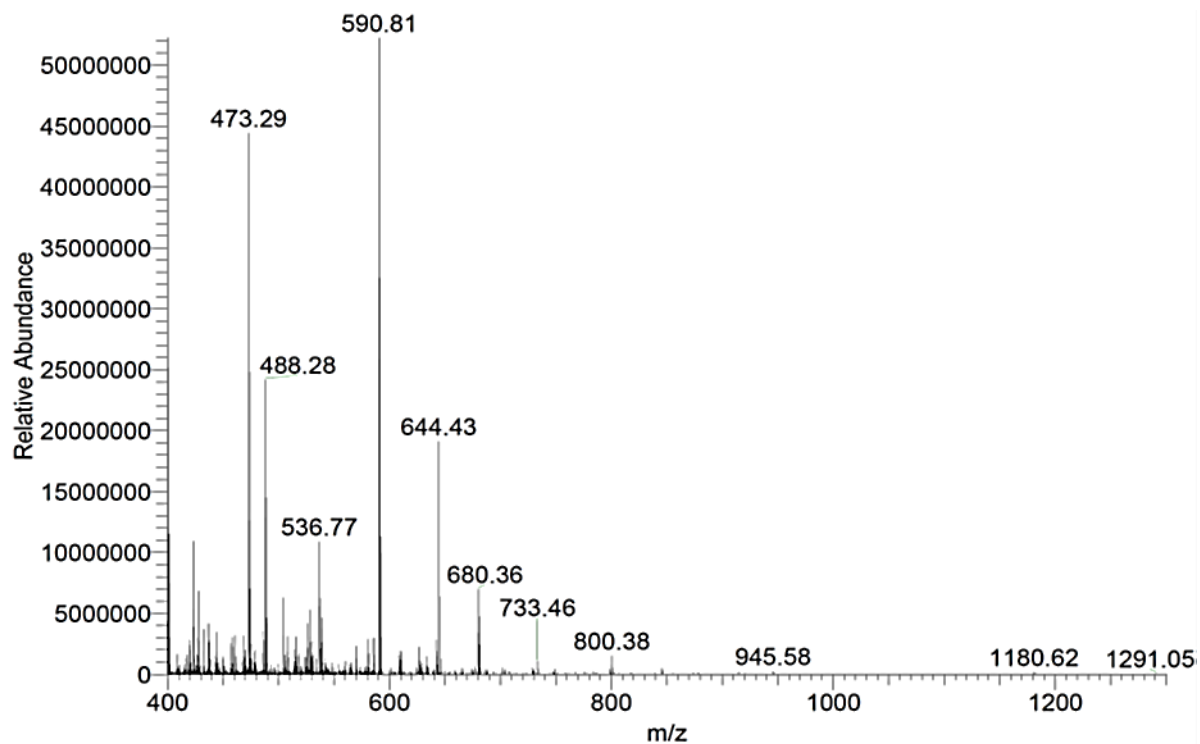


Figure 25. Full MS scan of the oxidized form of  $M_{ox}$  VVESAYEVIK, at RT 44.84 min.

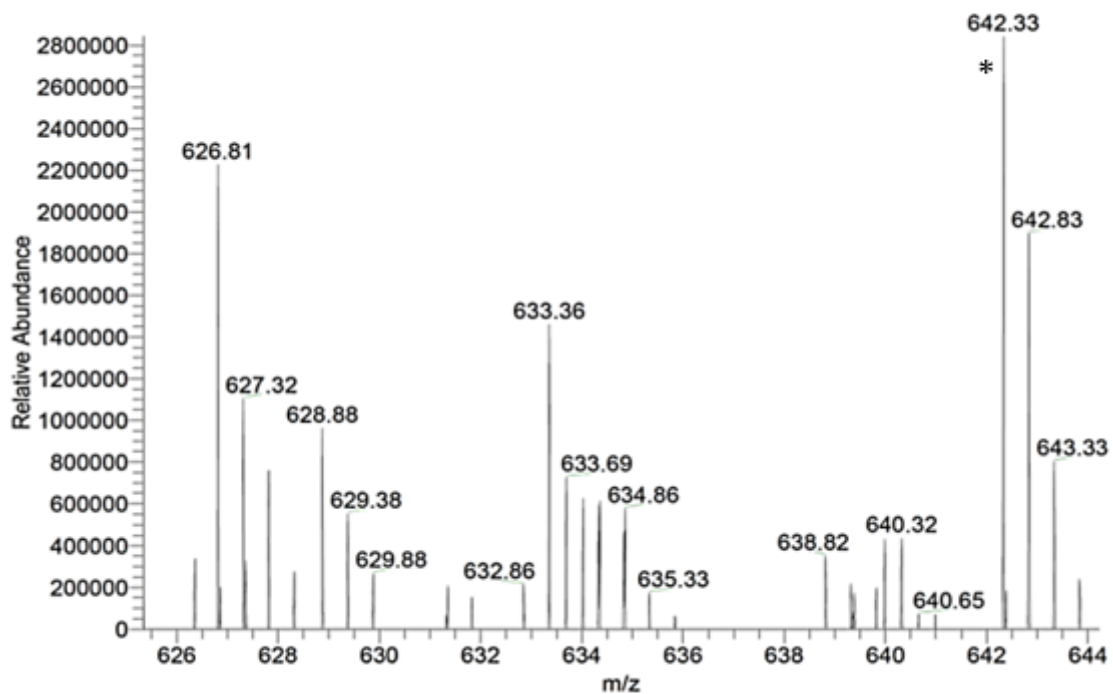


Figure 25A. Section of full MS scan of the oxidized form of  $M_{ox}$  VVESAYEVIK, at RT 44.84 min. \* representing the monoisotopic peak for the signal with (m/z, 642.33).

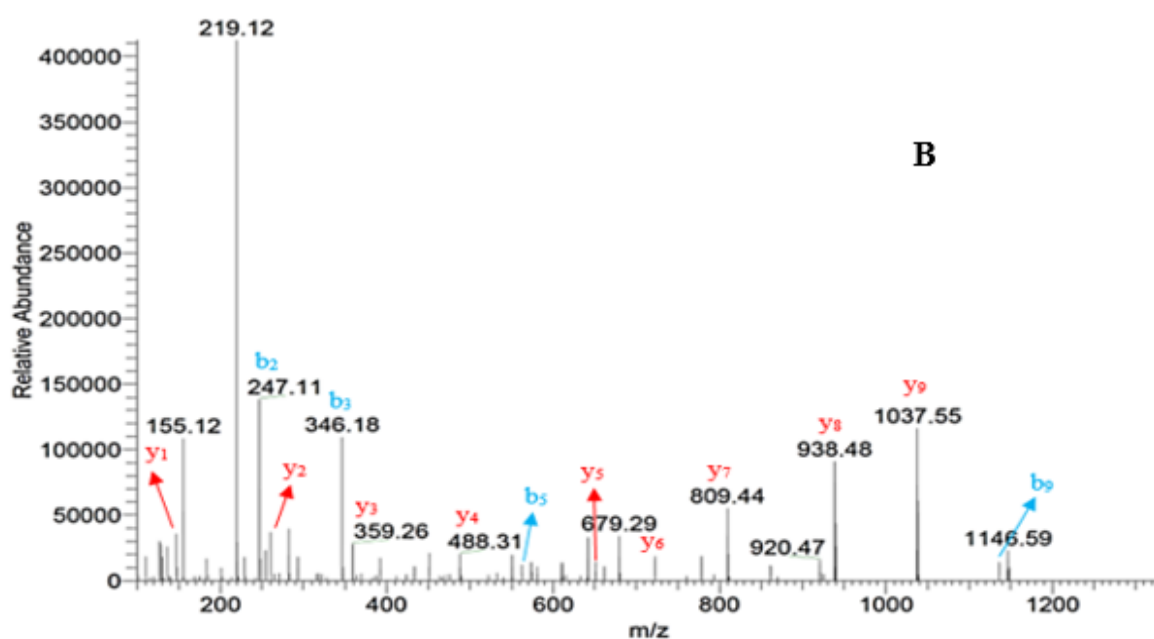
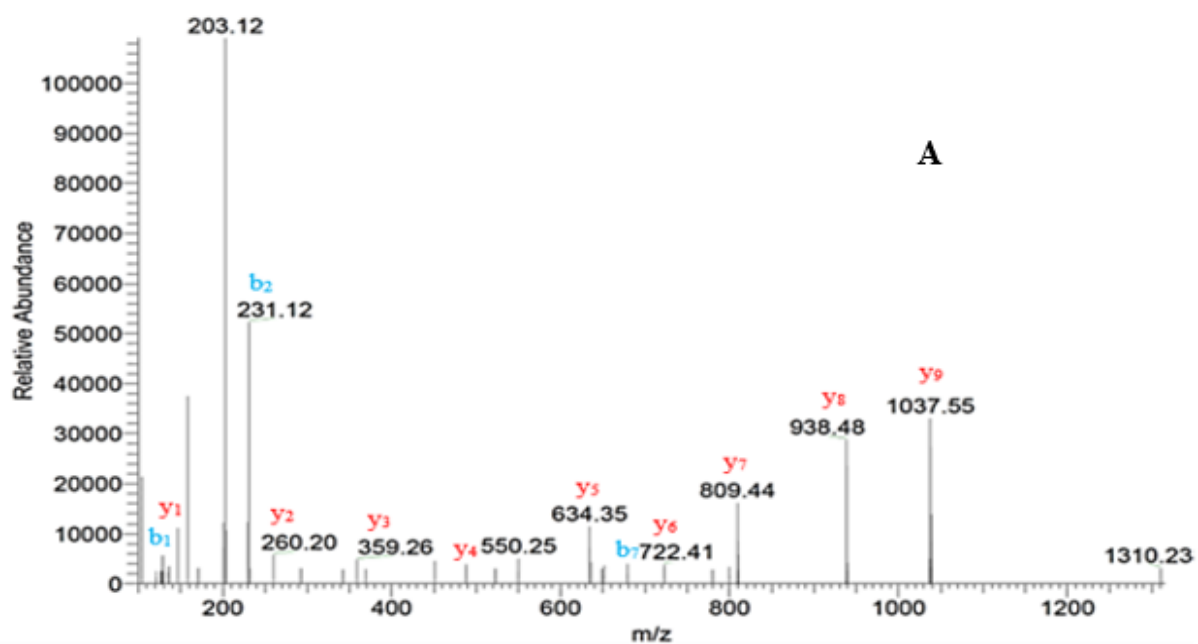


Figure 26. MS/MS spectra of the reduced MVVESAYEVIK (A) and the oxidized M<sub>ox</sub>VVESAYEVIK (B) representing the y- and b-ions of both methionine forms.

Table 7. Reduced and oxidized form of peptide, MVVESAYEVIK, including their retention time (RT), mass/charge (m/z) and molecular weight (MW).

Peptide sequence	Retention time (RT, min)	Mass/charge (m/z)	M.W
<b>M<sub>ox</sub></b> VVESAYEVIK	44.85	642.33 [M+2H] <sup>2+</sup>	1283.65
MVVESAYEVIK	46.50	634.33	1267.65

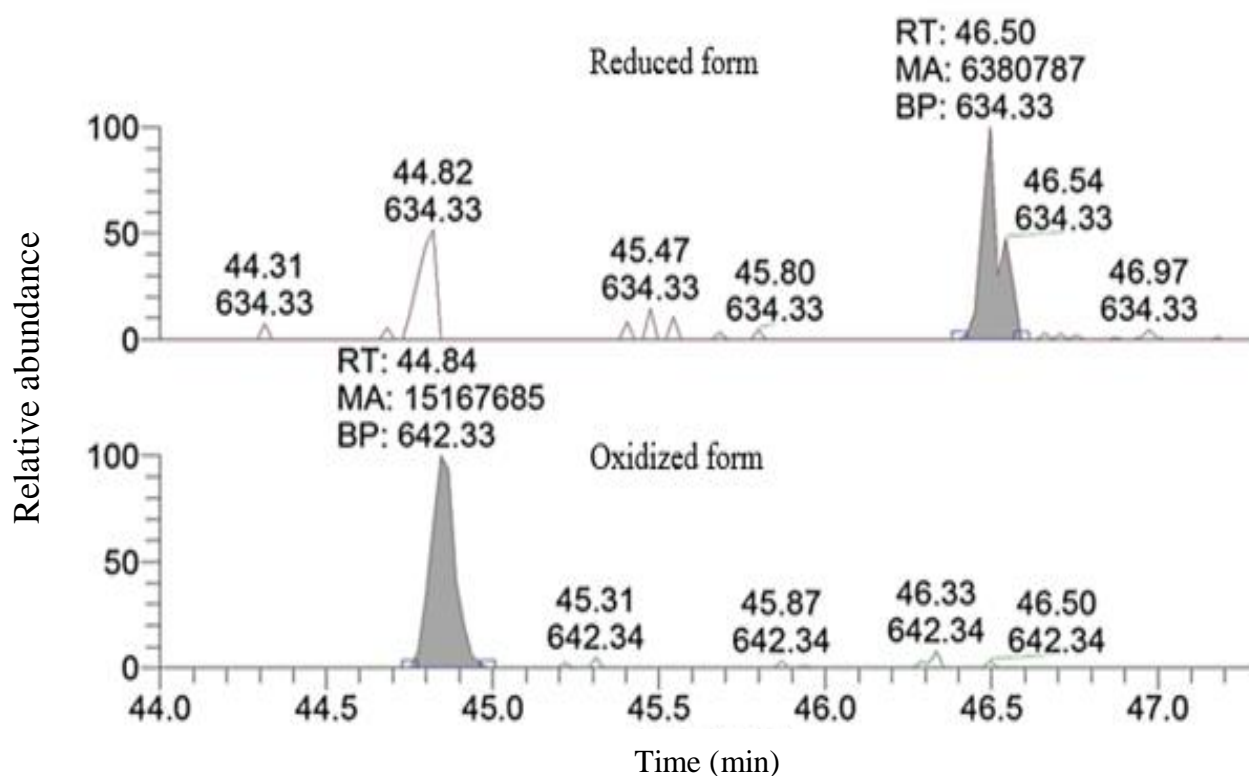


Figure 27. Extracted ion chromatogram (EIC) of the reduced MVVESAYEVIK and the oxidized **M<sub>ox</sub>**VVESAYEVIK representing the y- and b-ions of both methionine forms.

### 3.4.2. Peptide 4 (AILVDLEPGTMDSVR)

The peptide **4**, which was selected from methionine containing peptides, resulting from the tryptic digestion of proteins in Jurkat cells. After LC-MS/MS analysis, the (TIC, figure 28), the (BPC, figure 29), full MS scan of reduced (figure 30 ) and of oxidized (figure 31 ) form are presented below. The fragment ion spectra of peptide **4** is shown in figure 32 as well as AUC is shown in figure 33. The peptide **4** was found in both oxidized and reduced form has the parameters of the (RT, m/z and MW) which are represented in table 8.

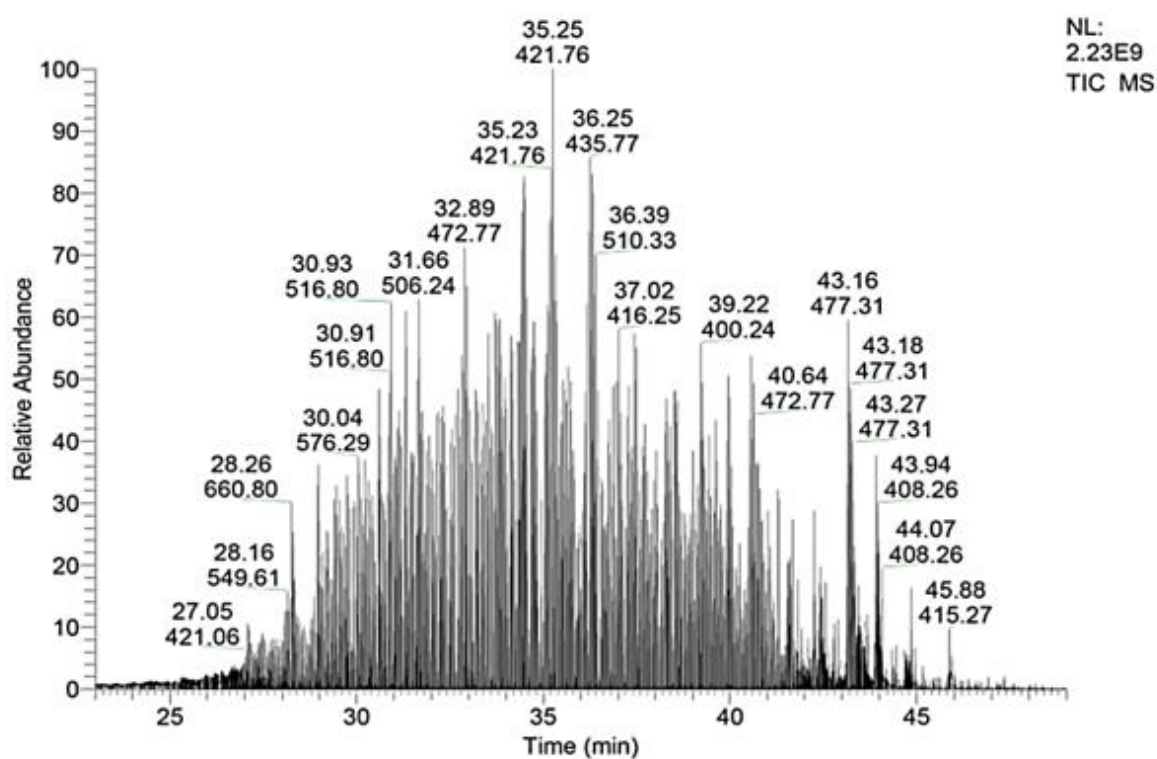


Figure 28. A part of total ion current (TIC) of Jurkat cell sample in case of PIRL homogenization, at RT (23.00-49.00 min).

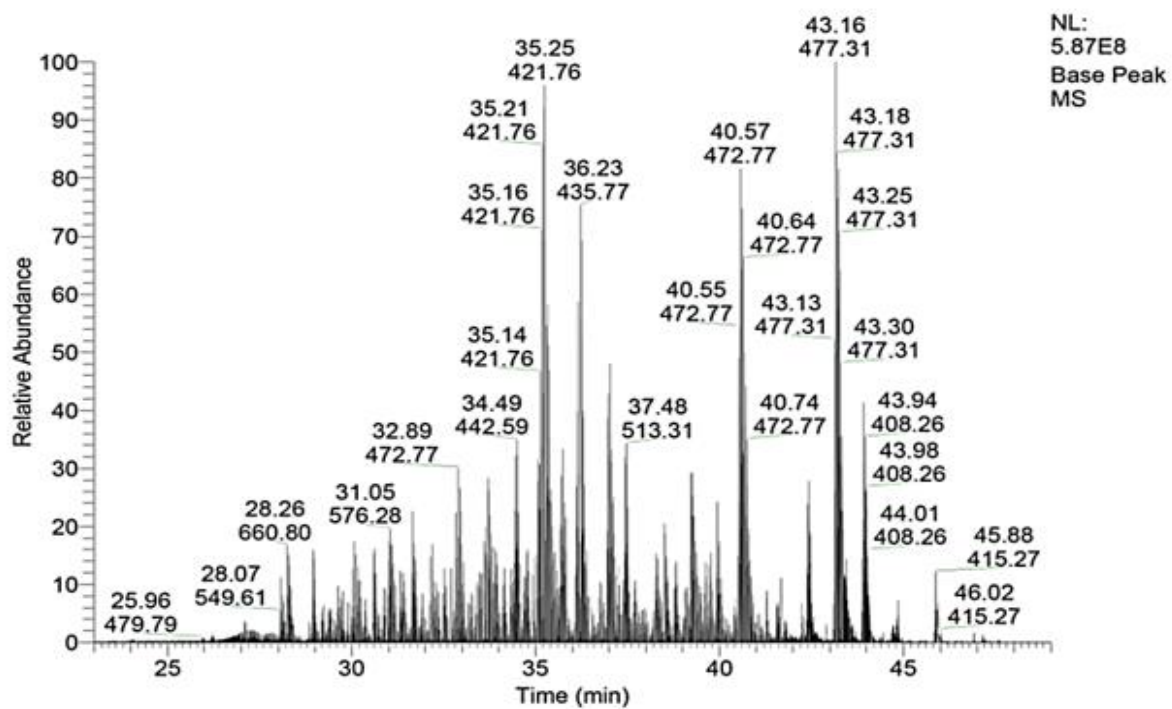


Figure 29. A part of base peak chromatogram (BPC) of Jurkat cell sample in case of PIRL homogenization, at RT (23.00-49.00 min).

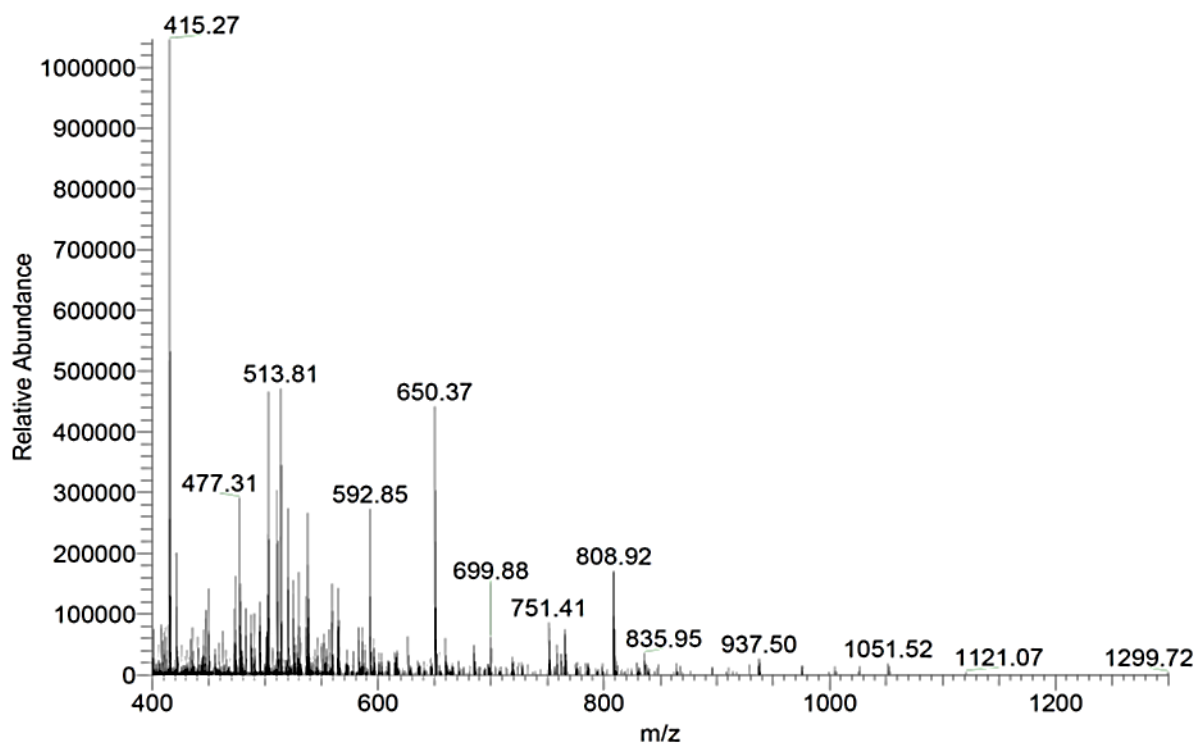


Figure 30. Full MS scan of the reduced form of AILVDLEPGTMDSVR,, at RT 46.40 min.

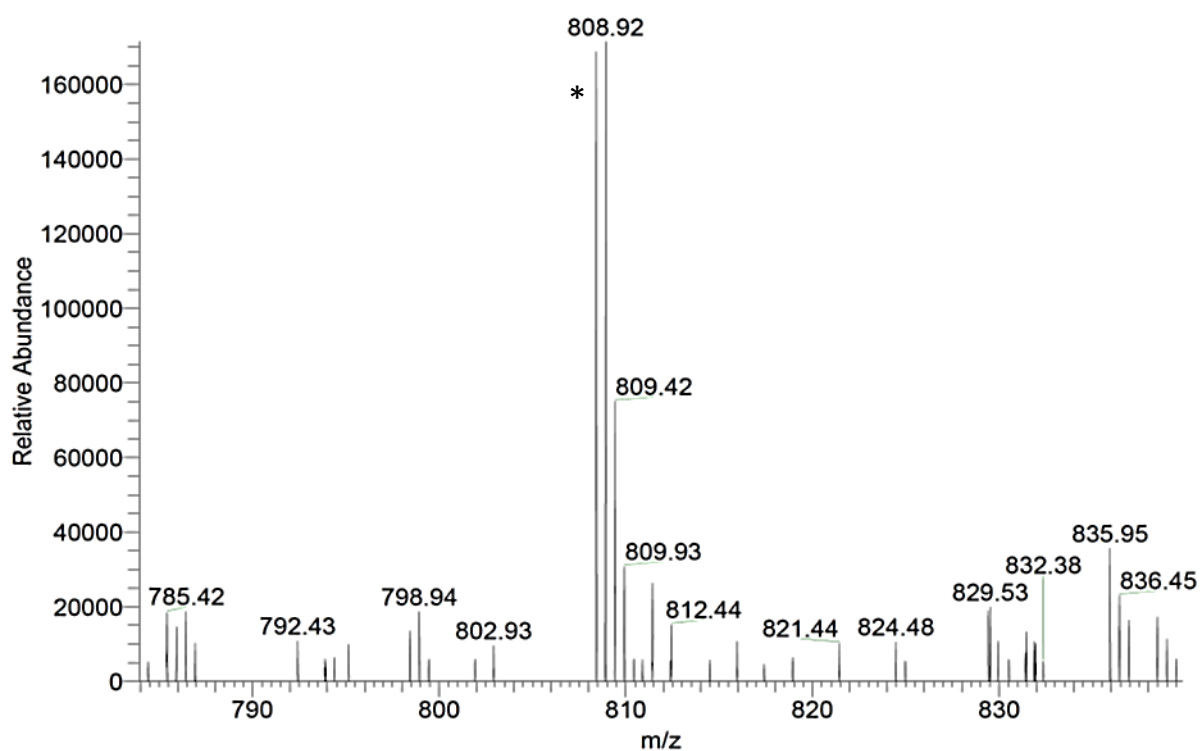


Figure 30A. Section of full MS scan of the reduced form of AILVDLEPGTMDSVR, at RT 46.40 min.  
\* representing the monoisotopic peak for the signal with (m/z, 808.42).



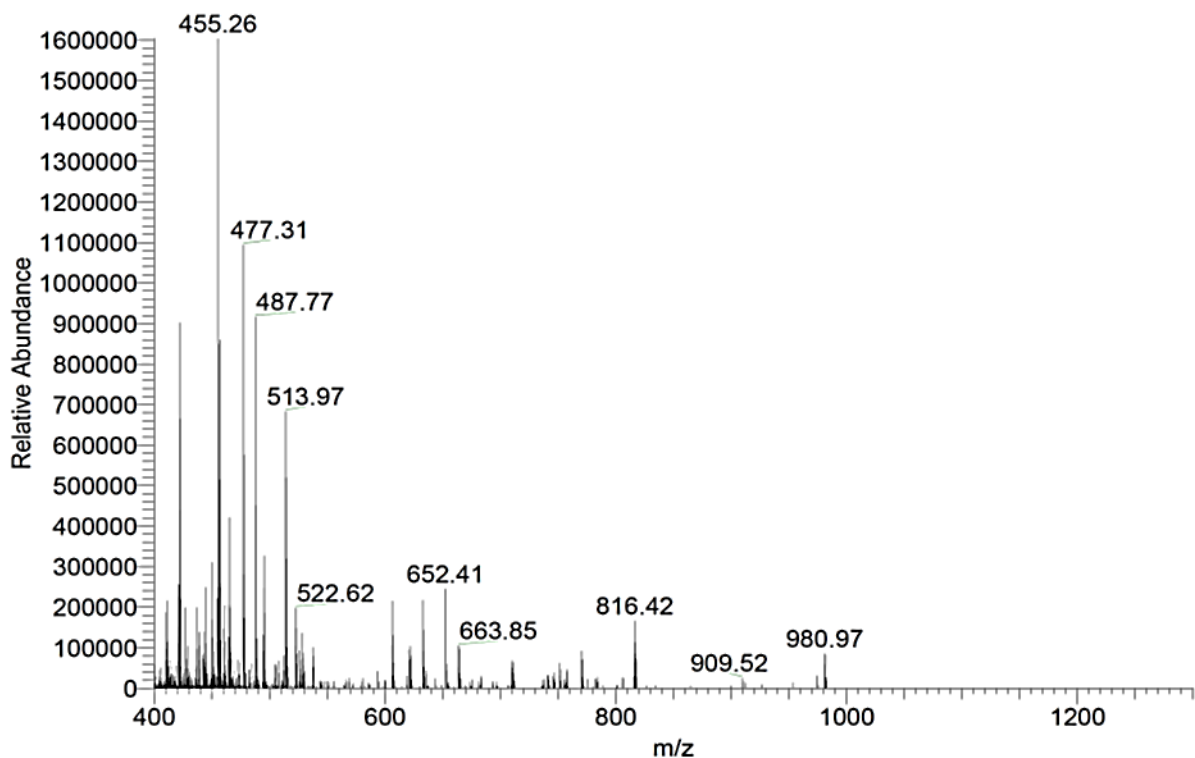


Figure 31. Full MS scan of the oxidized form of AILVDLEPGT  $M_{ox}$ DSVR, at RT 43.82 min.

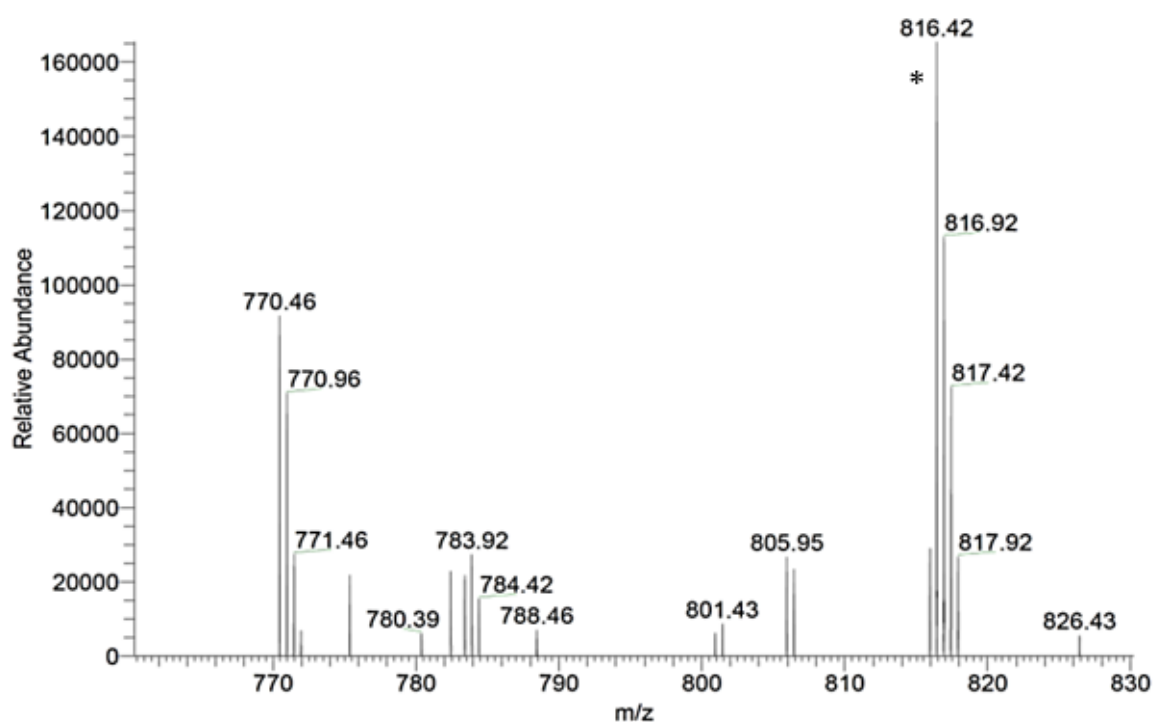


Figure 31A. Section of full MS scan of the oxidized form of AILVDLEPGT  $M_{ox}$ DSVR, at RT 43.82 min. \* representing the monoisotopic peak for the signal with (m/z, 816.42).

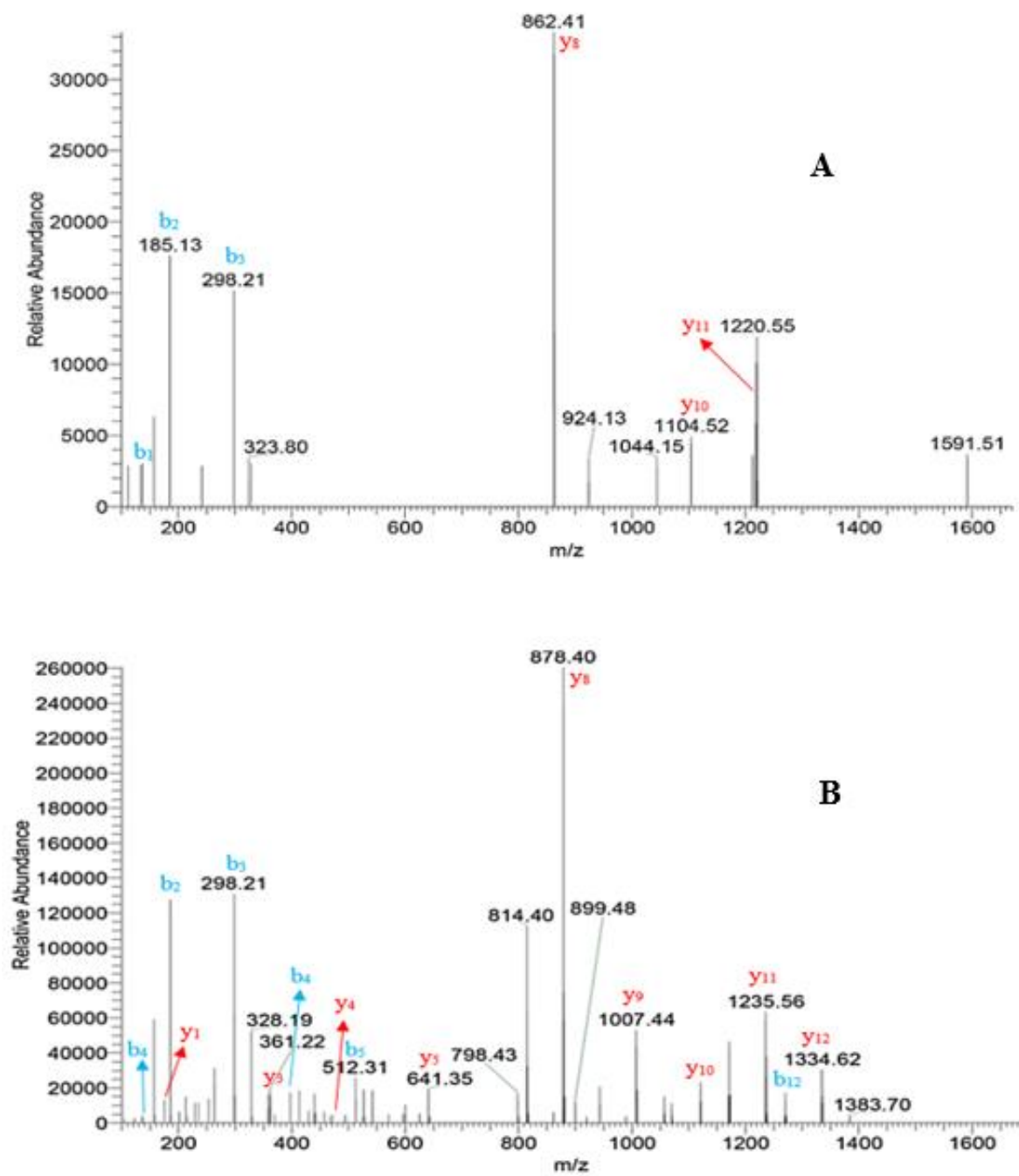


Figure 32. MS/MS spectra of the reduced AILVDLEPGTMDSVR (A) and the oxidized AILVDLEPGT M<sub>ox</sub>DSVR (B) representing the y- and b-ions of both methionine forms.

Table 8. Reduced and oxidized form of peptide, AILVDLEPGTMDSVR, including their retention time, mass/charge and molecular weight (MW).

Peptide sequence	Retention time (RT, min)	Mass/charge (m/z)	M.W
AILVDLEPGT $M_{ox}$ DSVR	43.83	816.42 $[M+2H]^{2+}$	1631.83
AILVDLEPGTMDSVR	46.41	808.42	1615.83

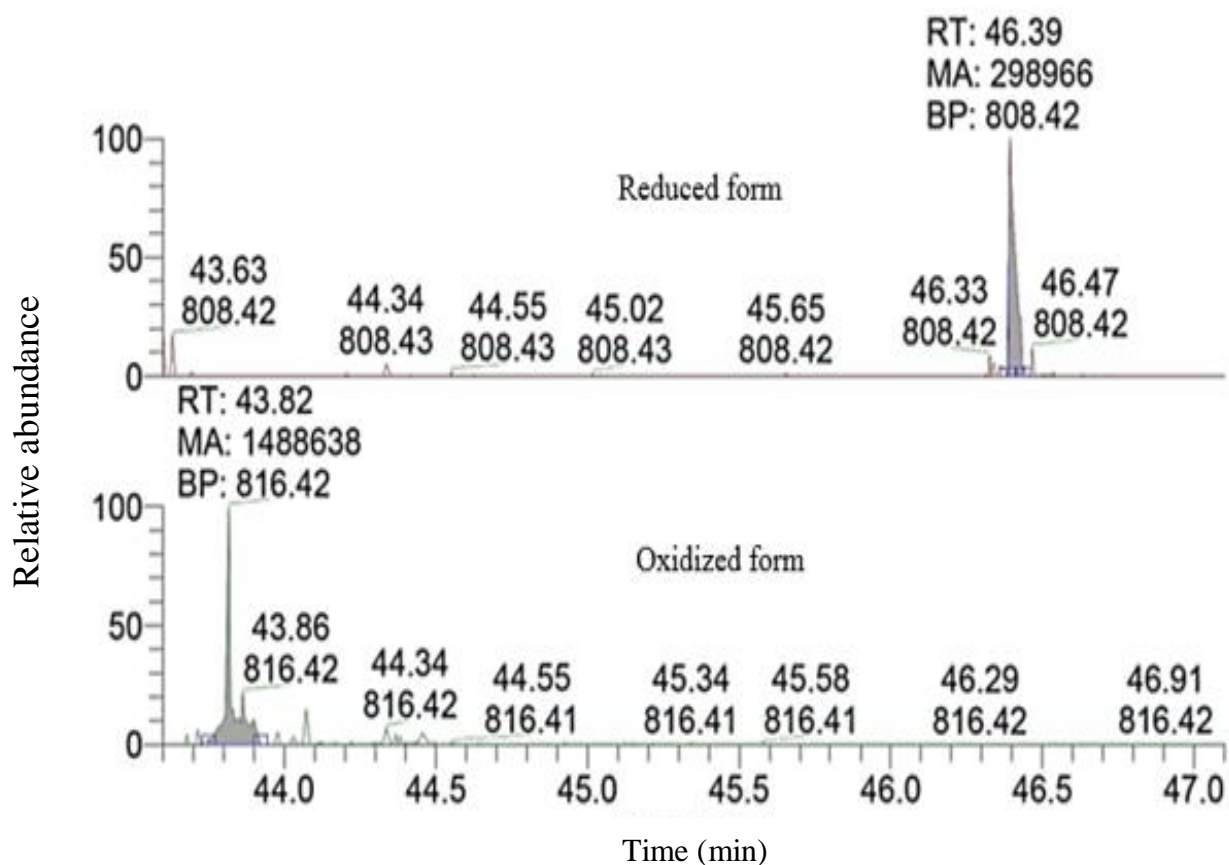


Figure 33. Extracted ion chromatogram (EIC) of the reduced AILVDLEPGTMDSVR and the oxidized AILVDLEPGT $M_{ox}$ DSVR representing the y- and b-ions of both methionine forms.

### 3.5. Classical versus PIRL homogenization

The peptide **5** observed in both homogenization methods was used to compare the extent of oxidation occurred.

#### 3.5.1. Peptide 5 (EITALAPSTMK)

The peptide **5** was found in both homogenization methods with oxidized and reduced form has the following parameters of the (RT, m/z and MW) are represented in tables (9, 10). In addition, it is shown the fragment spectra of reduced and oxidized state of the peptide **5** within two homogenization methods (figure 34).

The comparison between classical and PIRL-DIVE homogenization of peptide **5** (EITALAPSTMK) is shown in figure 46. Figure 35A, represents the classical homogenization; where the area under curve (AUC) of reduced form was found to be higher than oxidized form. However, data from PIRL-DIVE homogenization shows that the AUC of oxidized form was found to be higher than reduced form (figure 35B).

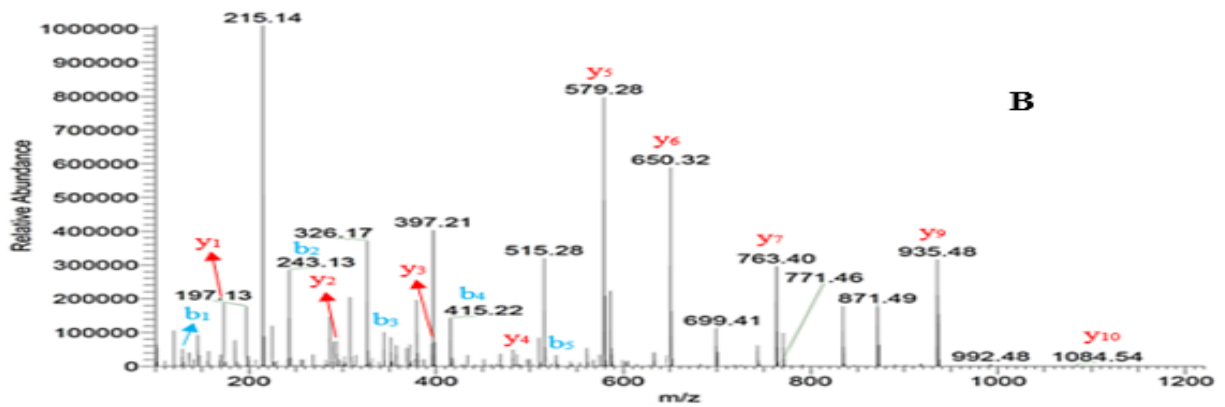
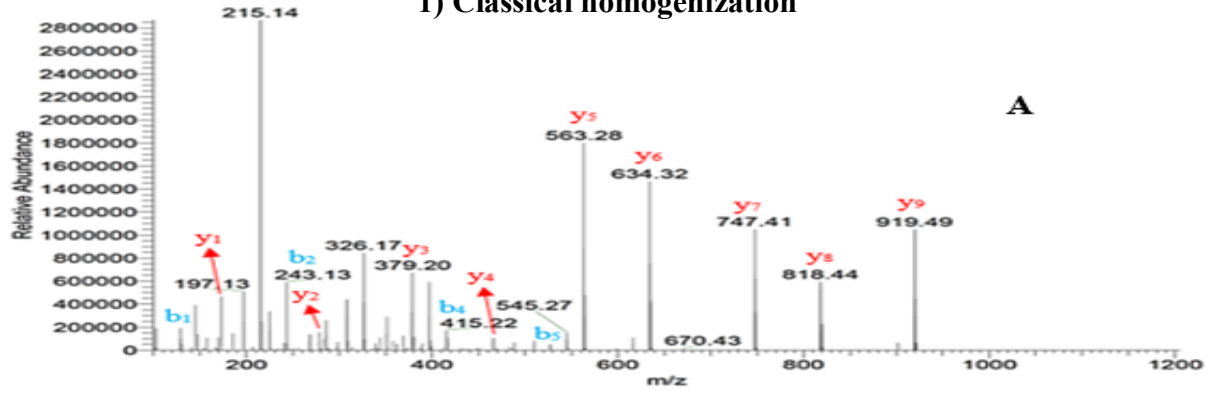
Table 9. Reduced and oxidized form of peptide, EITALAPSTMK, including their retention time, mass/charge and molecular weight (MW), after classical homogenization.

Peptide sequence	Retention time (RT, min)	Mass/charge (m/z)	M.W
EITALAPSTM <sub>ox</sub> K	28.29	589.31 [M+2H] <sup>2+</sup>	1177.61
EITALAPSTMK	31.25	581.31	1161.61

Table 10. Reduced and oxidized form of peptide, EITALAPSTMK, including their retention time, mass/charge and molecular weight (MW), after PIRL-DIVE homogenization.

Peptide sequence	Retention time (RT, min)	Mass/charge (m/z)	M.W
EITALAPSTM <sub>ox</sub> K	34.17	589.31 [M+2H] <sup>2+</sup>	1177.61
EITALAPSTMK	37.81	581.31	1161.61

## 1) Classical homogenization



## 2) PIRL-DIVE homogenization

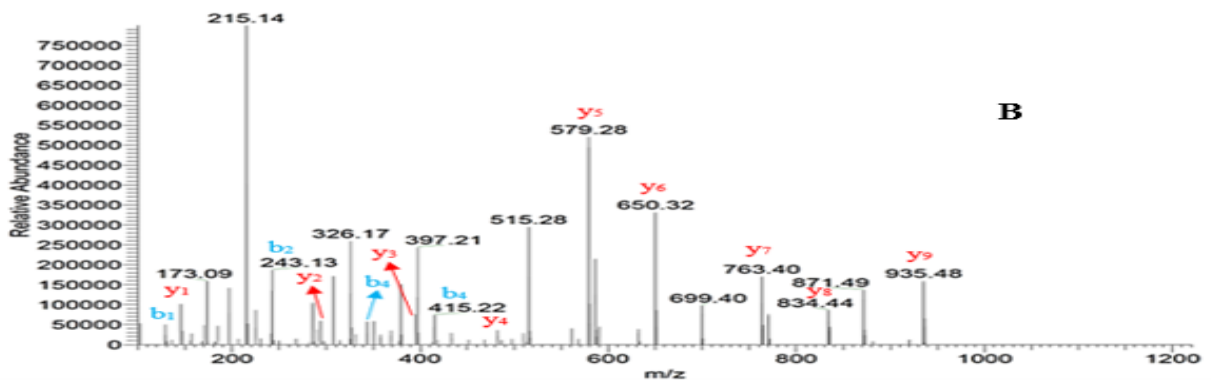
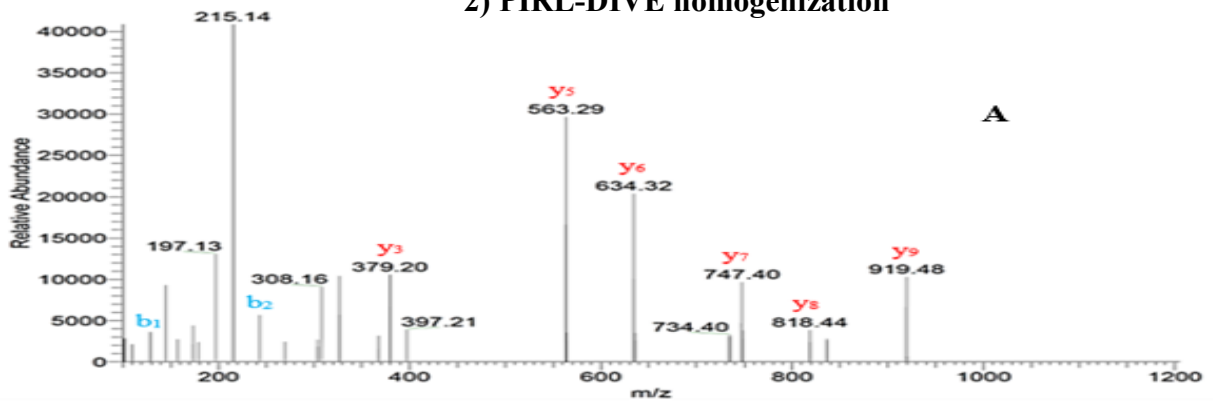


Figure 34. MS/MS spectra of the reduced EITALAPSTMK (A) and the oxidized EITALAPSTM<sub>ox</sub>K (B) representing the y- and b-ions of both methionine forms, for classical (1) and PIRL-DIVE (2) homogenization.

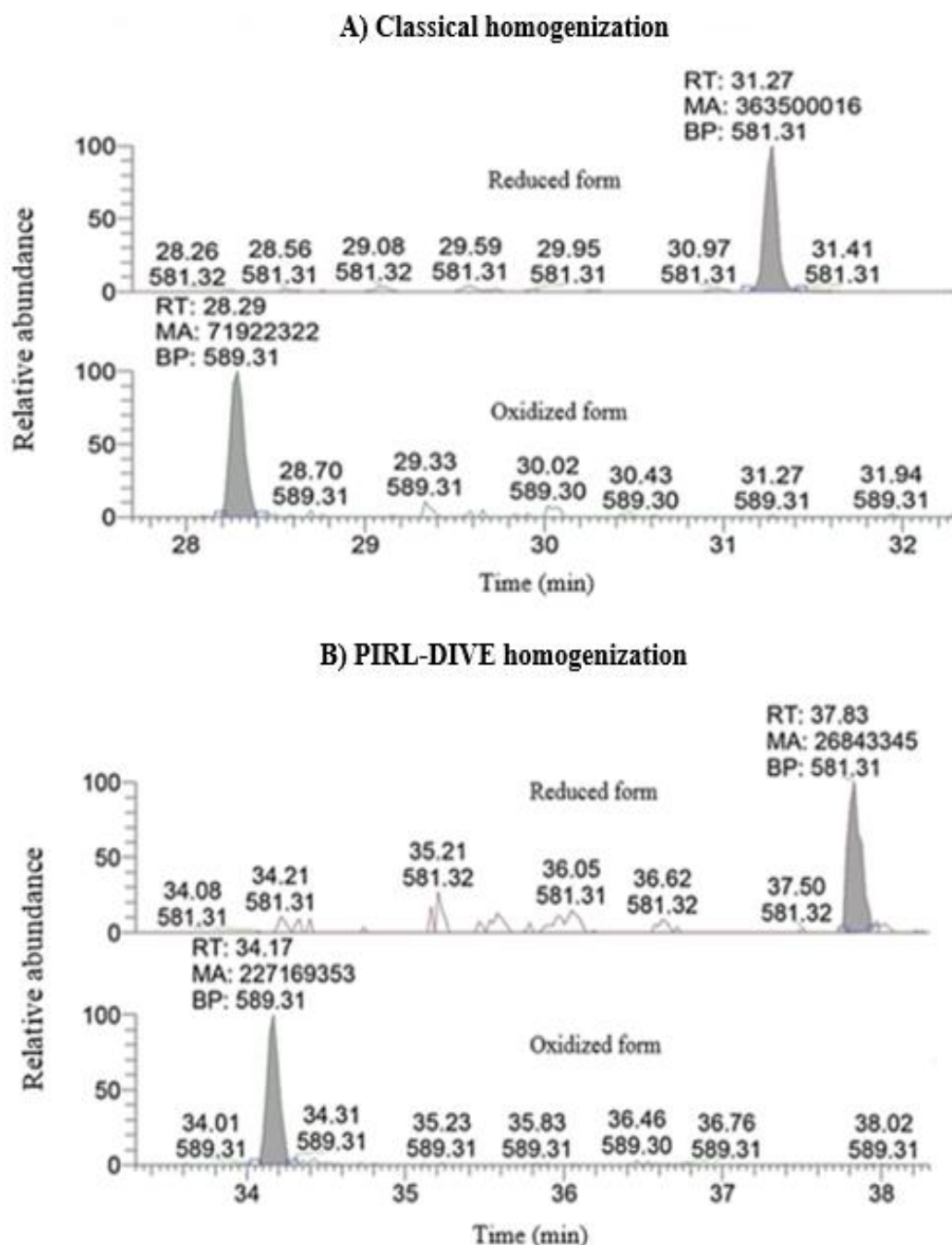


Figure 35. Extracted ion chromatogram (EIC) of the reduced EITALAPSTMK and the oxidized EITALAPSTM<sub>ox</sub>K representing the y- and b-ions of both methionine forms, in classical (A) and in PIRL-DIVE (B) homogenization. RT: retention time; BP: base peak; MA: measured area.

### 3.6. Validation of results

#### 3.6.1. Peptide 6 (AANEAGYFNEEMAPIEVK)

The validation of results was done by calculating the ratio of oxidized/reduced form of the peptide **6**, either manually using Xcallibur (figure 36) or automatically using MaxQuant software. The ratio was very similar in both cases (approx. 0.2)

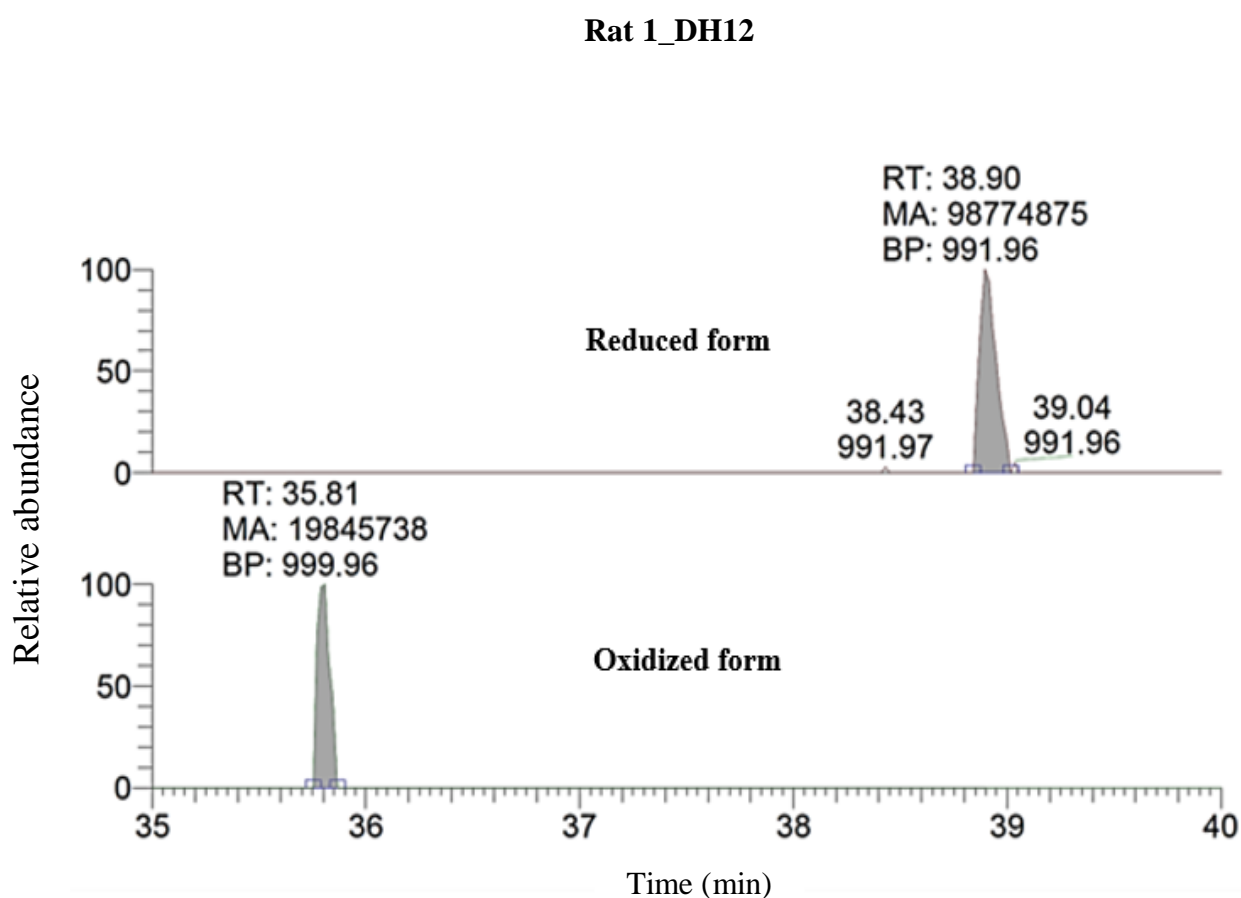
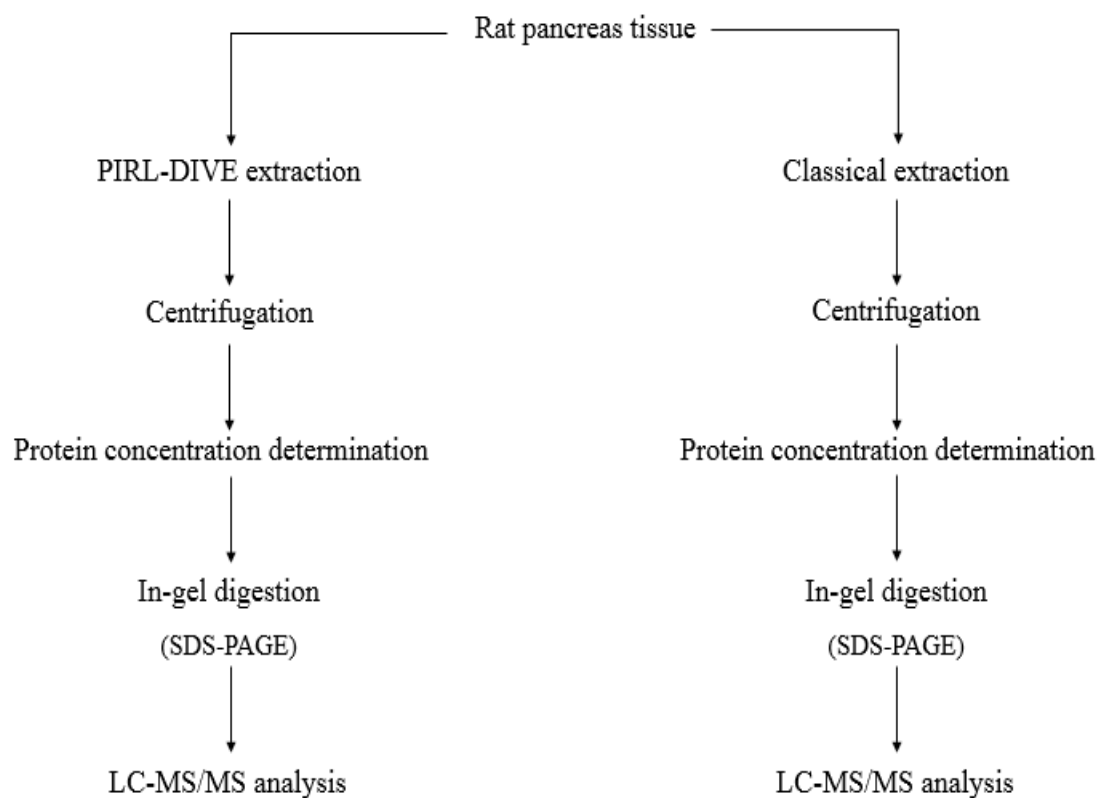


Figure 36. Extracted ion chromatogram (EIC) of the reduced AANEAGYFNEEMAPIEVK and the oxidized AANEAGYFNEEM<sub>ox</sub>APIEVK representing the y- and b-ions of both methionine forms.

### 3.7. Proteomics results of rat pancreas tissue

In order to investigate the rate of methionine oxidation between classical and PIRL-DIVE homogenization methods, a model of rat pancreas tissue was used. Equal pieces of pancreas tissues were used for classical and PIRL-DIVE homogenization.. The experimental workflow suggested is presented in scheme 2.



Scheme 2. The experimental workflow of rat pancreas tissue. Details are in materials and methods section.



### 3.7.1. Classical versus PIRL homogenization of rat pancreas

In three different rat pancreas tissues, the distribution of ratios of oxidized/reduced form of common peptides in each tissue separately shows that there is no significant difference between the both homogenization methods in rat 2 and rat 3 (figures 38 and 39). However, in rat 1, it is shown that with PIRL homogenization method, the very most of peptides are in reduced state (figure 37), which is the basic state of methionine containing peptides in the cell (reviewed in ref. 74, 75).

In case of rat 1, the classical homogenization, the number of peptides which have the ratio of oxidized/reduced form  $< 1$  is 316 peptides, and which have the ratio of oxidized/reduced form  $> 1$  is 355 peptides. In the PIRL homogenization, the number of peptides which have the ratio of oxidized/reduced form  $< 1$  is 651 peptides, and which have the ratio of oxidized/reduced form  $> 1$  is 20 peptides.

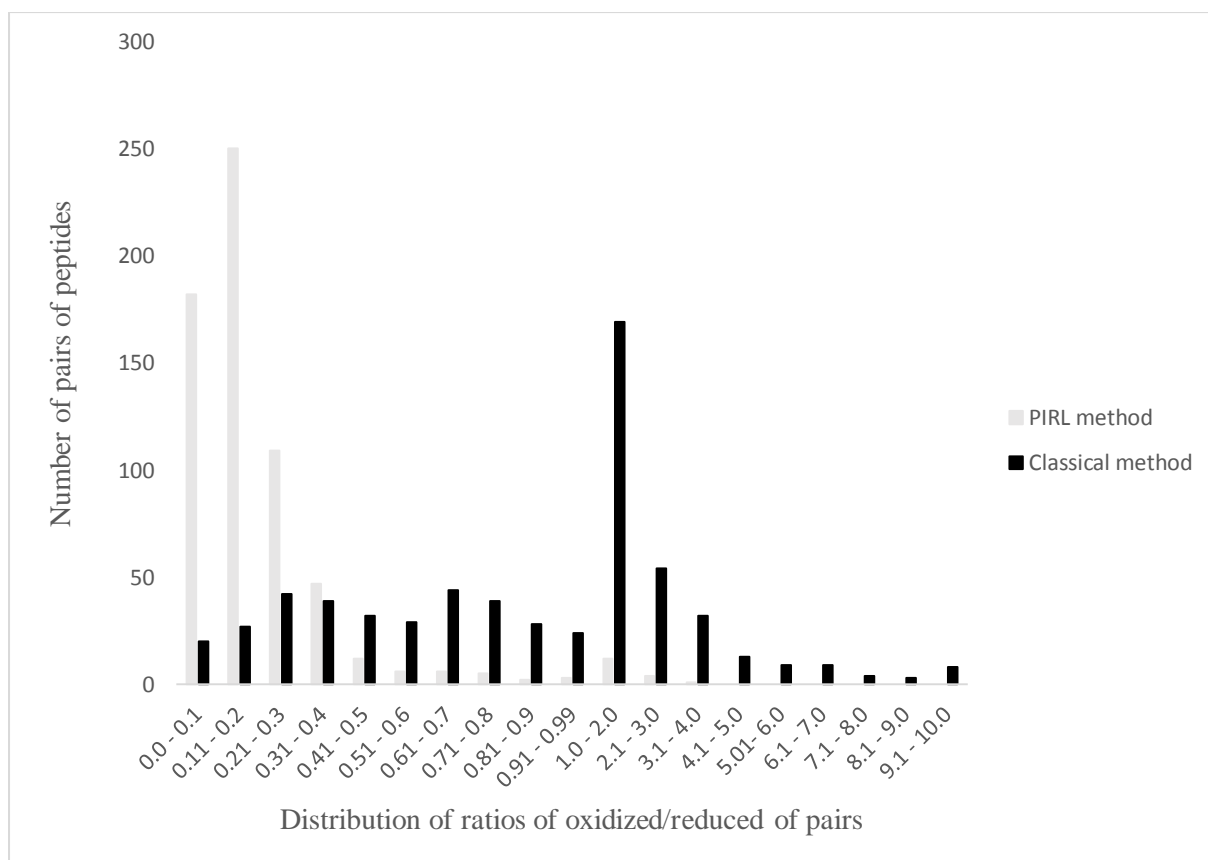


Figure 37. Distribution of ratios of peptides in both homogenization methods, in rat pancreas 1.

In case of rat 2, the classical homogenization, the number of peptides which have the ratio of oxidized/reduced form  $< 1$  is 616 peptides, and which have the ratio of oxidized/reduced form  $> 1$  is 53 peptides. In the PIRL homogenization, the number of peptides which have the ratio of oxidized/reduced form  $< 1$  is 619 peptides, and which have the ratio of oxidized/reduced form  $> 1$  is 50 peptides.

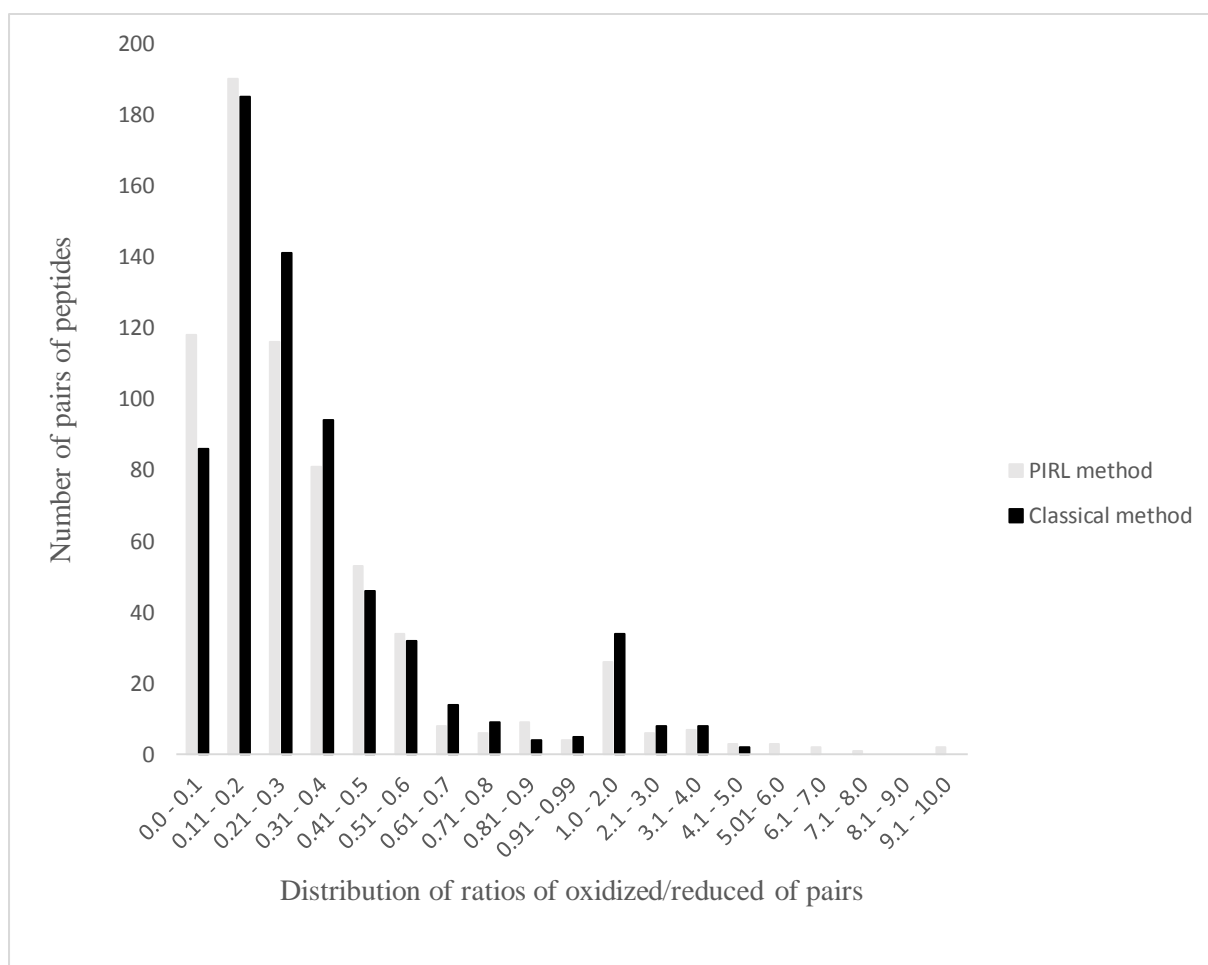


Figure 38. Distribution of ratios of peptides in both homogenization methods, in rat pancreas 2.

In case of rat 3, the classical homogenization, the number of peptides which have the ratio of oxidized/reduced form  $< 1$  is 781 peptides, and which have the ratio of oxidized/reduced form  $> 1$  is 28 peptides. In the PIRL homogenization, the number of peptides which have the ratio of oxidized/reduced form  $< 1$  is 770 peptides, and which have the ratio of oxidized/reduced form  $> 1$  is 39 peptides.

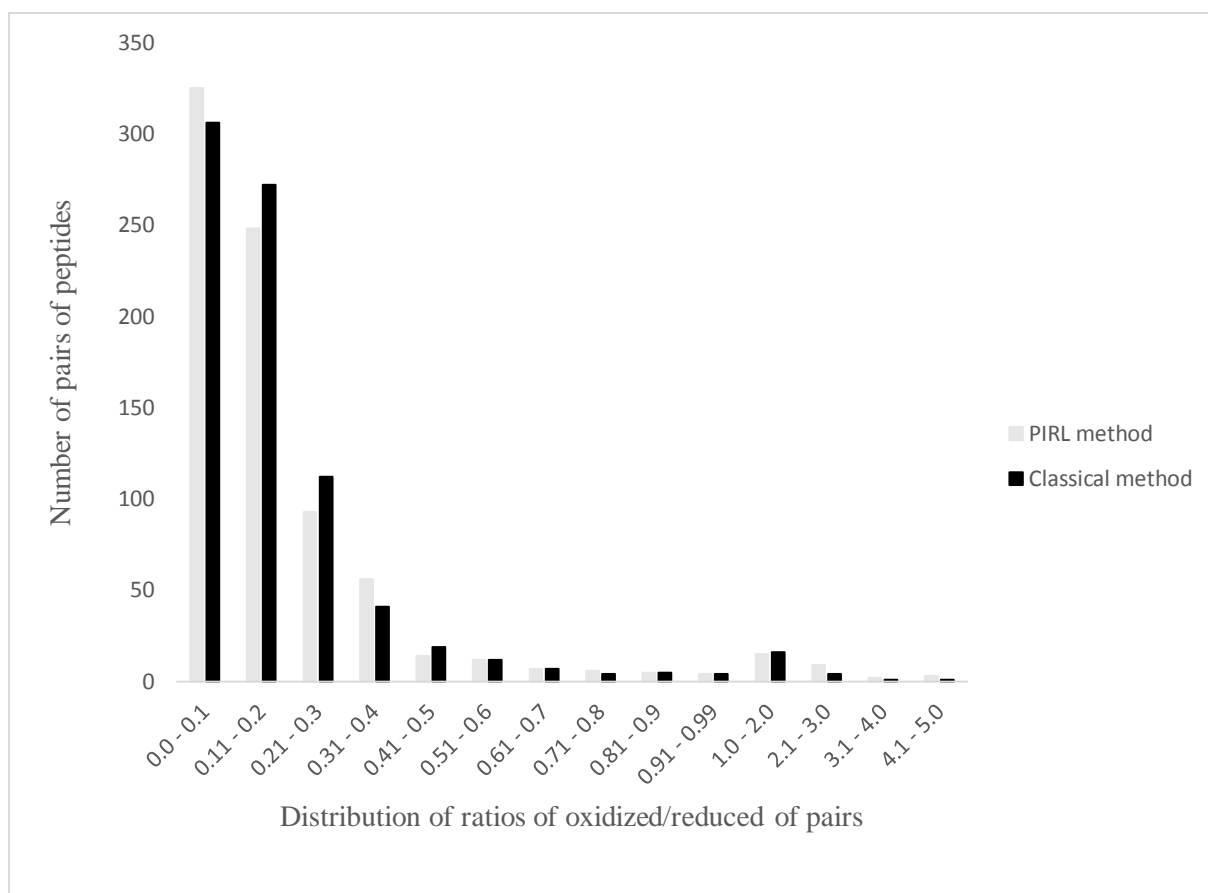


Figure 39. Distribution of ratios of peptides in both homogenization methods, in rat pancreas 3.

In three different rat pancreas tissues, by comparing the results for samples obtained by the classical and the PIRL method, the percentage of methionine containing peptides falling into category 1 was 92.80%, 57.80%, and 52.60% in rat 1, rat 2, and rat 3 respectively, while the percentage of methionine containing peptides in category 2 was 7.20%, 42.20% and 47.40% (figures 40, 41 and 42). For a few peptides a similar degree of oxidation (or: a similar ratio of oxidized/reduced methionines) were found by both methods in each tissue

Table 11. Number and percentage of oxidized methionine containing peptides of pairs of peptides in both homogenization methods in rat pancreas 1.

	<b>PIRL</b>	<b>Classical</b>
	< 1	> 1
Number of peptides	46	596
Percentage	7.17%	92.83%

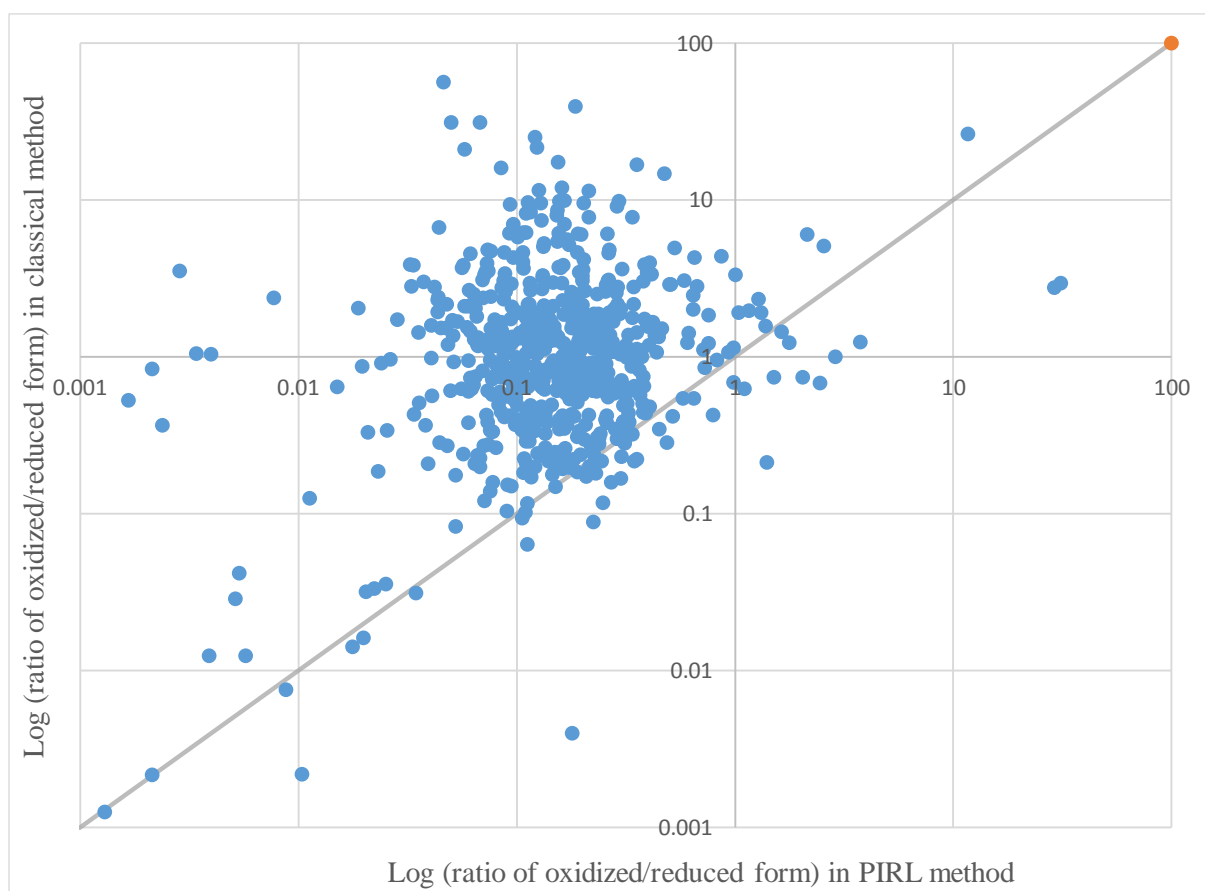


Figure 40. Two-dimensional scatter plot of rat pancreas 1. Each data point represents a peptide found in both approaches (classical and PIRL). Oxidized/reduced ratio in PIRL is plotted on the x-axis, while the ox/red ratio in classical is plotted on the y-axis. The scales of the axes are logarithmic.

Grey line displays linear function  $y=x$ . Data points above this line represent peptides that display a higher ox/red ratio in classical, whereas data point below  $y=x$  represent peptides with a higher ox/red ratio in PIRL.

Table 12. Number and percentage of oxidized methionine containing peptides of pairs of peptides in both homogenization methods in rat pancreas 2.

	<b>PIRL</b>	<b>Classical</b>
	< 1	> 1
Number of peptides	282	387
Percentage	42.15%	57.85%



Figure 41. Two-dimensional scatter plot of rat pancreas 2. Each data point represents a peptide found in both approaches (classical and PIRL). Oxidized/reduced ratio in PIRL is plotted on the x-axis, while the ox/red ratio in classical is plotted on the y-axis. The scales of the axes are logarithmic. Grey line displays linear function  $y=x$ . Data points above this line represent peptides that display a higher ox/red ratio in classical, whereas data point below  $y=x$  represent peptides with a higher ox/red ratio in PIRL.

Table 13. Number and percentage of oxidized methionine containing peptides of pairs of peptides in both homogenization methods in rat pancreas 3.

	<b>PIRL</b>	<b>Classical</b>
	< 1	> 1
Number of peptides	385	424
Percentage	47.59%	52.41%

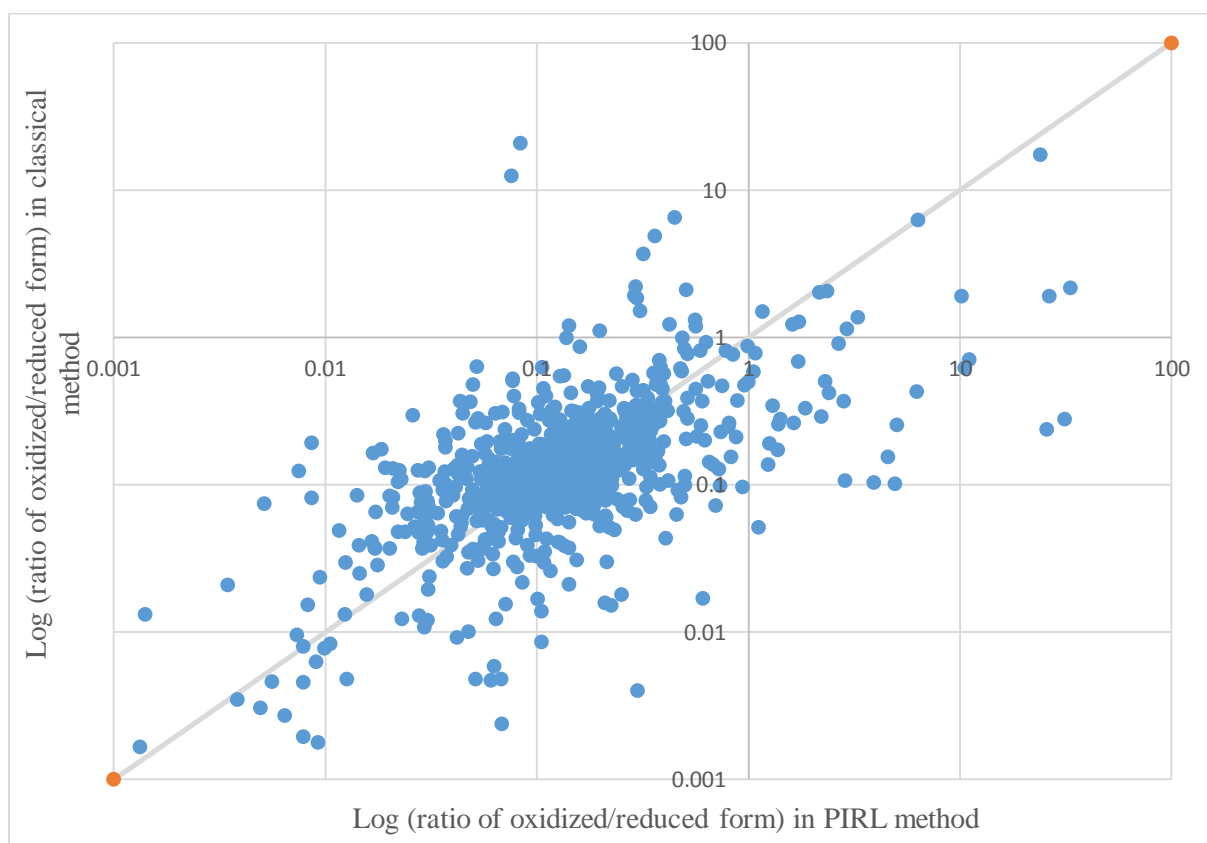
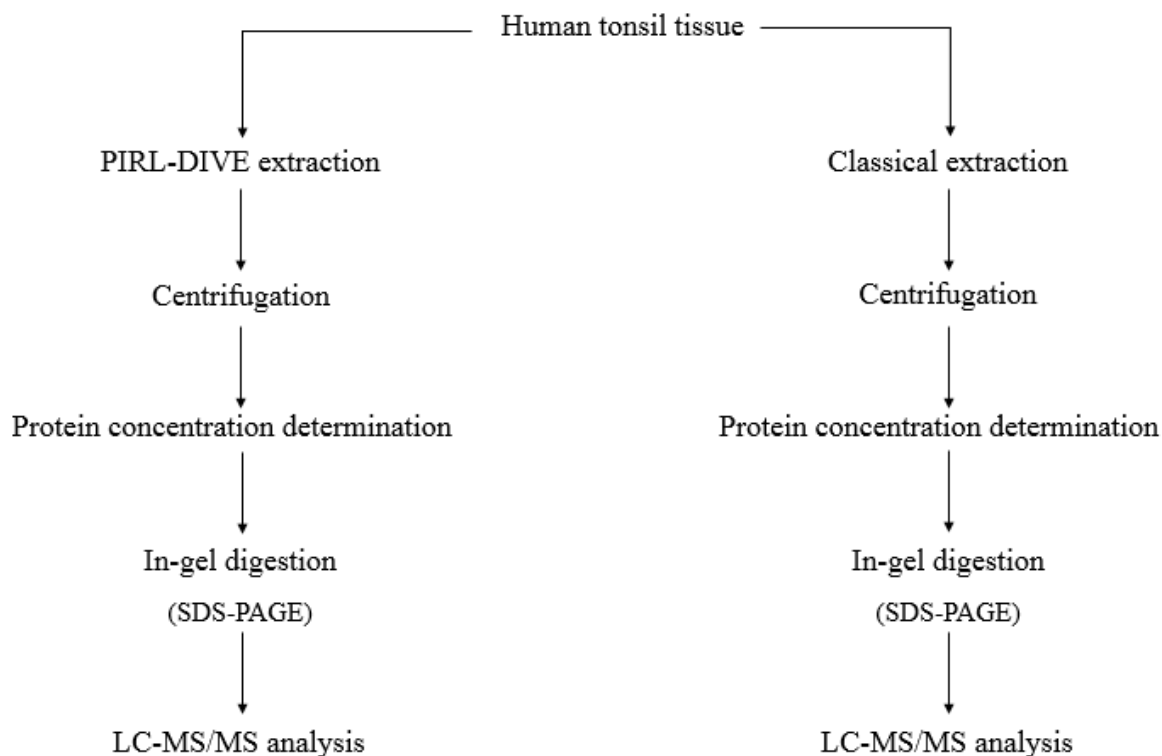


Figure 42. Two-dimensional scatter plot of rat pancreas 3. Each data point represents a peptide found in both approaches (classical and PIRL). Oxidized/reduced ratio in PIRL is plotted on the x-axis, while the ox/red ratio in classical is plotted on the y-axis. The scales of the axes are logarithmic. Grey line displays linear function  $y=x$ . Data points above this line represent peptides that display a higher ox/red ratio in classical, whereas data point below  $y=x$  represent peptides with a higher ox/red ratio in PIRL.

### 3.8. Proteomics results of human tonsil tissue

Another model; human tonsil tissue was used to investigate the rate of methionine oxidation between classical and PIRL-DIVE approaches. As it has been mentioned above, equal pieces of tonsil tissues were utilized for classical and PIRL-DIVE homogenization.. The experimental workflow suggested is presented in scheme 3.



Scheme 3. The experimental workflow of human tonsil tissue. Details are in materials and methods section.

#### 3.8.1. Classical versus PIRL homogenization of human tonsil

In three different human tonsil tissues, the distribution of ratios of oxidized/reduced form of common peptides in each tissue separately shows that there is no significant difference between the both homogenization methods in tonsil 2 and tonsil 3 (figures 44 and 45). However, in tonsil 1, it is shown that with PIRL homogenization method, the very most of peptides are in reduced state (figure 43), which is the basic state of methionine containing peptides in the cell (reviewed in ref. 74, 75).

In case of tonsil 1, the classical homogenization, the number of peptides which have the ratio of oxidized/reduced form  $< 1$  is 4 peptides, and which have the ratio of oxidized/reduced form  $> 1$  is 121 peptides. In the PIRL homogenization, the number of peptides which have the ratio of oxidized/reduced form  $< 1$  is 4 peptides, and which have the ratio of oxidized/reduced form  $> 1$  is 121 peptides.

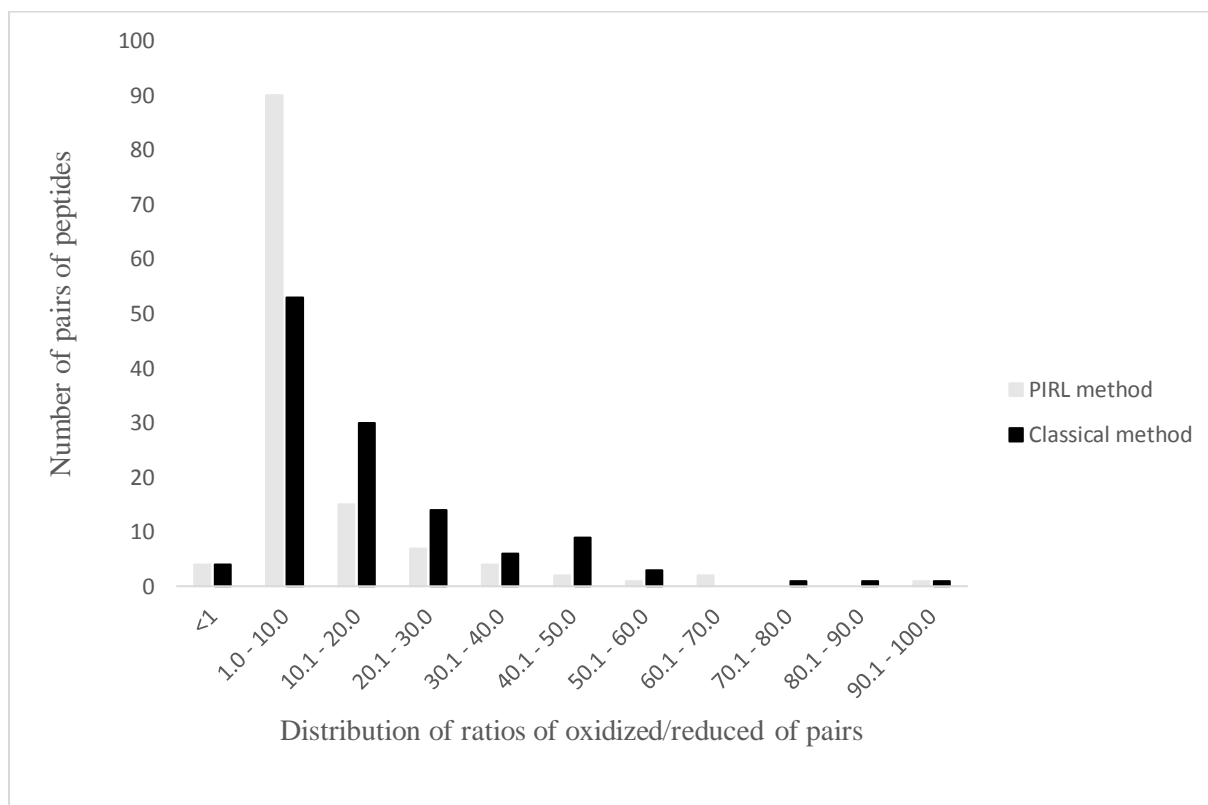


Figure 43. Distribution of ratios of peptides in both homogenization methods, in human tonsil 1.



In case of tonsil 2, the classical homogenization, the number of peptides which have the ratio of oxidized/reduced form  $< 1$  is 332 peptides, and which have the ratio of oxidized/reduced form  $> 1$  is 274 peptides. In the PIRL homogenization, the number of peptides which have the ratio of oxidized/reduced form  $< 1$  is 293 peptides, and which have the ratio of oxidized/reduced form  $> 1$  is 313 peptides.

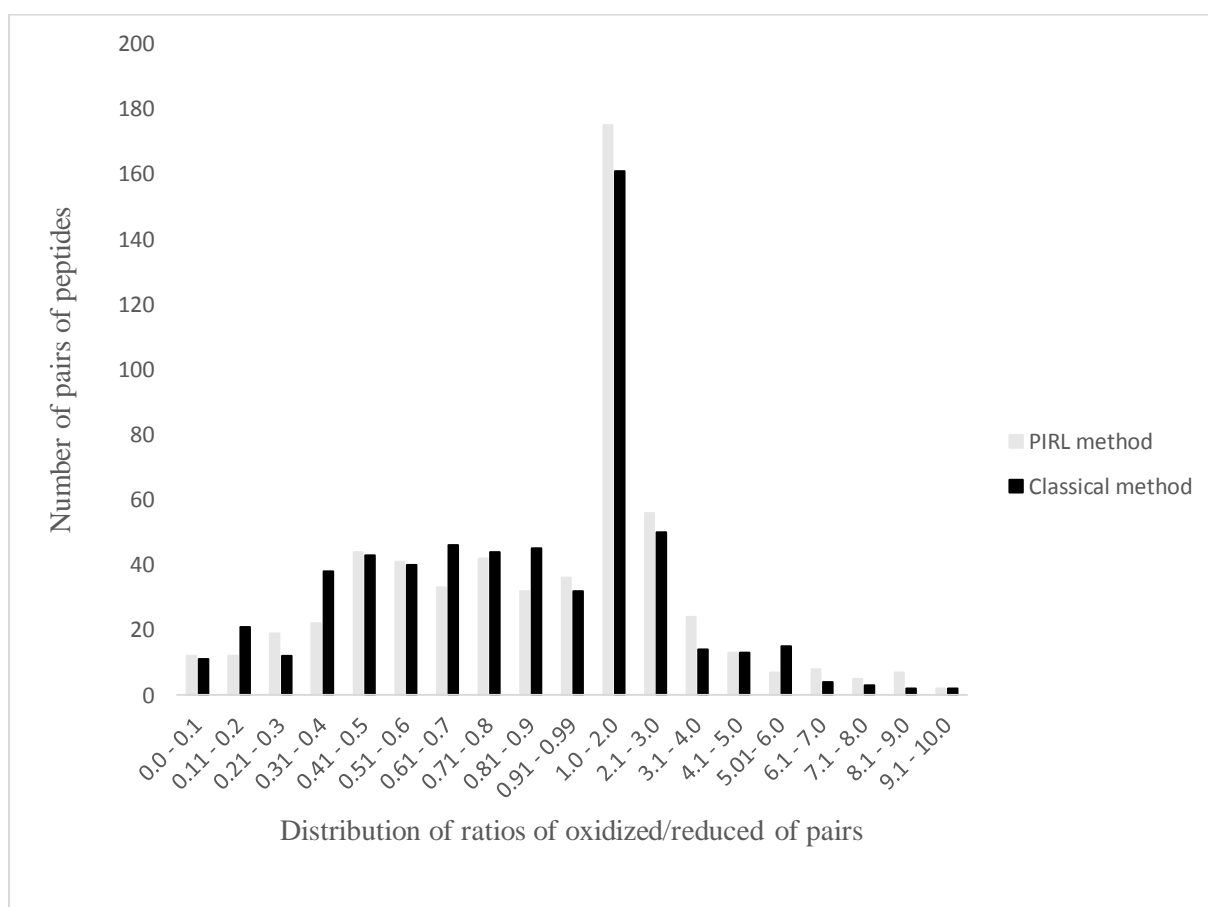


Figure 44. Distribution of ratios of peptides in both homogenization methods, in human tonsil 2.

In case of tonsil 3, the classical homogenization, the number of peptides which have the ratio of oxidized/reduced form  $< 1$  is 436 peptides, and which have the ratio of oxidized/reduced form  $> 1$  is 593 peptides. In the PIRL homogenization, the number of peptides which have the ratio of oxidized/reduced form  $< 1$  is 422 peptides, and which have the ratio of oxidized/reduced form  $> 1$  is 607 peptides.

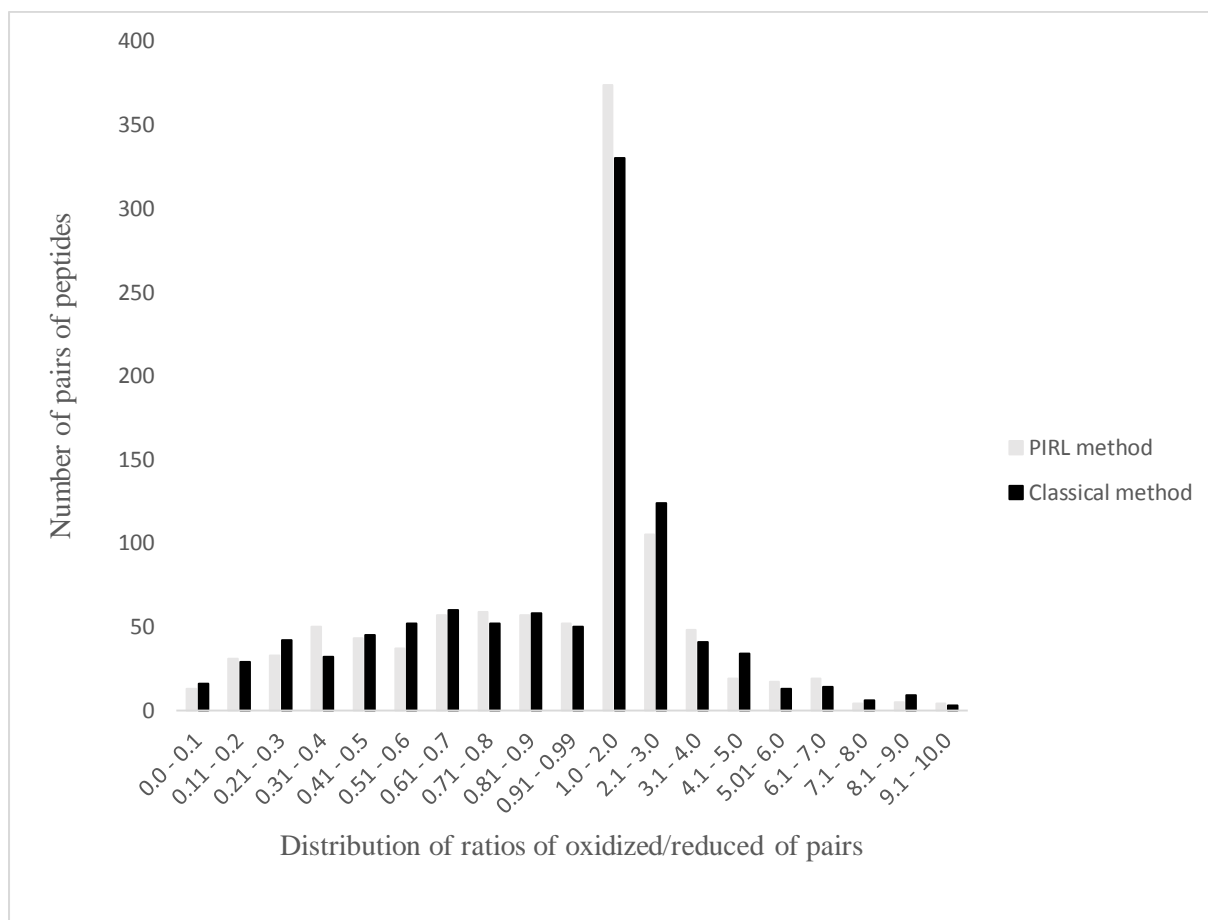


Figure 45. Distribution of ratios of peptides in both homogenization methods, in human tonsil 3.

In case of human tonsil tissues it was also found that in three different samples, by comparing the results for samples obtained by the classical and the PIRL method, the percentage of methionine containing peptides falling into category 1 was 80.80%, 42.60%, and 50.60% in tonsil 1, tonsil 2, and tonsil 3 respectively (figures 46, 47 and 48), while the percentage of methionine containing peptides in category 2 was 18.20%, 57.40% and 49.40%. in tonsil 1, tonsil 2, and tonsil 3, respectively.

Table 14. Number and percentage of oxidized methionine containing peptides of pairs of peptides in both homogenization methods in human tonsil 1.

	<b>PIRL</b>	<b>Classical</b>
	< 1	> 1
Number of peptides	24	101
Percentage	19.20%	80.80%

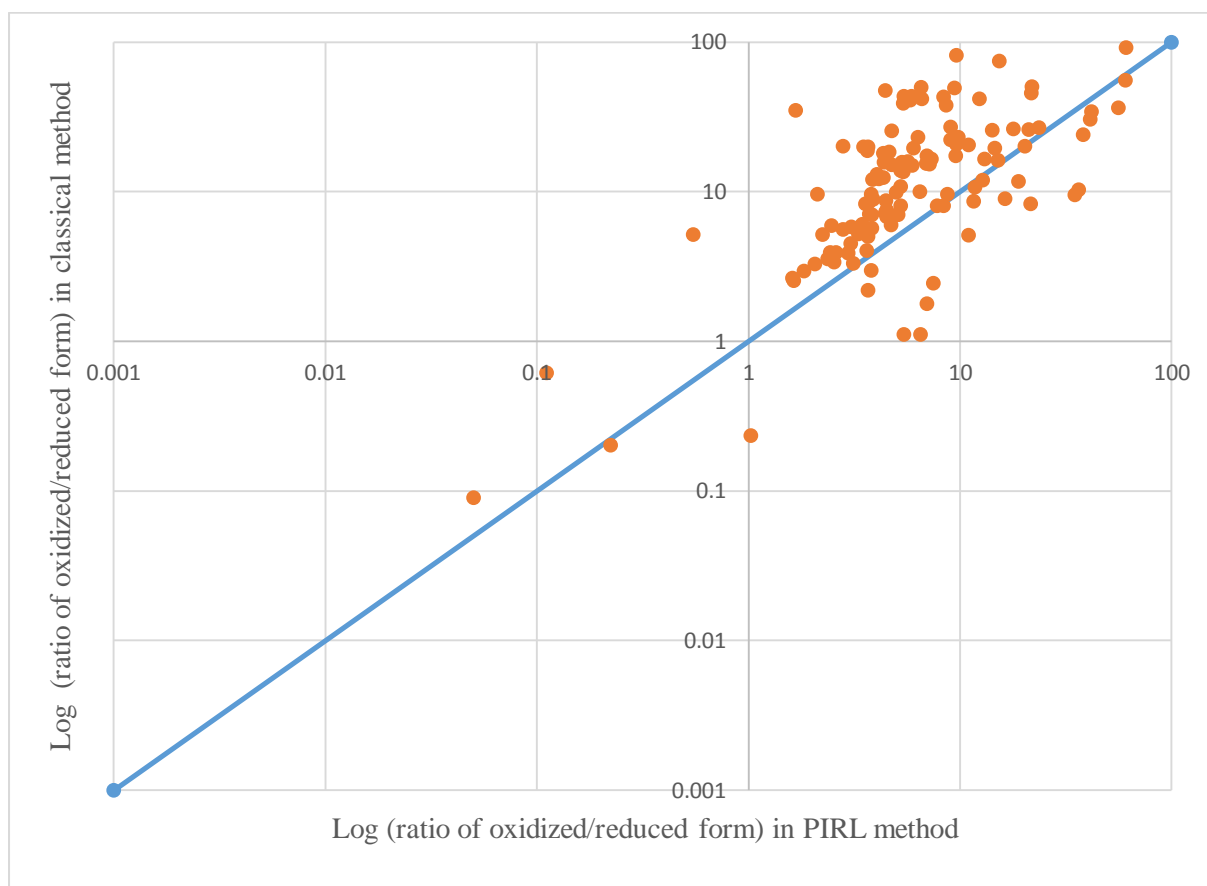


Figure 46. Two-dimensional scatter plot of human tonsil 1. Each data point represents a peptide found in both approaches (classical and PIRL). Oxidized/reduced ratio in PIRL is plotted on the x-axis, while the ox/red ratio in classical is plotted on the y-axis. The scales of the axes are logarithmic.

Grey line displays linear function  $y=x$ . Data points above this line represent peptides that display a higher ox/red ratio in classical, whereas data point below  $y=x$  represent peptides with a higher ox/red ratio in PIRL.

Table 15. Number and percentage of oxidized methionine containing peptides of pairs of peptides in both homogenization methods in human tonsil 2.

	<b>PIRL</b>	<b>Classical</b>
	< 1	> 1
Number of peptides	349	257
Percentage	57.59%	42.41%

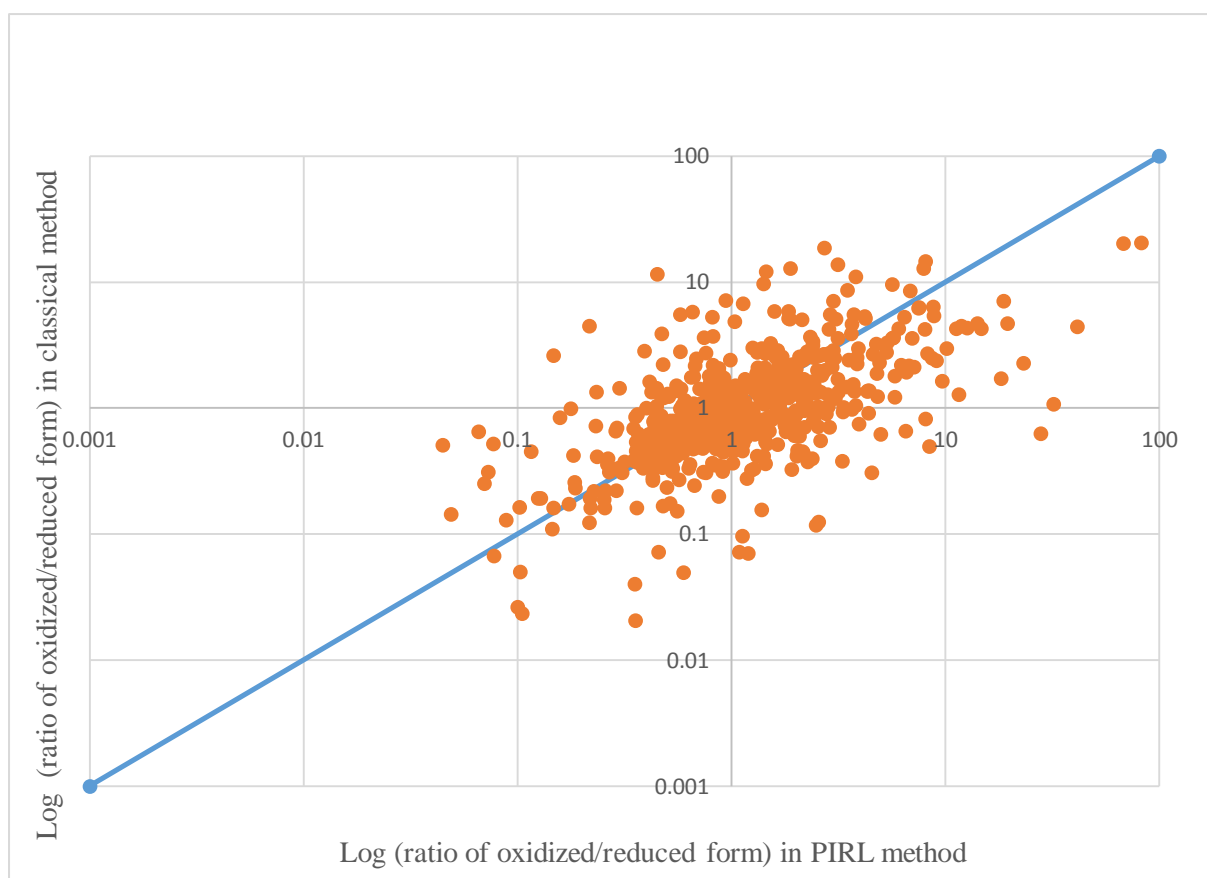


Figure 47. Two-dimensional scatter plot of human tonsil 2. Each data point represents a peptide found in both approaches (classical and PIRL). Oxidized/reduced ratio in PIRL is plotted on the x-axis, while the ox/red ratio in classical is plotted on the y-axis. The scales of the axes are logarithmic. Grey line displays linear function  $y=x$ . Data points above this line represent peptides that display a higher ox/red ratio in classical, whereas data point below  $y=x$  represent peptides with a higher ox/red ratio in PIRL.

Table 16. Number and percentage of oxidized methionine containing peptides of pairs of peptides in both homogenization methods in human tonsil 3.

	<b>PIRL</b>	<b>Classical</b>
	< 1	> 1
Number of peptides	508	521
Percentage	49.37%	50.63%

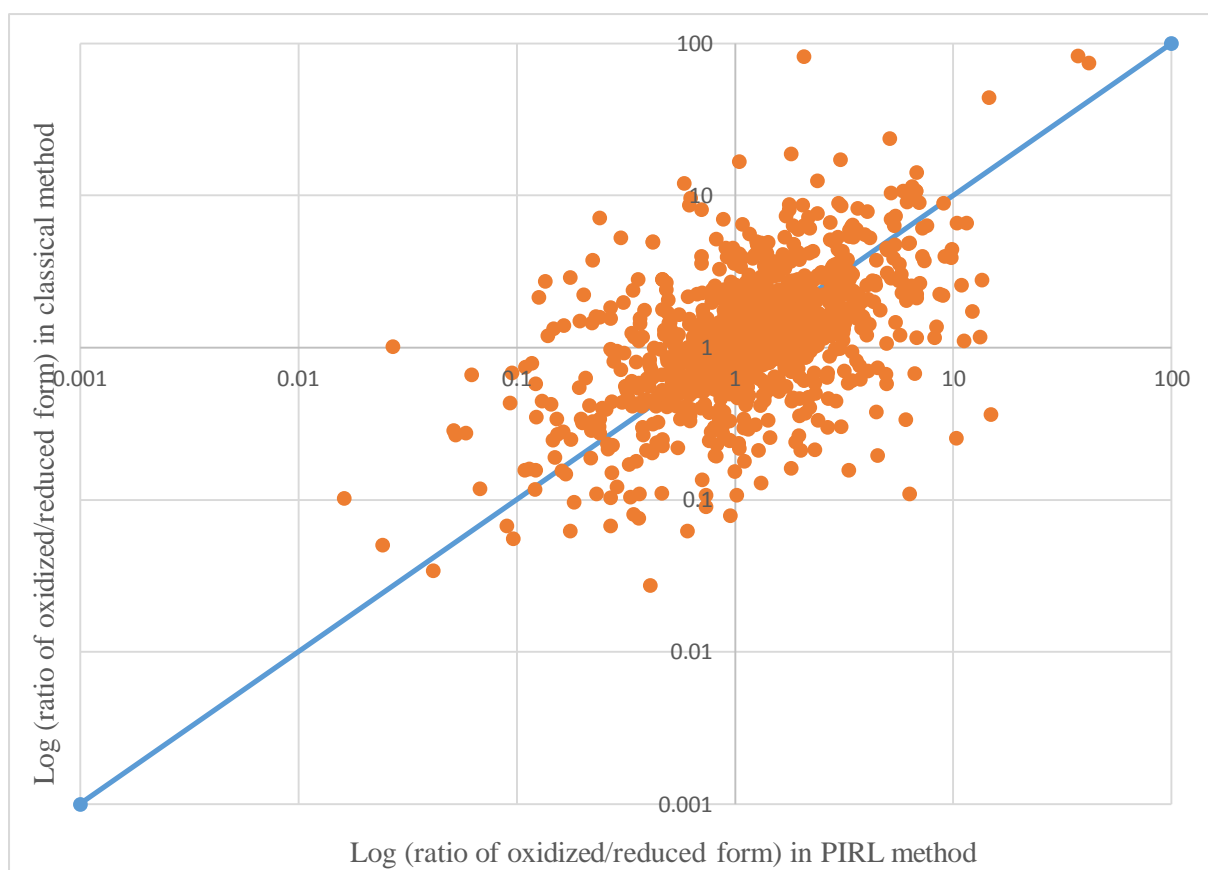


Figure 48. Two-dimensional scatter plot of human tonsil 3. Each data point represents a peptide found in both approaches (classical and PIRL). Oxidized/reduced ratio in PIRL is plotted on the x-axis, while the ox/red ratio in classical is plotted on the y-axis. The scales of the axes are logarithmic.

Grey line displays linear function  $y=x$ . Data points above this line represent peptides that display a higher ox/red ratio in classical, whereas data point below  $y=x$  represent peptides with a higher ox/red ratio in PIRL.

**4. Discussion**

Until now, classical (conventional) homogenization methods of tissues are most commonly used in the field of redox proteomics (as a part of sample preparation strategy). As these homogenization procedures are not performed under inert conditions (such as argon or nitrogen gases) which prevent or minimize the oxidation source from the surrounding environment to enter the buffer system during the homogenization process. Therefore, the possibility to obtain artificial elevated levels of oxidative modifications of proteins is high. As a result, false positive results including artificial oxidation of proteins may be generated. Applying the inert condition not only adds to the cost of sample preparation but also decrease the overall throughput. Therefore, search for other potentially advantageous homogenization tools that are less prone to artificial oxidation and are more efficient is desirable.

Homogenization is a process by which the target sample is transferred to the solution with the same structure and chemical composition. Thus, by performing the homogenization step in the sample preparation procedure, it is expected that the samples can change their physical properties without change in the chemical composition of components. Homogenization of biological samples such as tissues or cells is the first step during redox proteomics experiment. Proteins are included with cytoplasmic membrane and packed in different intracellular compartments. As a result, the extraction and solubilization of proteins demands the disruption of the cellular compartments. Different homogenization methods which are routinely used in field of redox proteomics are discussed below, including their advantages, limitations, and their comparison to PIRL technology

There are five common methods that are used for tissue homogenization prior to redox proteomic analysis, including: 1) ultrasonic, 2) mechanical, 3) freeze-thaw, 4) pressure, and 5) osmotic-detergent lysis. The choice of homogenization technique depends on the sample type.

In ultrasonic homogenization method, the sonicators are used to generate high energy or shock waves, that interacts with the target sample leading the disruption of cells [128]. One of the limitations of this homogenization method that is not suitable for a solid sample such as a tissue. In addition, there is a possibility that this method could result in the disruption of non-covalently bound molecular clusters such as multienzyme complexes. However, PIRL has been found to be suitable for tissue homogenization without significantly destroying the non-covalently bound protein complexes.

In mechanical homogenization method, the most common devices used are rotor-stator homogenizers and open blade mills. The homogenate obtained after mechanical homogenization is considered to be ideal when all proteins are released from the organelles and other cellular compartments as a free suspension of intact components [129]. Centrifugation is then applied to remove debris and other insoluble components (particles) from the cell sample. The mechanical homogenization method is appropriate for most of tissues (hard or soft tissues) compared to other conventional methods. One of the limitations of this method is loss of biomolecules such as proteins via the adsorption on the surface. Another limitation is the incomplete homogenization which can require additional homogenization step leading to the increase in sample loss. However, it has been reported that PIRL offers fine homogenate with much less sample loss compared to mechanical method (Kwiatkowski et al, 2016).

In freeze-thaw homogenization method, the homogenization mechanism relies on the effect of ice crystals formation in the target tissue within the freezing procedure [130]. It is appropriate for most of the bacteria, animal as well as plant cells suspended in water. This method could also be utilized as an additional step after ultrasonic or mechanical homogenization method. However, this homogenization technique may cause changes in the properties of bioactive molecules such as proteins. By using PIRL, the chemical composition of labile biomolecules such as proteins is not changed. Homogenates obtained with PIRL were found with significantly less enzymatic conversions of proteins compared to conventional homogenization methods (Kwiatkowski et al, 2015).

Pressure homogenization method (also called French press) can be efficiently used to homogenize eukaryotic cells and microorganisms in suspension [131]. Due to the construction of pressure homogenization technique, this type of homogenization is ineffective for tissue samples like ultrasonic method. In the osmotic and detergent homogenization methods, the disruption of cells rely on the action of osmotic pressure and/or detergent interactions leading to destruction of the cell walls and cell membranes. Nevertheless, their application is often limited, due to the cost and/or efficiency (Klimek-Ochab et al, 2011).

Therefore, the choice of single method capable of overcoming the various limitations described above is desired and it is suggested that PIRL offers solutions to many of them.

As described in the introduction section, it has been shown in previous studies that the tissue homogenization is possible by irradiating tissues with PIRL technique with the advantage that during this process the chemical composition of labile biomolecules like proteins is not changed. Furthermore, in homogenates obtained with PIRL significantly less enzymatic conversions of proteins were observed compared to classical homogenization approaches (Kwiatkowski et al, 2015). As a result, the total number of intact protein species detected in tissue homogenates, obtained with PIRL, was higher compared to classical homogenization techniques (Kwiatkowski et al, 2016). It was suggested that this advantage of PIRL induced homogenization of tissue is due to the extremely fast process of tissue disruption and transfer of the proteins from the intact tissue into the frozen condensate of the PIRL-induced tissue aerosol. Because this mechanism is very fast, enzymes, which are released from the compartments within the cells during homogenization, cannot degrade many of the other tissue molecules. In addition, another advantage of PIRL is that it does not induce reactive oxygen species (free radicals).

It was further hypothesized, that the special mechanism and the speed by which the tissue is homogenized with PIRL may also result in less oxidation of proteins occurring during this process and can be advantageous in the field of redox proteomics. In redox proteomics methionine oxidation can be studied as representative of the extent of oxidation of proteins/peptides. Thus, it was suggested that PIRL could give a better access to the redox state (e.g., oxidized methionine containing peptides) which is originally found in the cell or tissue compared to classical homogenization approaches. Therefore, PIRL technique was used to investigate the extent proteins oxidized during homogenization of tissues with PIRL in comparison to conventional homogenization.

Firstly, the homogenization of Jurkat cells via classical methodology was performed as a pilot experiment to examine if changes in the extent of methionine oxidation can be studied with the conventional proteomics LC-MS/MS strategy. During this study, an increase in the oxidized form of methionine containing peptides were successfully detected in response to the increasing concentration of hydrogen peroxide ( $H_2O_2$ ). Figures 8A and 8B represent the increase in levels of oxidized form of methionine containing peptides when exposed to the increasing  $H_2O_2$  concentrations.

After that, the degree of oxidation in methionine containing peptides was studied in two different tissue models i.e. rat pancreas and human tonsil tissues by using PIRL compared to the classical homogenization methods. In case of rat pancreatic tissues, the comparison of the



pairs (same) of methionine containing peptides was performed in three biological replicates. The acquired results show that in rat pancreas 2 and rat pancreas 3 samples, no significant difference was observed between the two homogenization techniques (figures 41 and 42). However, in the case of rat pancreas tissue 1, it is shown in figure 40, that majority of methionine containing peptides were found in more reduced state (which is the basic state of methionine residues in the cell “reviewed in ref. 74 and 75”) by using PIRL compared to classical homogenization method.

Three biological replicates of human tissue samples were also used to further verify results from the rat sample experiments. In case of human tonsil tissues, the results showed that in tonsil 2 and tonsil 3, there was no significant difference found between the two homogenization techniques as it is shown in figures 47 and 48. However, in the case of human tonsil tissue 1, it is shown in figure 46 that most of methionine containing peptides are found in more reduced state by using PIRL compared to classical homogenization method.

As displayed by the figures 40 and 46, the ratios of oxidized to reduced methionine containing peptides were found to be higher in the sample prepared with the classical homogenization method in rat pancreas 1, and human tonsil samples. This indicates that more methionine oxidation occurs after classical homogenization. This could be explained by the possibility of higher exposure to atmospheric oxygen compared to PIRL homogenization. Hence, one could claim a higher susceptibility of classical homogenization to environmental confounding variables.

There are few peptides that were found to have a similar degree of oxidation (or: a similar ratio of oxidized/reduced methionines) using both homogenization methods in each tissue. The suggested reason can be that the methionine residues in these peptides are buried within the three-dimensional (3D) structure of the proteins, therefore, being protected against oxidation in both homogenization methods. In this context, it has been experimentally demonstrated in previous studies that the efficiency of methionine oxidation is dependent on their solvent accessibility. This has been evaluated from a protein structure as the accessible surface area of the corresponding methionine residue [132]. Consequently, a set of 71 oxidized methionine containing peptides (involved in 31 proteins) have been analyzed by different bioinformatic tools. The results suggested that 41% of the methionines are exposed to solvent, 15% were found buried with different degrees of flexibility and 44% are buried and structured. It has been

shown that buried but highly flexible methionines can be oxidized. Buried and less flexible methionines can acquire additional local structural flexibility from flanking regions to facilitate the oxidation. Oxidation of buried and structured methionine can also be promoted by the oxidation of neighboring methionines that are more exposed and/or flexible. These results demonstrated that the protein structure flexibility constitutes a crucial factor in the methionine oxidation process .

The data shown in rat pancreas tissue 1 and human tonsil tissue 1 demonstrated that homogenization by PIRL-DIVE gives less oxidation compared to conventional methods. This suggests that PIRL mechanism itself does not generate oxidation. Consequently, it can be proposed that PIRL could be a promising method to be employed in the field of redox proteomics. The results also suggested that the major contribution in oxidation of methionine containing peptides is probably occurring in the steps following the homogenization steps, contrary to what was initially expected. The various sources of exposures of the samples to different sources of oxidative stress between after the homogenization step until the injection into the MS instrument, includes thawing of the sample, tryptic digestion etc. It is worth mentioning, that the previous studies suggested that oxidation of methionine can occur during the tryptic digestion step (reviewed in ref. 9). Therefore, the prevention of oxidation during tryptic digestion should minimize the artificial oxidation of methionine. Thus, a protocol which can prevent/ minimize the oxidation during mentioned steps such as tryptic digestion is feasible for further research. One possible solution could be to perform the experiments under inert gas (such as nitrogen or argon) in order to exclude atmospheric oxygen as an oxidation source. Furthermore, adding antioxidants can also be another solution for preventing the oxidation source.

It has also been demonstrated in previous studies that considerable extents of methionine oxidation in polypeptides can be generated during the sample manipulation steps other than tryptic digestion during their proteomic characterization. Several methionine residues were found converted into methionine sulfoxide (MetO) following their in-gel proteomic analysis in comparison to their extent of oxidation when in solution manipulations were performed. It has been suggested by the authors that high voltages used during electrophoresis might cause the formation of O<sub>3</sub> that may initiate a reaction cascade leading to the formation of methionine sulfoxide. It was also proposed that, the dissolved atmospheric O<sub>2</sub> in buffer solutions used for

the enzymatic digestion of proteins seems also to contribute, generating a background of MetO within samples. (Froelich et al, 2008). These buffers are generally known to have  $\text{pH} > 7$ .

Furthermore, it has been demonstrated that sequential corrosion of stainless steel ESI emitters, under common MS conditions, can induce electrochemical reactions associated with the spray process, eventually leading to artificial methionine oxidation (MetO). These electrical discharge processes can be avoided by repolishing the emitter, especially to a rounded geometry (Chen et al, 2007). This can lead to a method offering less artifacts originated by unwanted oxidation process. Consequently, this would enable one to more directly access to the peptides in their native redox state in cells or tissues.

In conclusion, the current results at hand on the application of PIRL-DIVE as a potential homogenization method for mass spectrometric redox proteome studies show that for the most of tissue samples there is no significant difference compared to classical methods but offering efficient tissue homogenization and better proteome coverage associated with PIRL technology. One tissue in each model (rat pancreas 1 and human tonsil 1) has shown less oxidation by using PIRL technology.

It is worth mentioning, that it has been experimentally reported by Houde et al, 2006 and by Huang et al, 2016 that oxidation of methionine can be taken place during tryptic digestion. This aspect has been also reviewed by Bachi et al, 2013. Therefore, artificial oxidation of methionine containing peptides is expected. As a result, it can be concluded from the presented results (rat pancreatic tissues 2 and 3 as well as human tonsil tissues 2 and 3) that tryptic digestion step is a critical confounding variable which is able to generate artifacts of methionine oxidation.

Caution should be taken after obtaining PIRL homogenate to avoid artificial oxidation. One possible addition can be the use of antioxidants to the PIRL homogenate to prevent artificial oxidation. Another solution can be working under an inert condition (e.g., nitrogen gas) to minimize the oxidation possibility. It was also suggested by Huang et al, 2016 and by Bachi et al, 2013 that digestion under milder conditions such as low pH can minimize the oxidation. This will result in data more closer in depicting the natural state of proteins and peptides in the

tissue samples. Hence, PIRL could be used as a promising alternative to conventional sample preparation methods in the field of redox proteomics.

**5. Future outlook**

Different conventional homogenization methods are applied in the field of redox proteomics, for example, studying the extent of methionine oxidation. The approach presented in the thesis at hand, representing the tissue homogenization via PIRL-DIVE, is found to be comparable to the methods of tissue homogenization already in use with the several additional advantages. For instance, it has been shown that PIRL-DIVE homogenization method preserves the native chemical composition of labile biomolecules of interest such as proteins. Also, tissue homogenates obtained with PIRL were found with significantly less proteins that were enzymatically converted due to their less exposure to active enzymes compared to classical homogenization methods (Kwiatkowski et al, 2015). The additional advantage offered by this method is the higher yield of intact protein species detected in tissue homogenates compared to classical approaches (Kwiatkowski et al, 2016). Furthermore, PIRL can be utilized to produce significantly finer homogenates of tissue such as cancer biopsies compared to other homogenization methods thus producing better representative tissue samples for proteomic applications. With these advantages PIRL DIVE will find broader applications in redox proteomics in particular.

Further work is required to fully benefit from these applications mentioned above such as efforts in optimizing PIRL for redox proteomics would be worth striving for. One possible improvement is to work under inert conditions to reduce the possibility of oxidation source from the surrounding environment which results in artificial oxidation (e.g., methionine oxidation) of proteins. Another plausible strategy would be to add antioxidants to the PIRL homogenate could also be another manner to prevent artificial oxidation. In contrast to inert gas, this approach would also inhibit artificial oxidation originating from other steps including the above-mentioned thawing of the sample, tryptic digestion etc. until the injection of the sample into the MS instrument. It is expected that either two solutions can minimize or prevent the possibility of artifacts of methionine sulfoxide.

Thus, taking all the aforesaid points into consideration, it is desirable to further improve PIRL in order to fully establish this method in the field of redox proteomics. Not only could this method improve basic research on redox proteomes of various cells and tissues, but it could also be used as a high-throughput, ultrafast homogenization method for clinical applications, possibly enabling new insights to identify and monitor redox protein disease markers.

**6. References**

1. Davies, K.J., *Oxidative stress: the paradox of aerobic life*. Biochem Soc Symp, 1995. **61**: p. 1-31.
2. Qu, B., et al., *Mitochondrial damage by the "pro-oxidant" peroxisomal proliferator clofibrate*. Free Radic Biol Med, 1999. **27**(9-10): p. 1095-102.
3. Gutteridge, J.M. and J. Mitchell, *Redox imbalance in the critically ill*. Br Med Bull, 1999. **55**(1): p. 49-75.
4. Monk, L.S., K.V. Fagerstedt, and R.M. Crawford, *Superoxide Dismutase as an Anaerobic Polypeptide : A Key Factor in Recovery from Oxygen Deprivation in *Iris pseudacorus*?* Plant Physiol, 1987. **85**(4): p. 1016-20.
5. Wu, J., et al., *The N-terminal domain of PILB from *Neisseria meningitidis* is a disulfide reductase that can recycle methionine sulfoxide reductases*. J Biol Chem, 2005. **280**(13): p. 12344-50.
6. Yang, W.S., et al., *Regulation of ferroptotic cancer cell death by GPX4*. Cell, 2014. **156**(1-2): p. 317-331.
7. Zhang, Y., et al., *Redox control of the survival of healthy and diseased cells*. Antioxid Redox Signal, 2011. **15**(11): p. 2867-908.
8. Bern, M., J. Saladino, and J.S. Sharp, *Conversion of methionine into homocysteic acid in heavily oxidized proteomics samples*. Rapid Commun Mass Spectrom, 2010. **24**(6): p. 768-72.
9. Dalle-Donne, I., et al., *Biomarkers of oxidative damage in human disease*. Clin Chem, 2006. **52**(4): p. 601-23.
10. Schafer, F.Q. and G.R. Buettner, *Redox environment of the cell as viewed through the redox state of the glutathione disulfide/glutathione couple*. Free Radic Biol Med, 2001. **30**(11): p. 1191-212.
11. Droge, W., *Free radicals in the physiological control of cell function*. Physiol Rev, 2002. **82**(1): p. 47-95.
12. Landis, G.N. and J. Tower, *Superoxide dismutase evolution and life span regulation*. Mech Ageing Dev, 2005. **126**(3): p. 365-79.
13. Pryor, W.A., *Vitamin E and heart disease: basic science to clinical intervention trials*. Free Radic Biol Med, 2000. **28**(1): p. 141-64.
14. Bachi, A., I. Dalle-Donne, and A. Scaloni, *Redox proteomics: chemical principles, methodological approaches and biological/biomedical promises*. Chem Rev, 2013. **113**(1): p. 596-698.

15. Kim, G., S.J. Weiss, and R.L. Levine, *Methionine oxidation and reduction in proteins*. Biochim Biophys Acta, 2014. **1840**(2): p. 901-5.
16. Brigelius-Flohe, R. and M. Maiorino, *Glutathione peroxidases*. Biochim Biophys Acta, 2013. **1830**(5): p. 3289-303.
17. Stadtman, E.R. and R.L. Levine, *Free radical-mediated oxidation of free amino acids and amino acid residues in proteins*. Amino Acids, 2003. **25**(3-4): p. 207-18.
18. Dalle-Donne, I., et al., *S-glutathionylation in protein redox regulation*. Free Radic Biol Med, 2007. **43**(6): p. 883-98.
19. Dalle-Donne, I., et al., *Protein S-glutathionylation: a regulatory device from bacteria to humans*. Trends Biochem Sci, 2009. **34**(2): p. 85-96.
20. Grimsrud, P.A., et al., *Oxidative stress and covalent modification of protein with bioactive aldehydes*. J Biol Chem, 2008. **283**(32): p. 21837-41.
21. Berlett, B.S. and E.R. Stadtman, *Protein oxidation in aging, disease, and oxidative stress*. J Biol Chem, 1997. **272**(33): p. 20313-6.
22. Jacobs, A.T. and L.J. Marnett, *Systems analysis of protein modification and cellular responses induced by electrophile stress*. Acc Chem Res, 2010. **43**(5): p. 673-83.
23. Boronat, S., S. Garcia-Santamarina, and E. Hidalgo, *Gel-free proteomic methodologies to study reversible cysteine oxidation and irreversible protein carbonyl formation*. Free Radic Res, 2015. **49**(5): p. 494-510.
24. Rogowska-Wrzesinska, A., et al., *Analysis of protein carbonylation--pitfalls and promise in commonly used methods*. Free Radic Res, 2014. **48**(10): p. 1145-62.
25. Boronat, S., et al., *Thiol-based H2O2 signalling in microbial systems*. Redox Biol, 2014. **2**: p. 395-9.
26. Butterfield, D.A. and C.M. Lauderback, *Lipid peroxidation and protein oxidation in Alzheimer's disease brain: potential causes and consequences involving amyloid beta-peptide-associated free radical oxidative stress*. Free Radic Biol Med, 2002. **32**(11): p. 1050-60.
27. Gorrini, C., I.S. Harris, and T.W. Mak, *Modulation of oxidative stress as an anticancer strategy*. Nat Rev Drug Discov, 2013. **12**(12): p. 931-47.
28. Keller, J.N., K.B. Hanni, and W.R. Markesbery, *Impaired proteasome function in Alzheimer's disease*. J Neurochem, 2000. **75**(1): p. 436-9.
29. D'Autreaux, B. and M.B. Toledano, *ROS as signalling molecules: mechanisms that generate specificity in ROS homeostasis*. Nat Rev Mol Cell Biol, 2007. **8**(10): p. 813-24.
30. Di Lisa, F. and P. Bernardi, *Mitochondrial function and myocardial aging. A critical analysis of the role of permeability transition*. Cardiovasc Res, 2005. **66**(2): p. 222-32.

31. Lambeth, J.D., *NOX enzymes and the biology of reactive oxygen*. Nat Rev Immunol, 2004. **4**(3): p. 181-9.
32. Janssen-Heininger, Y.M., et al., *Redox-based regulation of signal transduction: principles, pitfalls, and promises*. Free Radic Biol Med, 2008. **45**(1): p. 1-17.
33. Valko, M., H. Morris, and M.T. Cronin, *Metals, toxicity and oxidative stress*. Curr Med Chem, 2005. **12**(10): p. 1161-208.
34. Valko, M., et al., *Free radicals and antioxidants in normal physiological functions and human disease*. Int J Biochem Cell Biol, 2007. **39**(1): p. 44-84.
35. Bedard, K. and K.H. Krause, *The NOX family of ROS-generating NADPH oxidases: physiology and pathophysiology*. Physiol Rev, 2007. **87**(1): p. 245-313.
36. Avshalumov, M.V. and M.E. Rice, *Activation of ATP-sensitive K<sup>+</sup> (K(ATP)) channels by H<sub>2</sub>O<sub>2</sub> underlies glutamate-dependent inhibition of striatal dopamine release*. Proc Natl Acad Sci U S A, 2003. **100**(20): p. 11729-34.
37. Bao, L., et al., *Mitochondria are the source of hydrogen peroxide for dynamic brain-cell signaling*. J Neurosci, 2009. **29**(28): p. 9002-10.
38. Burgoyne, J.R., et al., *Hydrogen peroxide sensing and signaling by protein kinases in the cardiovascular system*. Antioxid Redox Signal, 2013. **18**(9): p. 1042-52.
39. Murphy, M.P., *How mitochondria produce reactive oxygen species*. Biochem J, 2009. **417**(1): p. 1-13.
40. Brown, D.I. and K.K. Griendling, *Nox proteins in signal transduction*. Free Radic Biol Med, 2009. **47**(9): p. 1239-53.
41. Schrader, M. and H.D. Fahimi, *Mammalian peroxisomes and reactive oxygen species*. Histochem Cell Biol, 2004. **122**(4): p. 383-93.
42. Hess, D.T., et al., *Protein S-nitrosylation: purview and parameters*. Nat Rev Mol Cell Biol, 2005. **6**(2): p. 150-66.
43. Fiaschi, T., et al., *Redox regulation of beta-actin during integrin-mediated cell adhesion*. J Biol Chem, 2006. **281**(32): p. 22983-91.
44. Masella, R., et al., *Novel mechanisms of natural antioxidant compounds in biological systems: involvement of glutathione and glutathione-related enzymes*. J Nutr Biochem, 2005. **16**(10): p. 577-86.
45. Powers, S.K. and M.J. Jackson, *Exercise-induced oxidative stress: cellular mechanisms and impact on muscle force production*. Physiol Rev, 2008. **88**(4): p. 1243-76.
46. Ristow, M., et al., *Antioxidants prevent health-promoting effects of physical exercise in humans*. Proc Natl Acad Sci U S A, 2009. **106**(21): p. 8665-70.



47. Powers, S.K., E.E. Talbert, and P.J. Adhietty, *Reactive oxygen and nitrogen species as intracellular signals in skeletal muscle*. J Physiol, 2011. **589**(Pt 9): p. 2129-38.
48. Dalle-Donne, I., et al., *Protein carbonylation in human diseases*. Trends Mol Med, 2003. **9**(4): p. 169-76.
49. Barnham, K.J., C.L. Masters, and A.I. Bush, *Neurodegenerative diseases and oxidative stress*. Nat Rev Drug Discov, 2004. **3**(3): p. 205-14.
50. Stocker, R. and J.F. Keaney, Jr., *Role of oxidative modifications in atherosclerosis*. Physiol Rev, 2004. **84**(4): p. 1381-478.
51. Butterfield, D.A. and I. Dalle-Donne, *Redox proteomics: from protein modifications to cellular dysfunction and disease*. Mass Spectrom Rev, 2014. **33**(1): p. 1-6.
52. Giacco, F. and M. Brownlee, *Oxidative stress and diabetic complications*. Circ Res, 2010. **107**(9): p. 1058-70.
53. Reed, T.T., et al., *Proteomic identification of nitrated brain proteins in early Alzheimer's disease inferior parietal lobule*. J Cell Mol Med, 2009. **13**(8b): p. 2019-29.
54. Negre-Salvayre, A., et al., *Pathological aspects of lipid peroxidation*. Free Radic Res, 2010. **44**(10): p. 1125-71.
55. Cadenas, E., *Basic mechanisms of antioxidant activity*. Biofactors, 1997. **6**(4): p. 391-7.
56. Sultana, R. and D.A. Butterfield, *Role of oxidative stress in the progression of Alzheimer's disease*. J Alzheimers Dis, 2010. **19**(1): p. 341-53.
57. Yan, L.J. and M.J. Forster, *Chemical probes for analysis of carbonylated proteins: a review*. J Chromatogr B Analyt Technol Biomed Life Sci, 2011. **879**(17-18): p. 1308-15.
58. Linares, M., et al., *Proteomic approaches to identifying carbonylated proteins in brain tissue*. J Proteome Res, 2011. **10**(4): p. 1719-27.
59. Brandes, N., S. Schmitt, and U. Jakob, *Thiol-based redox switches in eukaryotic proteins*. Antioxid Redox Signal, 2009. **11**(5): p. 997-1014.
60. Irazusta, V., et al., *Proteomic strategies for the analysis of carbonyl groups on proteins*. Curr Protein Pept Sci, 2010. **11**(8): p. 652-8.
61. Yuan, K., et al., *Thiol-based redox proteomics in cancer research*. Proteomics, 2015. **15**(2-3): p. 287-99.
62. Butterfield, D.A., et al., *Redox proteomics in selected neurodegenerative disorders: from its infancy to future applications*. Antioxid Redox Signal, 2012. **17**(11): p. 1610-55.

63. Butterfield, D.A., et al., *Mass spectrometry and redox proteomics: applications in disease*. Mass Spectrom Rev, 2014. **33**(4): p. 277-301.
64. Wittmann-Liebold, B., H.R. Graack, and T. Pohl, *Two-dimensional gel electrophoresis as tool for proteomics studies in combination with protein identification by mass spectrometry*. Proteomics, 2006. **6**(17): p. 4688-703.
65. Kim, H., et al., *2D gel proteomics: an approach to study age-related differences in protein abundance or isoform complexity in biological samples*. Methods Mol Biol, 2007. **371**: p. 349-91.
66. Rabilloud, T., et al., *Improvement of the solubilization of proteins in two-dimensional electrophoresis with immobilized pH gradients*. Electrophoresis, 1997. **18**(3-4): p. 307-16.
67. Rabilloud, T., et al., *Two-dimensional gel electrophoresis in proteomics: Past, present and future*. J Proteomics, 2010. **73**(11): p. 2064-77.
68. Sheehan, D., B. McDonagh, and J.A. Barcena, *Redox proteomics*. Expert Rev Proteomics, 2010. **7**(1): p. 1-4.
69. Perkins, D.N., et al., *Probability-based protein identification by searching sequence databases using mass spectrometry data*. Electrophoresis, 1999. **20**(18): p. 3551-67.
70. Roe, M.R. and T.J. Griffin, *Gel-free mass spectrometry-based high throughput proteomics: tools for studying biological response of proteins and proteomes*. Proteomics, 2006. **6**(17): p. 4678-87.
71. Eng, J.K., A.L. McCormack, and J.R. Yates, *An approach to correlate tandem mass spectral data of peptides with amino acid sequences in a protein database*. J Am Soc Mass Spectrom, 1994. **5**(11): p. 976-89.
72. Aebersold, R. and M. Mann, *Mass-spectrometric exploration of proteome structure and function*. Nature, 2016. **537**(7620): p. 347-55.
73. Gao, J., et al., *Loss of conformational stability in calmodulin upon methionine oxidation*. Biophys J, 1998. **74**(3): p. 1115-34.
74. Oien, D.B. and J. Moskovitz, *Substrates of the methionine sulfoxide reductase system and their physiological relevance*. Curr Top Dev Biol, 2008. **80**: p. 93-133.
75. Ezraty, B., L. Aussel, and F. Barras, *Methionine sulfoxide reductases in prokaryotes*. Biochim Biophys Acta, 2005. **1703**(2): p. 221-9.
76. Tarrago, L., E. Laugier, and P. Rey, *Protein-repairing methionine sulfoxide reductases in photosynthetic organisms: gene organization, reduction mechanisms, and physiological roles*. Mol Plant, 2009. **2**(2): p. 202-17.
77. Lowther, W.T., et al., *The mirrored methionine sulfoxide reductases of Neisseria gonorrhoeae pilB*. Nat Struct Biol, 2002. **9**(5): p. 348-52.

78. Oh, S.K., et al., *CaMsrB2, pepper methionine sulfoxide reductase B2, is a novel defense regulator against oxidative stress and pathogen attack*. *Plant Physiol*, 2010. **154**(1): p. 245-61.
79. Levine, R.L., et al., *Methionine residues may protect proteins from critical oxidative damage*. *Mech Ageing Dev*, 1999. **107**(3): p. 323-32.
80. Gu, S.X., J.W. Stevens, and S.R. Lentz, *Regulation of thrombosis and vascular function by protein methionine oxidation*. *Blood*, 2015. **125**(25): p. 3851-9.
81. Stadtman, E.R., et al., *Methionine oxidation and aging*. *Biochim Biophys Acta*, 2005. **1703**(2): p. 135-40.
82. Romero, H.M., et al., *Investigations into the role of the plastidial peptide methionine sulfoxide reductase in response to oxidative stress in Arabidopsis*. *Plant Physiol*, 2004. **136**(3): p. 3784-94.
83. Manta, B. and V.N. Gladyshev, *Regulated methionine oxidation by monooxygenases*. *Free Radic Biol Med*, 2017. **109**: p. 141-155.
84. St John, G., et al., *Peptide methionine sulfoxide reductase from Escherichia coli and Mycobacterium tuberculosis protects bacteria against oxidative damage from reactive nitrogen intermediates*. *Proc Natl Acad Sci U S A*, 2001. **98**(17): p. 9901-6.
85. Moskovitz, J., et al., *Methionine sulfoxide reductase (MsrA) is a regulator of antioxidant defense and lifespan in mammals*. *Proc Natl Acad Sci U S A*, 2001. **98**(23): p. 12920-5.
86. De Luca, A., et al., *Methionine sulfoxide reductase A down-regulation in human breast cancer cells results in a more aggressive phenotype*. *Proc Natl Acad Sci U S A*, 2010. **107**(43): p. 18628-33.
87. Lee, B.C., et al., *MsrB1 and MICALs regulate actin assembly and macrophage function via reversible stereoselective methionine oxidation*. *Mol Cell*, 2013. **51**(3): p. 397-404.
88. Butterfield, D.A., et al., *In vivo oxidative stress in brain of Alzheimer disease transgenic mice: Requirement for methionine 35 in amyloid beta-peptide of APP*. *Free Radic Biol Med*, 2010. **48**(1): p. 136-44.
89. Ghesquiere, B., et al., *Redox proteomics of protein-bound methionine oxidation*. *Mol Cell Proteomics*, 2011. **10**(5): p. M110.006866.
90. Oien, D.B., et al., *Detection of oxidized methionine in selected proteins, cellular extracts and blood serums by novel anti-methionine sulfoxide antibodies*. *Arch Biochem Biophys*, 2009. **485**(1): p. 35-40.
91. Rosen, H., et al., *Methionine oxidation contributes to bacterial killing by the myeloperoxidase system of neutrophils*. *Proc Natl Acad Sci U S A*, 2009. **106**(44): p. 18686-91.

92. Vogt, W., *Oxidation of methionyl residues in proteins: tools, targets, and reversal*. Free Radic Biol Med, 1995. **18**(1): p. 93-105.
93. Gevaert, K., et al., *Chromatographic isolation of methionine-containing peptides for gel-free proteome analysis: identification of more than 800 Escherichia coli proteins*. Mol Cell Proteomics, 2002. **1**(11): p. 896-903.
94. Wang, P.F., et al., *An unusually low pK(a) for Cys282 in the active site of human muscle creatine kinase*. Biochemistry, 2001. **40**(39): p. 11698-705.
95. Rhee, S.G., et al., *Hydrogen peroxide: a key messenger that modulates protein phosphorylation through cysteine oxidation*. Sci STKE, 2000. **2000**(53): p. pe1.
96. Ma, L.H., C.L. Takanishi, and M.J. Wood, *Molecular mechanism of oxidative stress perception by the Orp1 protein*. J Biol Chem, 2007. **282**(43): p. 31429-36.
97. Reddie, K.G. and K.S. Carroll, *Expanding the functional diversity of proteins through cysteine oxidation*. Curr Opin Chem Biol, 2008. **12**(6): p. 746-54.
98. Rehder, D.S. and C.R. Borges, *Cysteine sulfenic acid as an intermediate in disulfide bond formation and nonenzymatic protein folding*. Biochemistry, 2010. **49**(35): p. 7748-55.
99. Lindahl, M., A. Mata-Cabana, and T. Kieselbach, *The disulfide proteome and other reactive cysteine proteomes: analysis and functional significance*. Antioxid Redox Signal, 2011. **14**(12): p. 2581-642.
100. Yates, J.R., C.I. Ruse, and A. Nakorchevsky, *Proteomics by mass spectrometry: approaches, advances, and applications*. Annu Rev Biomed Eng, 2009. **11**: p. 49-79.
101. Aebersold, R. and M. Mann, *Mass spectrometry-based proteomics*. Nature, 2003. **422**(6928): p. 198-207.
102. Zhao, Y., et al., *Proteomic analysis of integral plasma membrane proteins*. Anal Chem, 2004. **76**(7): p. 1817-23.
103. Jeong, J.A., et al., *Proteomic analysis of the hydrophobic fraction of mesenchymal stem cells derived from human umbilical cord blood*. Mol Cells, 2006. **22**(1): p. 36-43.
104. Wu, C.C., et al., *A method for the comprehensive proteomic analysis of membrane proteins*. Nat Biotechnol, 2003. **21**(5): p. 532-8.
105. Chao, C.C., Y.S. Ma, and E.R. Stadtman, *Modification of protein surface hydrophobicity and methionine oxidation by oxidative systems*. Proc Natl Acad Sci U S A, 1997. **94**(7): p. 2969-74.
106. Griffiths, S.W. and C.L. Cooney, *Development of a peptide mapping procedure to identify and quantify methionine oxidation in recombinant human alpha1-antitrypsin*. J Chromatogr A, 2002. **942**(1-2): p. 133-43.

107. McHugh, L. and J.W. Arthur, *Computational Methods for Protein Identification from Mass Spectrometry Data*. PLoS Computational Biology, 2008. **4**(2): p. e12.
108. Fenn, J.B., et al., *Electrospray ionization for mass spectrometry of large biomolecules*. Science, 1989. **246**(4926): p. 64-71.
109. Karas, M., D. Bachmann, and F. Hillenkamp, *Influence of the wavelength in high-irradiance ultraviolet laser desorption mass spectrometry of organic molecules*. Analytical Chemistry, 1985. **57**(14): p. 2935-2939.
110. Cottrell, J.S., *Protein identification using MS/MS data*. J Proteomics, 2011. **74**(10): p. 1842-51.
111. McGuff, P.E., et al., *STUDIES OF THE SURGICAL APPLICATIONS OF LASER (LIGHT AMPLIFICATION BY STIMULATED EMISSION OF RADIATION)*. Surg Forum, 1963. **14**: p. 143-5.
112. Mann, M., R.C. Hendrickson, and A. Pandey, *Analysis of proteins and proteomes by mass spectrometry*. Annu Rev Biochem, 2001. **70**: p. 437-73.
113. Elavarasu, S., D. Naveen, and A. Thangavelu, *Lasers in periodontics*. J Pharm Bioallied Sci, 2012. **4**(Suppl 2): p. S260-3.
114. Solon, L.R., R. Aronson, and G. Gould, *Physiological implications of laser beams*. Science, 1961. **134**(3489): p. 1506-8.
115. Carruth, J.A., *Lasers in medicine and surgery*. J Med Eng Technol, 1984. **8**(4): p. 161-7.
116. Franjic, K., et al., *Laser selective cutting of biological tissues by impulsive heat deposition through ultrafast vibrational excitations*. Opt Express, 2009. **17**(25): p. 22937-59.
117. Franjic, K. and D. Miller, *Vibrationally excited ultrafast thermodynamic phase transitions at the water/air interface*. Phys Chem Chem Phys, 2010. **12**(20): p. 5225-39.
118. Hess, M., et al., *Picosecond infrared laser (PIRL): an ideal phonomicrosurgical laser?* Eur Arch Otorhinolaryngol, 2013. **270**(11): p. 2927-37.
119. Amini-Nik, S., et al., *Ultrafast mid-IR laser scalpel: protein signals of the fundamental limits to minimally invasive surgery*. PLoS One, 2010. **5**(9).
120. Paltauf, G. and P.E. Dyer, *Photomechanical processes and effects in ablation*. Chem Rev, 2003. **103**(2): p. 487-518.
121. Miller, R.J., *Mapping atomic motions with ultrabright electrons: the chemists' gedanken experiment enters the lab frame*. Annu Rev Phys Chem, 2014. **65**: p. 583-604.
122. Kwiatkowski, M., et al., *Ultrafast extraction of proteins from tissues using desorption by impulsive vibrational excitation*. Angew Chem Int Ed Engl, 2015. **54**(1): p. 285-8.












123. Kwiatkowski, M., et al., *Homogenization of tissues via picosecond-infrared laser (PIRL) ablation: Giving a closer view on the in-vivo composition of protein species as compared to mechanical homogenization*. J Proteomics, 2016. **134**: p. 193-202.
124. Linke, S.J., et al., *A new technology for appplanation free corneal trephination: the picosecond infrared laser (PIRL)*. PLoS One, 2015. **10**(3): p. e0120944.
125. Lubran, M.M., *The measurement of total serum proteins by the Biuret method*. Ann Clin Lab Sci, 1978. **8**(2): p. 106-10.
126. Smith, P.K., et al., *Measurement of protein using bicinchoninic acid*. Anal Biochem, 1985. **150**(1): p. 76-85.
127. Shevchenko, A., et al., *In-gel digestion for mass spectrometric characterization of proteins and proteomes*. Nat Protoc, 2006. **1**(6): p. 2856-60.
128. Wu, Q., et al., *Proteome studies on liver tissue in a phenobarbital-induced rat model*. Eur J Pharmacol, 2011. **670**(2-3): p. 333-40.
129. Huber, L.A., K. Pfaller, and I. Vietor, *Organelle proteomics: implications for subcellular fractionation in proteomics*. Circ Res, 2003. **92**(9): p. 962-8.
130. Chaiyarit, S. and V. Thongboonkerd, *Comparative analyses of cell disruption methods for mitochondrial isolation in high-throughput proteomics study*. Anal Biochem, 2009. **394**(2): p. 249-58.
131. Bodzon-Kulakowska, A., et al., *Methods for samples preparation in proteomic research*. J Chromatogr B Analyt Technol Biomed Life Sci, 2007. **849**(1-2): p. 1-31.
132. Xu, K., V.N. Uversky, and B. Xue, *Local flexibility facilitates oxidization of buried methionine residues*. Protein Pept Lett, 2012. **19**(6): p. 688-97.













## 7. Appendix

## Risk and safety statements/List of hazards substances utilized according to GSH

Source: <http://www.bgrci.de/fachwissen-portal/themenspektrum/gefahrstoffe/ghs/inhalt-von-ghs/kennzeichnung/>

<http://www.sigmaaldrich.com/catalog/product/sigma/h1009?lang=de&region=DE>

Chemical name	GHS symbol	Hazard statements	Precautionary statements
Acetonitril		H225, H332, H302, H312, H319	P210, P305+P351+P338, P403+P235
Dithiothreitol		H302, H315, H319, H335	P302+352, P305+351+338
Iodacetamide		H301, H317, H334, H413	P261, P280, P301+P310, P342+P311
Methanol		H225, H301, H311, H331, H370	P210, P280, P233, P302+P352, P309, P310
Tris		H315, H319, H335	P261, P305+351+338
Thiourea		H302, H351, H361d, H411	P273, P281, P308+P313
Oligo R3 Bulk Medium		H335	P261, P304+P340, P312, P403+P233, P405
Trifluoroacetic acid		H332, H314, H412	P271, P273, P301+P330+P331, P305+P351+P338, P309+P310
Trypsin		H319, H335, H315, H334	P285, P261, P305+351+338, P321, P405, P501
Ammonium hydrogen carbonat		H302	---
Hydrogen peroxide		H302, H318, H412	<u>P280, P301 + P312 + P330, P305 + P351 + P338 + P310</u>

Reducing agent 20x		H319	P260, P303+P361+P353, P305+P351+P338, P310, P405, P501
Liquid nitrogen		H281	P282, P336+P315, P403
Hydrochloric acid (37%)		H290, H314, H335	P234, P260, P304+P340, P303+P361+P353, P305+P351+P338, P309+P311, P501
Formic acid		<u>H226, H302,</u> <u>H314, H331</u>	<u>P210, P280, P303 +</u> <u>P361 + P353, P304</u> <u>+ P340 + P310,</u> <u>P305 + P351 +</u> <u>P338, P403 + P233</u>
Ethanol		H225	P210
Sample buffer 4x		H319	P280, P264, P305+P351+P338, P310, P405, P501
2-Mercaptoethanol		H302, H411, H315, H335, H311, H319	P280, P312, P302+P350, P261, P273, P301+P312, P305+P351+P3 38
Isopropanol		H225, H319, H336.	P210, P233, P305+351+338
SDS		<u>H228, H302 +</u> <u>H332, H315,</u> <u>H318, H335,</u> <u>H412</u>	<u>P210, P261, P273,</u> <u>P280, P305 + P351</u> <u>+ P338</u>
BCA test kit		H410	<u>P273, P391, P501</u>
2D-Quant kit		H301, H302, H314, H315, H318, H319, H400, H410, H411, H412	P273, P280, P302+P352, P305+P351+P338
Protease inhibitors cocktail (complete tablet mini), EDTA free		H315, H319	P264, P280, P302 + P352, P332 + P313, P337 + P313, P362 + P364



### 8. Acknowledgement

First of all I pray and thank ALLAH for giving me the patience and strength to finish my PhD work.

I would like to express my deepest and massive thanks to my Supervisor Professor Dr. Hartmut Schlüter, for offering me the chance to join his group and do my PhD research under his supervision, providing me with an impressive topic, his support, kind supervision, giving me a lot from his time, improving my scientific knowledge and helping me to achieve my goals. I thank him for his humble manner, his patience and for his advices the whole time. I learned a lot from discussing scientific issues, his way in generating ideas and simplifying concepts.

Professor Schlüter is not only my supervisor but someone I trust him, respect him and learned a lot from him.

Many thanks and appreciation to PD Dr. Friedrich Buck for his time, his valuable discussions of the theoretical and practical aspects in a friendly and understandable manner, and for his proof-reading of my thesis.

Many thanks to my co-advisor Prof. Dr. Dr. Christian Betzel (Chemistry Department) for his acceptance to be my co-advisor for my PhD research, his time and effort.

I also want to thank Prof. Dr. Dwayne Miller, for giving me the opportunity to work with the impressive new technology, PIRL “picosecond infrared laser”.

Special thanks to the members in the working group of Prof. Miller: Dr. Nils-Owe Hansen and Stephanie Uschold for their kind assistance during ablation experiments.

I also would like to thank PD Dr. Malte Kriegs and Konstantin Hoffer (Laboratory for Radiobiology & Experimental Radiation Oncology) for providing me with Jurkat cell samples.

Many thanks to my colleague Marcus Wurlitzer for his assistance in statistical and bioinformatical sections, his beneficial discussions.

Many thanks also to Sönke Harder, for spreading a nice lab work atmosphere and for his practical assistance.

Many thanks to all my colleagues in the working group: Laura Heikaus, Yudong Guan, Pascal Steffen, Dennis Krösser, Benjamin Dreyer, Arslan Ali, Manka Fuh, Lorena Hänel, Parnian Kiani, Christina Johannsen, Jonas Klein and Christine Lefert, wishing you the best and hoping a bright future for all of you.

I would also like to thank PD Dr. Buck and Dr. Christoph Krips for German translation of the abstract.

Many thanks for my previous colleagues Dr. Marcel Kwiatkowski Dr. Refat Nimer, Dr. Maryam Omid, Ramin Fazel and Andrey Kurittin

Lots of love and appreciation to my parents. I deeply thank my mother Zeinab, my father Mahmoud, my brothers Mohammad and Ahmad and my sister Eman, my wife Eman and my son Mahmoud for supporting me and pushing me to seek my PhD.

Without my parents I would not reach this point.

Finally, my deepest thanks to my closet friend Matin Kohsar for supporting me with his advices during my stay in Germany.

With my best wishes for all

**9. Declaration on oath**

I hereby declare on oath, that I have written the present dissertation by my own and have not used other than the acknowledged resources and aids. The submitted written version corresponds to the version on the electronic storage medium. I hereby declare that I have not previously applied or pursued for a doctorate (Ph.D. studies).

Name: Atef Manna

Location: Hamburg

Date: 19.09.2017